Universidade de Lisboa

Faculdade de Farmácia

BIMODAL PROBES FOR IMAGING OF PROSTATE CANCER

Sofia Margarida Alves Batanete

Dissertation supervised by Professor Doutor António Rocha Paulo and co-supervised by Professor Doutor António J. I. Alfaia

MSc Course in Pharmaceutical and Medicinal Chemistry

2019

Universidade de Lisboa

Faculdade de Farmácia

BIMODAL PROBES FOR IMAGING OF PROSTATE CANCER

Sofia Margarida Alves Batanete

Dissertation supervised by Professor Doutor António Rocha Paulo and co-supervised by Professor Doutor António J. I. Alfaia

MSc Course in Pharmaceutical and Medicinal Chemistry

2019

Acknowledgements

First of all, I thank Dr. António Paulo for accepting my participation in this project of the Radiopharmaceutical Sciences Group (RSG) of the Center for Nuclear Sciences and Technologies (C^2TN) and for his enormous scientific knowledge, his demand and the guidance of the work that led to the conclusion of this thesis. I also thank Francisco Silva for his availability for the introduction and integration in laboratory work, the co-supervision of the project and the knowledge wisely transmitted. I thank my co-adviser, Professor António Alfaia, for the encouragement given to this work.

To all the professionals in this group, I thank you, above all, for the hospitality and kindness with which you received me and my colleagues from the Chemical Synthesis laboratories, thank you for your warm inclusion, support and good working environment. Thank you all for your willingness to perform and assist in the interpretation of the ESI-MS spectras, as well as the NMR spectras and the tips provided for their interpretation. I also thank Elisa Palma and Polatom investigator Arek, for sharing their experience for the synthesis of pyrazolyl - diamine derivatives and the PSMA inhibitor, respectively.

A special thanks goes to Dr. Paula Campello for having received me in her laboratory and for all the knowledge transmitted, as well as for the encouragement, availability and for all the practical suggestions and advices.

Last but not least, I thank my family (especially!) and my friends for the unconditional support given to me along this course. Thank you so much for your encouragement and your ability to give me the perseverance and patience needed to continue this work, even when frustration set in and giving up seemed like the easy way out.

Abstract

Prostate cancer (PCa) is the most common malignancy found in men affecting one in six and is the second leading cause of cancer-related death in men. Recently, new radioactive probes targeted at the prostate-specific membrane antigen (PSMA) have been introduced, which have revealed a high potential for PCa detection and staging based on nuclear imaging techniques, like Single-Photon Emission Computed Tomography (SPECT) or Position Emission Tomography (PET). In particular, very promising results were obtained for complexes prepared with the ^{99m}Tc and ^{68}Ga radiometals and functionalized with a PSMA inhibitor, which includes glutamic acid (Glu) and lysine (Lys) as amino acids linked by an urea bond.

The PET or SPECT probes allow the detection of PCa and its metastases through the acquisition of whole body images. However, the use of similar fluorescent probes is more favorable in intraoperative procedures for a more selective excision of tumor tissue. To this end, encouraging results have been described for PSMA inhibitors functionalized with indocyanine green (ICG) dyes. The design of PSMA-specific dual probes containing either a PET or SPECT radionuclide or a fluorophore for optical imaging may simultaneously profit from the advantages of nuclear and optical medical imaging modalities.

The main goal of this thesis was the design, synthesis and biological evaluation of bimodal probes, with PET / SPECT and Near-infrared fluorescence **(**NIRF) valences for PCa detection, starting from the base structure of ^{99m}Tc and ^{68}Ga complexes functionalized with PSMA inhibitors that have already shown clinical relevance and that should be functionalized with fluorophores of the ICG type.

In this work it was devised the synthesis of bimodal probes for PCa imaging, wherein the general structure included a PSMA inhibitor (PSMA11), a chelating agent, like (N,N′-Bis[2-hydroxy-5-(carboxyethyl)-benzyl]ethylenediamine-N,N- diacetic acid) (HBED-CC) or pyrazolyl diamine, and a derivative of the fluorophore IR820 (aromatic and aliphatic). Concerning the required organic precursors, a solid phase synthesis strategy allowed the synthesis of the Glu-urea-Lys scaffold needed for PSMA inhibition, while two synthetic approaches were tried out to obtain an aliphatic and an aromatic derivative of IR820. The synthesis of two ligands, suitable for further coupling to the fluorophore and PSMA inhibitor, was successfully achieved in this work: HBED-CC, a two-fold carboxylic acid substituted HBED, was synthesized as the chelating agent for ^{68}Ga, while for labeling with ^{99m}Tc and for SPECT imaging a pyrazolyl-diamine ligand was obtained.

Keywords:

Prostate Cancer

PSMA

Radiopharmaceuticals

Fluorescent Probes

Bimodal Probes

Resumo

O cancro da próstata (PCa) é a neoplasia maligna mais comum em homens, afetando um em cada seis, sendo a segunda principal causa de morte por cancro em homens. Recentemente, foram introduzidas novas sondas radioactivas direcionadas ao antigénio de membrana específico da próstata (PSMA), que revelaram um elevado potencial para detecção e estadiamento do PCa com base em técnicas de imagiologia nuclear, como a Tomografia por Emissão de Fotão Único (SPECT) ou a Tomografia por Emissão de Positrões (PET). Em particular, foram obtidos resultados muito promissores para complexos preparados com os radioisótopos ^{99m}Tc e ^{68}Ga e funcionalizados com um inibidor de PSMA, cuja estrutura incluí ácido glutâmico (Glu) e lisina (Lys) como aminoácidos ligados por uma ligação de ureia.

As sondas radioactivas para PET ou SPECT permitem a detecção do cancro da próstata e das suas metástases, mediante aquisição de imagens de corpo inteiro. No entanto, o uso de sondas congéneres fluorescentes, de preferência na zona do infravermelho próximo (NIR), é mais favorável em procedimentos intraoperativos que visem a excisão, o mais selectiva possível, do tecido tumoral. Para este efeito, foram descritos resultados encorajadores para inibidores do PSMA funcionalizados com fluoróforos do tipo “indocyanine green” (ICG). O desenho de sondas duais específicas para o PSMA, contendo um radionuclídeo para imagiologia PET ou SPECT ou um fluoróforo para imagiologia óptica, poderá permitir aproveitar simultaneamente as vantagens inerentes às modalidades nucleares e ópticas de imagem médica.

O principal objetivo desta tese foi a concepção, síntese e avaliação biológica de sondas bimodais (PET/SPECT e NIRF) para detecção do cancro da próstata, partindo da estrutura base de complexos de ^{99m}Tc e ^{68}Ga funcionalizados com inibidores do PSMA com relevância clínica e que deveriam ser funcionalizados com fluoróforos do tipo ICG.

Relativamente à seleção do radionuclídeo para a síntese das sondas duais, várias possibilidades estão disponíveis para diagnóstico, terapia ou teranóstica. O ^{99m}Tc é o radioisótopo mais utilizado em SPECT, enquanto o ^{68}Ga é um radioisótopo com crescente importância para PET, o que justifica seu o interesse na oncologia nuclear, principalmente na detecção do PCa. Vale a pena ressaltar que um dos complexos de ^{68}Ga direcionados ao PSMA já foi clinicamente testado em vários centros europeus de Medicina Nuclear e conduziu a resultados promissores na detecção de PCa e das suas metástases quando comparado a outras sondas PET ou outras técnicas de imagem. Relativamente à valência de imagem óptica das sondas bimodais, a mesma seria conseguida através da conjugação a um fluoróforo

NIRF, a heptametina IR820, cuja estrutura apresenta semelhanças com a ICG (único fluoróforo NIRF aprovado pela FDA para uso clínico). O IR820 é estruturalmente semelhante à ICG, mas apresenta maior estabilidade em solução devido à presença de grupos de ácido sulfónico nas duas cadeias laterais que permitem ainda uma melhor solubilidade em água e menor toxicidade através da rápida depuração *in vivo*. O aumento da estabilidade *in vitro* do IR820 traduz-se igualmente num aumento da estabilidade *in vivo*, permitindo obter imagens ao longo de um maior período de tempo. Por estes motivos, o IR820 foi selecionado como o cromóforo NIRF a ser avaliado neste trabalho na concepção das sondas bimodais.

Neste trabalho, foi estudada a síntese de sondas bimodais para imagiologia do PCa, em que a estrutura geral visava a inclusão de um inibidor do PSMA (PSMA11), um agente quelante bifuncional (HBED-CC ou pirazolilo - diamina) e um derivado do fluoróforo IR820 (aromático e alifático). Em relação aos precursores orgânicos que foram objecto de estudo, a síntese em fase sólida permitiu obter o *scaffold* Glu-ureia-Lys necessário para a inibição do PSMA, apesar de ter sido também testada, previamente, a síntese em fase líquida para obtenção do mesmo *scaffold*, sendo que a mesma não conduziu a resultados promissores uma vez que não foi possível sintetizar o análogo da lisina desejado. Duas abordagens sintéticas foram testadas para obter um derivado alifático e aromático do IR820. A funcionalização do fluoróforo - IR820 - para posterior acoplamento aos ligandos bifuncionais foi testada com recurso a dois *linkers* contendo uma função amina: 4-aminotiofenol e hexametildiamina. A síntese dos derivados do IR820 envolveu a modificação do ciclohexenil central com um cloro reactivo na posição *meso* para obtenção dos derivados do IR820. Foi efectuada com sucesso a síntese de dois ligandos bifuncionais. Sintetizou-se o (N,N′-Bis[2-hidroxi-5-(carboxietil)-benzil]etilenodiamina-N,N-ácido diacético) (HBED-CC), um derivado do HBED substituído por dois ácidos carboxílicos que actua como um ligando bifuncional eficiente para o radionuclídeo ^{68}Ga. Um complexo de Fe(III) do ligando HBED-CC foi também sintetizado neste trabalho, o qual pode ser usado diretamente para acoplamento do inibidor do PSMA ou da sonda fluorescente, sem necessidade de inclusão de grupos protectores adicionais. Espera-se que a posterior descomplexação do ferro conduza à obtenção dos produtos desejados. Tendo em vista a marcação com ^{99m}Tc e para estudos SPECT foi sintetizado um agente quelante do tipo pirazolilo-diamina. Inicialmente, foi testada a formação de um éster ativado na posição 4- do anel pirazolilo, para a síntese de um composto que ao possuir uma função éster ativado deverá reagir com os grupos amina dos fluoróforos estudados neste trabalho, sendo esperada a formação de uma ligação amida estável.

Em relação ao acoplamento entre o ligando pirazolilo-diamina e o derivado aromático do fluoróforo IR820, a síntese proposta não se mostrou eficaz. Esta falha poderá ser explicada pela menor reatividade do derivado aromático do IR820, comparativamente ao derivado

alifático. Também é importante considerar que o éster ativado testado poderá hidrolisar na presença de água residual e mesmo durante o armazenamento, de acordo com a experiência dos investigadores do Grupo de Ciências Radiofarmacêuticas (RSG) do C^2TN/IST que desenvolveram inicialmente o ligando do tipo pirazolilo-diamina.

Durante o desenvolvimento deste trabalho, foram testadas várias técnicas para caracterização e identificação estrutural dos compostos estudados, nomeadamente TLC, ESI-MS, HPLC e RMN de ^{1}H e ^{13}C. Como métodos de purificação recorreu-se a técnicas cromatográficas em coluna (SiO_2 ou Al_2O_3) e também à técnica de HPLC. Deve ter-se em consideração que foram encontradas várias dificuldades na obtenção dos produtos no seu estado puro, apesar de terem sido estudados diferentes métodos de purificação.

A necessidade de otimização das sínteses propostas, para maximização dos rendimentos e selecção dos métodos de purificação mais adequados, levou ao atraso na obtenção dos compostos previstos neste trabalho. Por estes motivos, não foi possível obter os compostos finais propostos. No entanto, foi possível obter vários dos precursores necessários para a síntese das sondas bimodais pretendidas. No futuro, e aproveitando a estratégia de síntese desenvolvida para o derivado alifático do IR820, deve-se considerar a otimização dos métodos de síntese e purificação propostos para efectivamente realizar com sucesso a síntese das sondas bimodais e avançar para a sua avaliação biológica, nomeadamente a avaliação dos complexos duais de ^{99m}Tc e ^{68}Ga em células de PCa e em modelos animais com tumor induzido. No futuro, assim que os ligandos finais e os complexos radiomarcados estejam disponíveis, será crucial realizar essa avaliação biológica para verificar qual o potencial dos complexos previstos como sondas bimodais para a imagiologia e detecção de PCa.

Palavras chave:

Cancro da próstata

PSMA

Radiofármacos

Sondas Fluorescentes

Sondas bimodais

Table of contents

Abbreviations

A

ACN: Acetonitrile

Ahx: 6-aminohexanoic acid

Alloc: allyloxycarbonyl

B

BOC: tert-butyloxycarbonyl

BFC: Bifunctional chelator

BFLs: Bifunctional ligands

BCR: Biochemical recurrence

BODIPY: Borondipyrromethane

C

C²TN: Center for Nuclear Sciences and Technologies

CT: Computed tomography

D

d: Days

DCC: Dicyclohexylcarbodiimide

DCM: Dichloromethane

DIPEA: N,N-Diisopropylethylamine

DMF: Dimethylformamide

DOTA: (1,4,7,10-tetraazacyclododecane-1,4,7,10-tetraacetic acid)

E

EC: Electronic Capture

EDC: Ethyl(dimethylaminopropyl) carbodiimide

EDDA: N,N' ethylenediamine diacetic acid

ESI-MS: Electrospray ionization - Mass Spectrometry

EtOAc: Ethyl acetate

Et_3N: Triethylamine

EtOH: Ethanol

F

Fmoc: Fluorenylmethyloxycarbonyl

FOLH1: Folate hydrolase

FDA: Foods and Drugs Administration

G

Glu: Glutamic acid or glutamate

GCPII: Glutamate carboxypeptidase II

H

h: Hours

HBED-CC: (N,N′-Bis[2-hydroxy-5-(carboxyethyl)-benzyl]ethylenediamine-N,N- diacetic acid)

HCl: hydrogen chloride or hydrochloride

HBTU: Hexafluorophosphate benzotriazole tetramethyl uronium

HPLC: High performance liquid chromatography

I

ICG: Indocyanine green

IT: Isomeric transition

L

Lys: Lysine

LET: Linear energy transfer

M

mCRPC: Metastatic castration-resistant prostate cancer

MeOH: Methanol

MRI: Magnetic resonance imaging

Min: Minutes

N

NAAG: *N*-acetyl aspartyl glutamate

NIRF: Near-infrared

NIRF: Near-infrared fluorescence

NHS: N-Hydroxysuccinimide

NM: Nuclear medicine

NMR: Nuclear Magnetic Resonance

P

PCa: Prostate cancer

PET: Position Emission Tomography

PMB: *p*-methoxybenzyl

PSA: Prostate-specific antigen

PSMA: Prostate-specific membrane antigen

R

RN: Radionuclide

rt: Retention time

RT: Room temperature

RSG: Radiopharmaceutical Sciences Group

S

SAAC: Single-amino-acid chelator

SPECT: Single-Photon Emission Computed Tomography

T

TEA: Triethylamine

TFA: Trifluoroacetic acid

TFP: Tetrafluorophenol

THF: Tetrahydrofuran

TLC: Thin-layer chromatography

TMS: Trimethylsilane

TsOH: p-Toluenesulfonic acid

U

US: Ultrasound

List of Tables

List of Figures

List of Schemes

1. Introduction

1. Introduction

1.1. PCa incidence, diagnosis and therapy

PCa is the most common malignancy found in men [1-2], affecting one in six [3] and is the second leading cause of cancer-related death in men[1],[4]. According to a study published in 2018 about the overall cancer incidence and mortality patterns in Europe, PCa was the fourth most common cancer (450,000 cases), being only surpassed by female breast (523,000 cases), colorectal (500,000 cases) and lung (470,000 cases) cancers[5].The occurrence of metastases is one of the major causes of morbidity and mortality in PCa patients[6] The early detection of these metastatic or recurrent lesions is of high clinical relevance for staging, prognosis, and therapy management[6-7].

Due to the high incidence of PCa and the resistance to androgen therapy and chemotherapy of the advanced disease, extensive research is focused on the development of many types of technologies both for the high resolution visualization/detection of PCa lesions and for cost effective and selective therapies[8].

PCa is a complex and biologically heterogeneous disease and cannot be fully assessed with conventional imaging alone[1]. In the radiology arena, a variety of imaging technologies, including ultrasound (US), computed tomography (CT), and magnetic resonance imaging (MRI) are widely used, where imaging obtained by primary external energy sources is utilized for detection and evaluation of structural/anatomical abnormalities[8]. However, these techniques also show the limitations of current cancer imaging and cannot reliably delineate the occurrence, the location, and the biochemical status of PCa cancer and its metastases[9].

Several nuclear medicine (NM) procedures have also been developed in the past for imaging PCa. The advantage of the NM procedures is that these methods assess, noninvasively, the functional and not just anatomical abnormalities as is evaluated in conventional imaging methods, allowing the monitorization of the metabolic and molecular characteristics of cancer cells[8]. The NM imaging approaches utilize short-lived nuclear tracers and acquire signals emanating from the body after administration of imaging agents that target cancer-specific alterations, including glucose, amino acid and fatty acid metabolism, receptor status, cellular proliferation, tumor hypoxia and blood flow[9]. So far, several radiopharmaceuticals have been used either for diagnosis or therapy of PCa cancer[10], as shown in table 1.1.

Table 1.1. Radiopharmaceuticals in use or tested for diagnosis and therapy of PCa.

Tracer	**Principle**	**Application**
^{18}F-FDG	Glucose metabolism	Diagnosis, PET
^{11}C-acetate	Fatty acid *de novo* synthesis	Diagnosis, PET
^{11}C-choline ^{18}F-choline ^{18}F-methylcholine ^{18}F-ethylcholine	Phospholipid biosynthesis	Diagnosis, PET
^{18}F-FACBC	Amino acid transport; synthetic leucine analogue	Diagnosis, PET
^{111}In-J591	PSMA ligand; antibody	Diagnosis, SPECT
^{64}Cu-J591	PSMA ligand; antibody	Diagnosis, PET
^{89}Zr-J591	PSMA ligand; antibody	Diagnosis, PET
^{99m}Tc-MIP-1404	PSMA ligand; small-molecule inhibitor	Diagnosis, SPECT
^{123}I-MIP-1072 ^{123}I-MIP-1095	PSMA ligand; small-molecule inhibitor	Diagnosis, SPECT
^{18}F-DCFBC	PSMA ligand; small-molecule inhibitor	Diagnosis, PET
^{68}Ga-PSMA-HBED-CC (PSMA-11)	PSMA ligand; small-molecule inhibitor	Diagnosis, PET
^{90}Y-J591	PSMA ligand; antibody	Therapy
^{177}Lu-J591	PSMA ligand; antibody	Therapy
^{131}I-MIP-1466	PSMA ligand; small-molecule inhibitor	Therapy
^{177}Lu-PSMA-617	PSMA ligand; small-molecule inhibitor	Therapy

Nuclear molecular imaging with SPECT and PET is poised to fill the need of the noninvasive detection of the multiple molecular and cellular processes that are active in PCa patients[1]. Furthermore, the hybrid imaging techniques, such as SPECT/CT and PET/CT, combine functional and morphological information leading to high diagnostic accuracy[1], as they combine the innate advantages of the fused imaging technologies in a synergetic way as the CT modality provide anatomical details and also attenuation correction to the functional data from nuclear molecular imaging modalities[11-12].Nowadays, both hybrid imaging techniques are used in the clinical routine, not only as the primary staging tool in PCa cancer, but also in patients with suspected disease recurrence[1]. Also, these imaging techniques are useful for restaging patients with PCa before and after RN therapy, as shown in figure 1.1. [adapted from [13-14]].

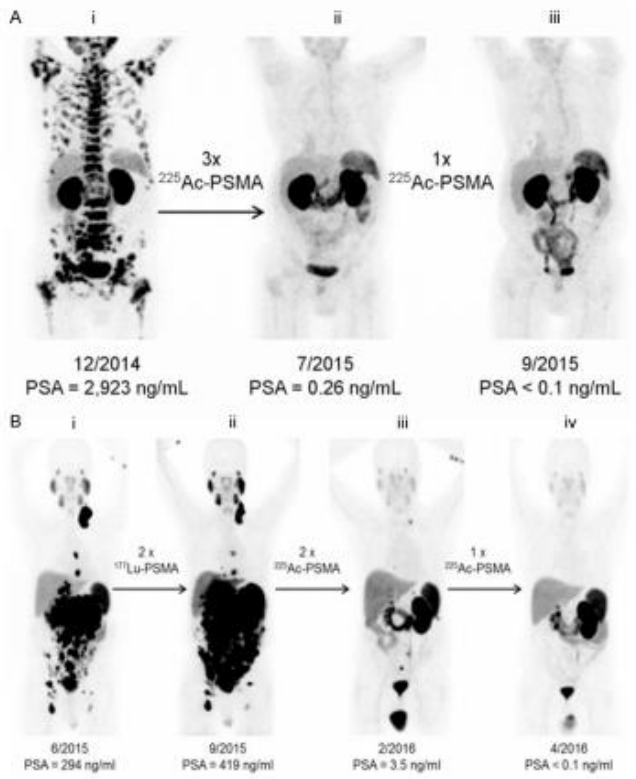

Figure 1.1. (A) ^{68}Ga-PSMA-11 PET/CT scans of a PCa patient. Pretherapeutic tumor spread (i), restaging 2 months after third cycle of ^{225}Ac-PSMA-617 (ii), and restaging 2 months after one additional consolidation therapy (iii). (B) ^{68}Ga-PSMA-11 PET/CT scans of another PCa patient. In comparison to initial tumor spread (i), restaging after 2 cycles of β-emitting ^{177}Lu-PSMA-617 presented progression (ii). In contrast, restaging after second (iii) and third (iv) cycles of ^{225}Ac-PSMA-617 therapy presented impressive response.

Over the past decade, optical imaging has also emerged as a real-time, sensitive, high resolution and noninvasive modality for visualization, localization, and measurement of bioactive molecules *in vivo*[15]. The optical signals can provide molecular information of biological tissues and are related to the tumor anatomical structure as well as the tumor metabolism and biochemistry[16]. NIRF imaging is an attractive novel modality for cancer detection and acquisition of real-time pathophysiological information[17]. It was demonstrated to be a feasible and practicable method for PCa detection in addition to the predominant modalities for clinical detection and diagnosis of this pathology[17].

There are several therapeutic options for PCa which include surgery, chemotherapy, cryotherapy, brachytherapy with radioactive seeds, and the use of external radiation which is now being highly promoted with the use of proton therapy machines using conformal targeting technologies[8].

It is described that approximately 30%–40% of patients will fail primary treatment, and a rising prostate-specific antigen (PSA) level will herald the onset of biochemical recurrence (BCR) [2]. After potential salvage procedures (radiation and surgery), patients usually undergo androgen deprivation therapy[2]. This treatment is typically followed by an increase in the prostate-specific antigen (PSA) level after 2–8 y; this increase indicates the onset of metastatic castration-resistant PC (mCRPC)—the lethal form of the disease[2]. Reactivation of androgen receptor signaling occurs in early mCRPC; therefore, second-line agents targeting the androgen receptor signaling axis have extended survival in clinical trials[2]. Treatment with other systemic agents, including taxane-based chemotherapy (e.g., docetaxel), the immunotherapeutic agent sipuleucel-T and the bone-seeking α-emitter $^{223}RaCl_2$, has been shown to improve overall survival and quality of life[2]. Nevertheless, patients with mCRPC have a poor prognosis and a median survival of 19 months[2].

However, there is lack of effective imaging methods for early diagnosis, localization and identification of metastases, choice of postoperative treatment and prevention of postoperative recurrence[18]. Accurate staging in primary PCa and early assessment of BCR for tailoring initial and subsequent treatment strategies are unmet clinical needs[2]. Once mCRPC is diagnosed, effective therapy for improving overall survival and quality of life is desperately needed[2]. PSMA ligands are currently being investigated intensively, as they hold promise for extending the frontier in PCa imaging and RN therapy[2]. Therefore, thanks to certain recent developments in radiopharmaceutical chemistry, the role of NM for the diagnosis as well as therapy of PCa is expected to significantly grow in the future[8].

1.2. PSMA and its targeting

Among the markers of PCa, PSMA is the most well-established[15],[19]. PSMA corresponds to a highly specific prostate epithelia cell membrane antigen[20] and, recently, has emerged as one of the most extensively investigated and exploited targets for molecular imaging and RN therapy of PCa[21]. PSMA represents a highly valuable molecular marker in PCa, for both diagnostic and therapeutic application, due to the following reasons: i) strong upregulation in poorly differentiated, metastatic, and hormone-refractory PCa; ii) low basal expression in nonprostatic tissues; iii) direct correlation between PSMA expression levels and androgen independence, metastasis, and PCa progression[21].

PSMA is a type II transmembrane glycoprotein that contains 750 amino acids and has a molecular weight of 100 kDa[1-3],[10],[18],[22]. It has a unique structure containing three distinct parts; a 707-amino acid extracellular region, a cell membrane part of 24 amino acids and a cytoplasmic tail which contains 19 amino acids[1],[8].PSMA is a key player in prostate carcinogenesis and disease progression, glutamatergic neurotransmission and folate absorption[1] (see figure 1.2.). These various functions and the tissue distribution of the protein result in different designations[1]. The name which is also frequently used for this enzyme is glutamate carboxypeptidase II, or GCPII[1],[3],[8],[14],[22-23]. Furthermore, in central nervous system, it metabolizes the brain neurotransmitter *N*-acetyl aspartyl glutamate (NAAG), and is named NAALADase[1],[8],[14]. In the proximal small intestine, it removes γ-linked glutamates from poly-g-glutamated folate, which is reflected in its name, folate hydrolase FOLH1[1],[18].

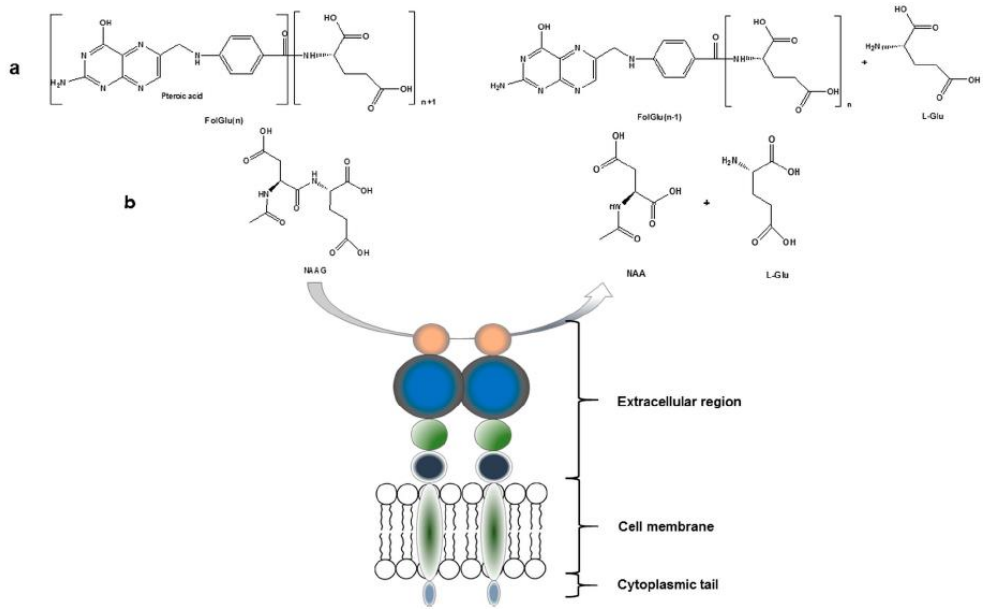

Figure 1.2. Enzymatic actions of PSMA. (a) Glu is released from folate polyglutamate resulting in the release of folic acid; (B) NAAG is hydrolyzed to aspartate (NAA) and L-Glu. Adapted from[1].

PSMA expression and localization in the normal human prostate are associated with the cytoplasm and apical side of the epithelium surrounding the prostatic ducts[2]. PSMA is enzymatically active only in its dimeric form[2]. Its function for prostate cells is still unknown[2] but it has been described that PSMA undergoes constitutive receptor-mediated endocytosis via clathrin-coated pits[1],[3],[6],[14]. Dysplastic and neoplastic transformation of prostate tissue results in the transfer of PSMA from the apical membrane to the luminal surface of the ducts[2].

PSMA possesses the criteria of a promising target for PCa, i.e., abundant and restricted (to prostate) expression at all stages of the disease, presentation at the cell surface but not shed into the circulation as it is not secreted and is membrane bound, and association with enzymatic or signaling activity[23].

It is described that PSMA is significantly over expressed (100–1000 fold) on nearly all PCa cells[2], compared to the physiologic levels found in other tissues such as , small intestine, or brain[24] and its expression is further increased in advanced stages and in mCRPC[2]. Also, after binding to the active center of the extracellular domain, PSMA ligands are internalized and subsequent endosomal recycling leads to enhanced tumor uptake, retention, and subsequent high image quality for diagnostic procedures and a high local dose for therapeutic applications[2].

Available tools for PSMA targeting include monoclonal antibodies and a variety of small molecule or peptide ligands, each of which has advantages and limitations associated with its use[3].

Antibody-based probes, like the FDA-approved imaging agent for targeting PSMA in PCa – ProstaScint - are attractive because of the high level of specificity for the target and the picomolar range affinities that can often be achieved[3]. The major disadvantages of antibodies are the slow target binding and background clearance in an appropriate time frame for diagnostic imaging, reduced utility for image-guided surgical approaches and their potentially immunogenic behavior [20]. In contrast, small molecule probes can often be generated with nanomolar affinity ranges and rapid clearance rates that not only facilitate tissue penetration but also minimize potential toxicity resulting from exposure times[3].

In the search for PSMA targeting agents with more favorable characteristics compared to antibody molecules[25], the development of highly PSMA-specific small peptides referred to as PSMA ligands or PSMA inhibitors was pursued. PSMA inhibitors bind to the active center located in the extracellular domain and are subsequently internalized[2]. The recognition of the structural and functional homology between NAAG peptidase I and PSMA supported the

development of these small molecules[2], which is based on modifications of NAALADase inhibitors and on the known crystal structure of PSMA, as discussed below.

The PSMA internal inhibitor–binding cavity can be roughly divided into 3 continuous parts: the S19 Glu recognition pocket (S1'), the dinuclear zinc(II) active site, and an irregularly shaped entrance funnel connecting the active site to the external surface of PSMA (see figure 1.3.)[26]. Crystal structure investigations also indicated that, besides the electrostatic interactions of urea and carboxylic groups at the active Zn(II)-containing center of PSMA, there are lipophilic interactions resulting from a hydrophobic pocket (S1) located next to the active site[24].

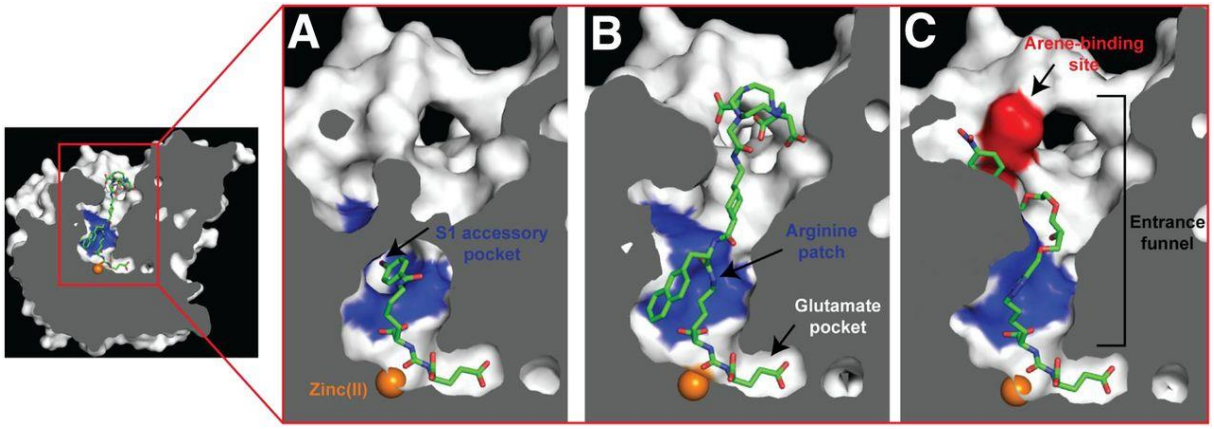

Figure 1.3. Representation of a cross-section of PSMA. The internal inhibitor-binding cavity presents a S1' Glu recognition pocket, dinuclear zinc(II) active site and irregularly shaped entrance funnel, where an arginine patch, a S1 accessory hydrophobic pocket and an arene-biding site are significant structural features for inhibitor design. Zinc ions are shown as orange spheres and some PSMA ligands are shown as stick representations: DCIBzL (A) (PDB code 3D7H), PSMA-617 (B) (unpublished data) and ARM-P4 (C) (PDB code 2XEG). Adapted from[26].

Taking into consideration the PSMA structure, the design of small-molecule PSMA ligands includes, as common features, the presence of pentanedioic acid groups as glutamate mimics and a zinc-binding group to interact with the catalytic zinc atom at the PSMA active site[27]. Since 2-PMPA (see figure 1.4.) was firstly reported as a potent PSMA inhibitor in 1996, many efforts have been devoted to generate other molecules with inhibitory action towards PSMA[1]. The main strategy for the discovery of those inhibitors is to find zinc-binding groups to be linked to a glutamate moiety (or its mimics)[1]. Different functionalities with affinity for zinc, including phosphonates, phosphates, phosphoramidates, thiols and ureas, were identified and evaluated[1], as exemplified in figure 1.4. In the field of radiopharmaceutical development, a great number of urea-based PSMA inhibitors have been synthesized and modified accordingly in order to be labeled with a variety of RNs[1], as discussed in the next section.

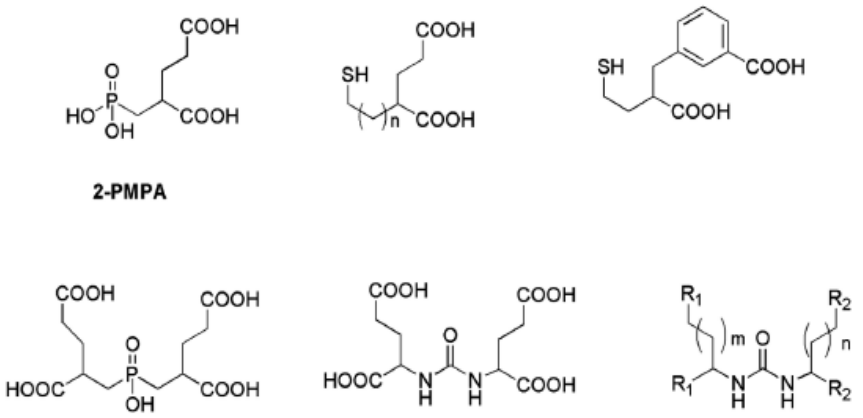

Figure 1.4. Some examples of small molecules for PSMA targeting.

1.3. Radioligands for PSMA targeting

Low molecular-weight peptidomimetic Glu-ureido–based PSMA inhibitors are the most studied class of targeting molecules in the design of radioligands suitable for PCa imaging by nuclear techniques or for RN therapy[1],[26]. The designed and evaluated radioligands usually consist of 3 components: i) the binding motif (e.g. Glu-urea-Lys, the most widely used scaffold); ii) a linker; iii) a radiolabel-bearing moiety, comprising a chelator molecule for labeling with radiometals or a prosthetic group for labeling with radiohalogens[2] (see figure 1.5).

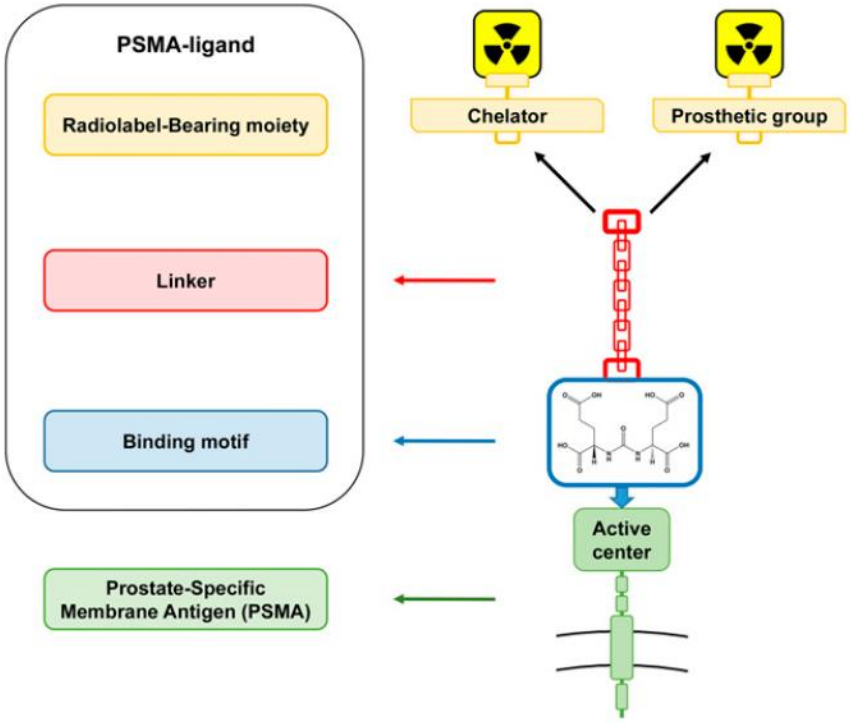

Figure 1.5. General structure of a Urea-based PSMA radioligand. Adapted from[2].

Regarding the selection of the RN, several possibilities are available either for diagnosis, therapy or theranostic. Theranostic is a new and emerging approach that provides a transition from conventional medicine to personalized and precision medicine, as it combines diagnostic and therapeutic applications in a single agent (or related ones), allowing targeted diagnosis, drug delivery and treatment response monitoring[28]. For imaging purposes, besides a relatively physical short half-life, the isotope must be a pure gamma emitter or positron emitter, i.e. have no particle emission such as alpha and beta particles (these particles increase the radiation dose to the patient while not providing any diagnostic information)[29]. However, for therapy purposes a suitable range of the physical half-life for therapeutic RNs is between 6 h and 7 days[30], because a very short physical half-life limits the delivery flexibility and is very impractical, while a long half-life will retain the radiation dose in the patients and expose surrounding tissues[30]. α- and β- emitters are preferable for therapy purposes, as α and β particles present high-linear energy transfer (LET) that leads to its fully deposition within a small range of tissue (usually in mm) not allowing the radiation to penetrate through the patient's body[30]. However, some β-emitting RNs also decay with γ-radiation, which can be advantageous if the energy and intensity are within the diagnostic range, as it also allows the visualization of the radiopharmaceutical distribution within the patient's body using gamma scintigraphy methods[30]. The physical characteristics of some relevant medical RNs[30-37] are shown in table 1.2.

Table 1.2. Physical characteristics of some medical RNs for imaging and therapy.

RN	**Use**	**Half-life**	**Main types of decay**	**E_{max} (MeV)**
^{99m}Tc	SPECT imaging	6 h	IT	0.141
^{123}I	SPECT imaging	13.2 h	EC	0.16
^{111}In	SPECT imaging	67.9 h	EC	0.17/0.25
^{201}Tl	SPECT imaging	73.1 h	EC	0.17
^{67}Ga	SPECT imaging	78.3 h	EC	0.09/0.19/0.30
^{11}C	PET imaging	20.3 min	β^+	0.97
^{13}N	PET imaging	9.97 min	β^+	1.20

^{15}O	PET imaging	2.03 min	β^+	1.74
^{18}F	PET imaging	110 min	β^+	0.64
^{64}Cu	PET imaging and therapy	12.7 h	β^+ (17.5%) EC (43.5%) β^- (38.5%)	0.653 1.675 0.579
^{68}Ga	PET imaging	68.1 min	β^+ (87.7%) EC (8.9%) γ (3.2%)	1.899 2.921 1.077
^{124}I	PET imaging	4.18 d	β^+ (25.6%) EC (74.4%)	1.532/2.135 0.603/1.691
^{131}I	Therapy	8 d	β^- (89.9%) γ (7.27%)	0.606 0.364
^{177}Lu	Therapy	6.7 d	β^- (79.3%) γ (11.6%)	0.498 0.177
^{225}Ac	Therapy	10 d	α	5.7

Some medical RNs are easily obtained *in situ* through elution of a RN generator, being readily available for the preparation of radiopharmaceuticals. For example, ^{99m}Tc is obtained daily in NM centers from commercially available $^{99}Mo/^{99m}Tc$ generators (see table 1.3. and figure 1.6.)[29],[31],[38]. ^{99m}Tc still is the most important RN used in conventional NM. The parent ^{99}Mo, which has a longer half-life (67 hours), continually produces ^{99m}Tc that presents a short half-life (6 hours) suitable for SPECT imaging[29],[31],[37-38].

^{68}Ga is a positron emitter that can be also obtained, *in situ*, by elution of a $^{68}Ge/^{68}Ga$ generator (see table 1.3. and figure 1.6.)[29],[31],[39],[40-41]. ^{68}Ga presents a physical half-life of 68 min[29],[40-41], suitable for many PET exams and, for this reason, is assuming a growing importance in diagnostic imaging studies and in theranostic applications when combined with a therapeutic radiometal (e.g. ^{177}Lu)[1],[8],[41].

Table 1.3. Characteristics of $^{68}Ge/^{68}Ga$ and $^{99}Mo/^{99m}Tc$ generators.

Parent	Decay mode/ Half-life	Daughter	Time of maximal ingrowth (equilibrium)	Decay mode/ Half -life	Decay product
^{68}Ge	EC 271 d	^{68}Ga	≈ 6.5 h (S)	β^+, EC 68 min	^{68}Zn
^{99}Mo	β^- 67 h	^{99m}Tc	≈ 24 h (T)	IT 6 h	^{99}Tc

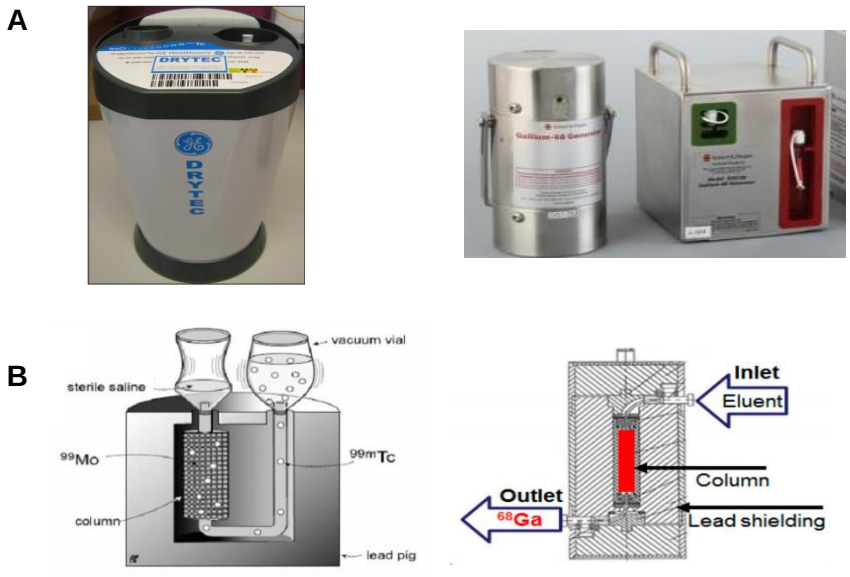

Figure 1.6. (A) Examples of commercially available $^{99}Mo/^{99m}Tc$ and $^{68}Ge/^{68}Ga$ generators, respectively. (B) Schematic presentation of the cross section of both column-based generators. Adapted from [39], [41].

A variety of urea-based PSMA inhibitors have been labeled with different medical RNs, bearing in most cases the Glu-urea-Lys as scaffold[8],[10],[26],[42]. The resulting radioligands can be synthesized in a simple and standardized fashion and, in some cases, have already entered clinical settings and are being used either for SPECT or PET imaging and/or therapy purposes[26]. Some examples of clinically relevant urea-based PSMA radioligands are listed in table 1.4.

Table 1.4. Glu-ureido-based PSMA radioligands of clinical relevance.

Cpd.	Chemical Structure	Class	RN	Ref.
MIP-1095	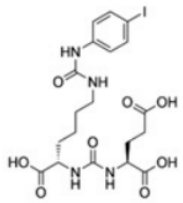	Theranostic	^{123}I ^{124}I ^{131}I	(25-26),(43-44)
DCFBC	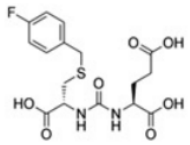	Diagnostic PET	^{18}F	(25-26),(45)
DCFPyL	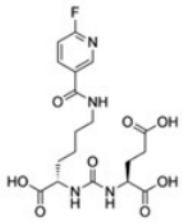	Diagnostic PET	^{18}F	(25-26),(46-47)
MIP-1404 Trofolastat	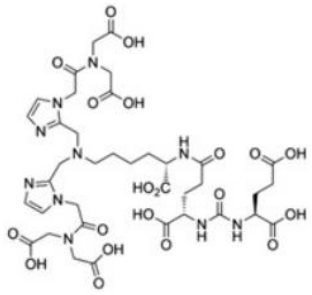	Diagnostic SPECT	^{99m}Tc	(22),(25-26)
PSMA I&T	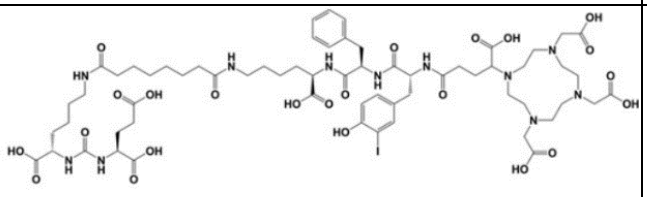	Theranostic	^{68}Ga; ^{177}Lu; ^{111}In	(26),(48-49)

PSMA-617	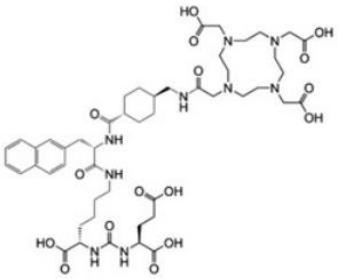	Theranostic	^{68}Ga; ^{177}Lu; ^{64}Cu ^{225}Ac	(13),(26), (50-51)
PSMA-11	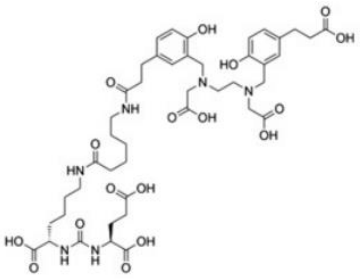	Diagnostic PET	^{68}Ga	(24-26)
PSMA-1007	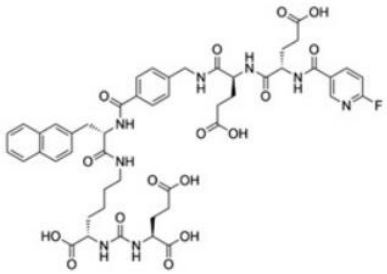	Diagnostic PET	^{18}F	(26)(52)
PSMA I&S	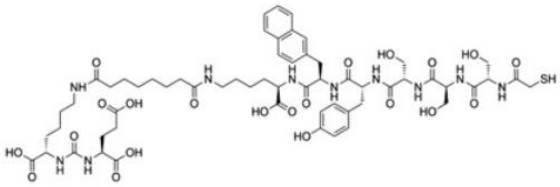	Diagnostic SPECT	^{99m}Tc	(21)(26)

Cpd. = compound; Ref. = reference

Concerning the chelator choice and modifications, Eder *et al.* compared the pharmacokinetics and targeting characteristics of the same Glu-urea-Lys binding motif coupled to either the acyclic HBED-CC chelator or the macrocyclic DOTA (1,4,7,10-tetraazacyclododecane-1,4,7,10-tetraacetic acid) chelator[24]. HBED-CC shows fast ^{68}Ga-complexation kinetics and affords complexes with high *in vitro* and *in vivo* stability[7],[24],[53-55]. DOTA is a chelator that is suitable for the labeling of biomolecules with a variety of trivalent radiometals, which includes ^{68}Ga and its therapeutic counterpart ^{177}Lu[55]. This study showed that the ^{68}Ga-radioconjugate obtained using HBED-CC as the bifunctional chelator (BFC) exhibited reduced non-specific accumulation and higher specific internalization in PSMA-expressing LNCaP cells, when compared with the DOTA congener[24]. These results might be due to the lipophilicity of the HBED-CC moiety, since the active binding site of PSMA consists of two motifs, one interacting

with urea-based ligands and one representing a lipophilic pocket[7],[24]. This idea is supported by the suggestion that the binding site has a pocket that interacts with hydrophobic aromatic groups[7],[24].

Worldwide, ^{68}Ga-PSMA-11 ([^{68}Ga]Glu-urea-Lys(Ahx)-HBED-CC) (see table 1.4.) is currently the most prominent radioligand for the PET imaging of PSMA-positive PCa. ^{68}Ga-PSMA-11 was clinically introduced several years ago and is commonly used for diagnostic imaging of PCa in the clinics, especially in Europe[26]. This PSMA inhibitor exhibits the Glu- NH-CO-NH-Lys pharmacophore and HBED-CC as an efficient ^{68}Ga chelator. The success of ^{68}Ga-PSMA-11 reflects the favorable physical properties of ^{68}Ga, as mentioned above, which allow high-resolution PET images with the option of accurate quantification.

Because ^{99m}Tc is the preferred RN for developing SPECT radiopharmaceuticals, efforts have been made to obtain ^{99m}Tc-labelled PSMA inhibitors suitable for PCa imaging[25]. The more encouraging results were obtained for a Glu-urea-Glu pharmacophore, MIP-1404 (see table 1.4.), functionalized with a single-amino-acid chelator (SAAC) containing imidazolyl rings as coordinating units[56]. The resulting conjugate is labeled with ^{99m}Tc based on the so-called tricarbonyl chemistry[22],[25]. The SAACs allows facile labeling with ^{99m}Tc, forms a robust ^{99m}Tc(I) tricarbonyl complex, and was designed to minimize hepatobiliary uptake[25],[56]. Preclinical studies showed that ^{99m}Tc-MIP-1404 has high tumor uptake and high tumor-to-blood ratios in PCa-tumor bearing mice, early after injection of ^{99m}Tc-MIP-1404, leading to SPECT images with excellent tumor-to-background contrast[25]. These favorable features revealed that this PSMA ligand is feasible for ^{99m}Tc-SPECT/CT detection of PCa lesions[25]. It is expected that ^{99m}Tc-MIP-1404 (Trofolastat) will be launched on the market as the first low-molecular-weight SPECT PSMA radioligand, as a phase 3 clinical trial with this tracer is already under way[44],[57]. Besides this promising SPECT PSMA radioligands, also an ^{99m}Tc urea-based PSMA radioligand for imaging and surgery - PSMA I&S (see table 1.4.) - is also in clinical development[21].

1.4. NIRF Probes for PSMA-targeting

Cancer near infrared (NIR) molecular imaging relies greatly on the development of stable, highly specific and sensitive fluorescent probes[16]. In particular, it has been dedicated immense attention to NIRF imaging with probes emitting within the wavelength range of 700-1000 nm, owing to its low absorption and autofluorescence from organisms and tissues in this NIR spectral range[16]. This can minimize background interference, improve tissue depth penetration, and enhance image sensitivity[16]. For these reasons, an ideal NIR probe must

function in the NIR spectral range, with large Stokes shift for minimum interference between absorption and emission spectra[16]. Moreover, it must display high molar absorption coefficient and quantum yield for intense fluorescence, sufficient chemical and photostability in solvents, buffers or biological conditions for imaging or detection, and good water solubility to avoid dye aggregation in aqueous environment[16]. Additionally, a promising NIR probe should have suitable chemical functionalities for bioconjugation with specific ligands for targeting purpose[16], to obtain minimal background and enhanced sensitivity[58].

Current NIR probes generally comprise two categories: inorganic and organic molecules. The organic probes present more favorable features than the inorganic ones, which show some disadvantages, such as potential cytotoxicity of their heavy metals, small-scale and expensive preparation[16]. So, NIR organic dyes have attracted increasing attention in biomedical applications as they show improved photophysical properties and easy availability by large-scale chemical synthesis, leading to promising clinical implications for optical imaging[16]. In the past few years, several classes of NIR organic dyes were developed and evaluated: cyanine dyes, squaraines, phthalocyanines, porphyrin derivatives and BODIPY (borondipyrromethene) analogues (see figure 1.7.).

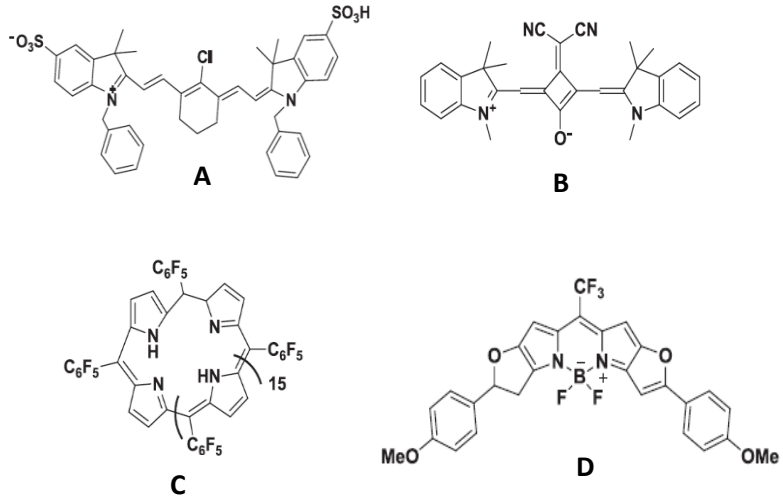

Figure 1.7. Some examples of newly developed NIR fluorescent dyes. (A) Cyanine dyes: small organic molecules with two aromatic nitrogen-containing heterocycles with a delocalized charge linked by a polymethine bridge. (B) Squaraines derivatives: consist of an oxocyclobutenolate core with aromatic or heterocyclic components at both ends of the molecules. (C) Phthalocyanines: two-dimensional 18π-electron aromatic porphyrin derivatives, consisting of four bridged pyrrole subunits linked together through nitrogen atoms. (D) BODIPY dyes: have a general structure of 4,40-difluoro- 4-bora-3a, 4a-diaza-s-indacene. Adapted from[16].

One of the most prominent classes of NIR probes corresponds to cyanine dyes (also called as polymethine cyanine dyes) (see figures 1.7. and 1.8.). The monomethine and trimethine cyanines (Cy3) generally show absorption in the visible region, but the extension of the chromophore by one vinylene moiety causes a bathochromic shift of about 100 nm[16]. Thus, pentamethine (Cy5) derivatives can reach a near-infrared region (>700 nm), and heptamethine cyanines (Cy7) may show absorption beyond 1000 nm[16]. Some cyanine dyes (such as Cy5, Cy5.5, Cy7 and their derivatives) are among the most common NIR fluorescent dyes with high molar absorption coefficient and fluorescence quantum yield[16].

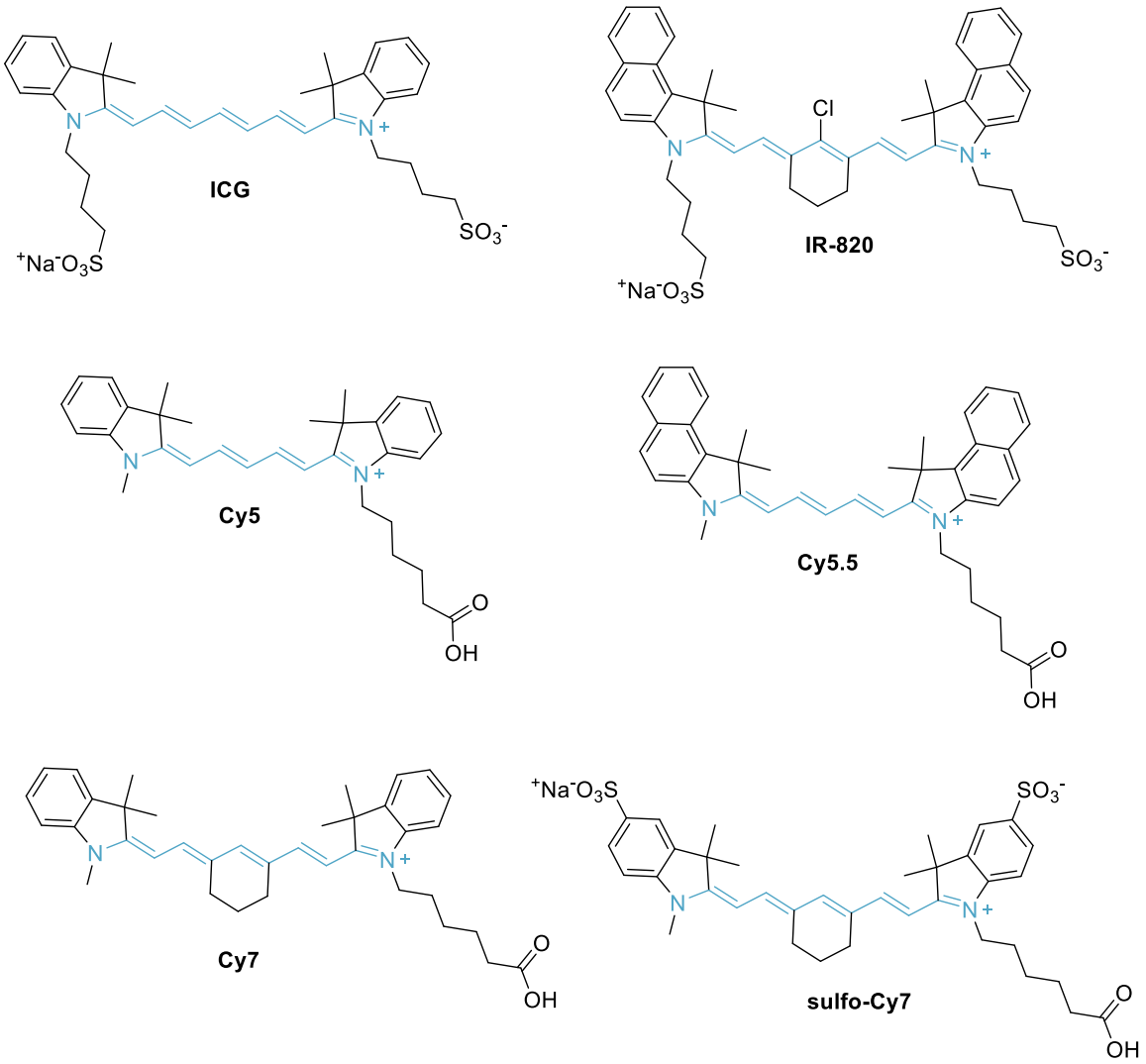

Figure 1.8. Chemical structure of some cyanine dyes: first digit identifies the number of carbon atoms between the indolenine groups and the suffix .5 is added for benzo-fused cyanines.

However, many cyanine dyes suffer from poor photostability, low quantum yield, high plasma protein binding rate, undesired aggregation and mild fluorescence in aqueous solution[16]. To overcome these limitations several modifications have been studied, such as:

a) introduction of a rigid cyclohexenyl substitution in the middle of polymethine linker to increase the photostability and fluorescence quantum yield[16];

b) introduction of electron-donating groups on N-position of 3H-indolenine and substitution of the central chlorine atom at the cyclohexene ring by electron-donor groups to improve the photochemical stability[16],[59];

c) introduction of carboxylic or sulfonic acid groups to increase Stokes shift, fluorescence quantum yield and water solubility[16],[60].

Cyanine dyes have gained much attention in biomedical applications because of their optimal spectral, chemical, and biological properties[61]. Moreover, it is worthwhile to mention the excellent safety profile of ICG dye, which has been approved by the FDA almost for over 50 years for ophthalmic angiography and to determine cardiac output and liver blood flow and function[9].

Besides ICG, other heptamethine indocyanine dyes have emerged as potential tools for in vivo tumor diagnostic and therapeutic applications[16], due to their excellent photophysical properties and ease of synthetic modifications[61]. ICG can accumulate in normal tissues and emit fluorescence signals with high intensity during some surgical procedures, largely compromising the potential use of ICG for tumor visualization as it lacks tumor-targeting capability, similarly to other conventional NIRF polymethine cyanine organic dyes[60].

As clinically approved NIR dyes (ICG and methylene blue) are contrast agents with no tumor specificity, efforts have been made to develop agents that are designed to recognize biochemical features of the tumor cells in a specific manner, leading to effective targeting of tumor cells[3]. Particularly promising results have been obtained in the targeting of PSMA, which is overexpressed in primary and metastatic PCa as mentioned above[3]. This comprised NIRF probes carrying a variety of cancer specific ligands (such as humanized anti-PSMA antibodies, peptide ligands or small-molecule PSMA inhibitors)[3],[16],[62]. These target specific NIRF probes (see table 1.5.) are expected to increase the signal-to-background ratios, presenting clinical utility for image-guided surgery and tumor resections[3],[16], as they allow a precise discrimination between tumor and healthy tissue leading to a better outcome of PCa patients.

Table 1.5. Some NIR fluorophore-labeled PSMA targeting probes.

NIR dyes	PSMA ligands	Chemical Structure	Ref.
Cy5.5	CTT-54.2	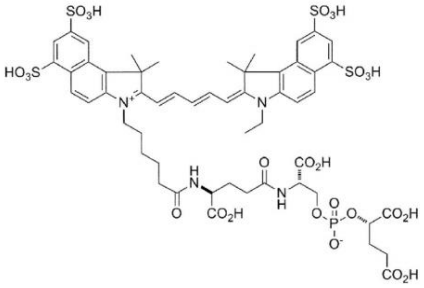	(63)
IRDye800CW	YC-27	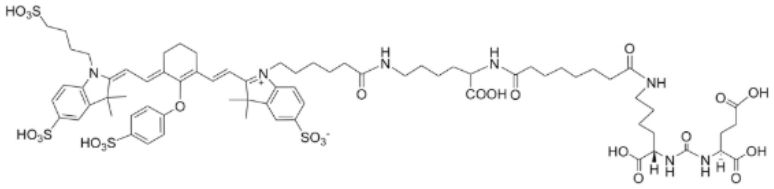	(3),(64)
IRDye800CW	PSMA-1	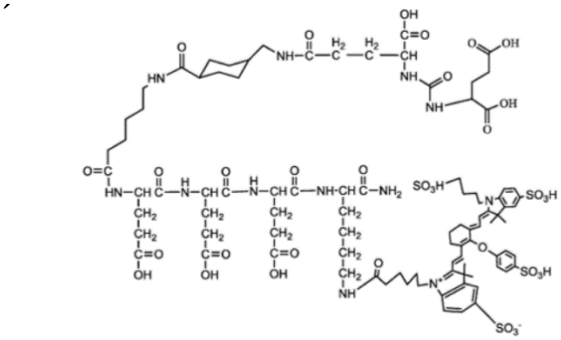	(15)
Cy5.5	PSMA-1	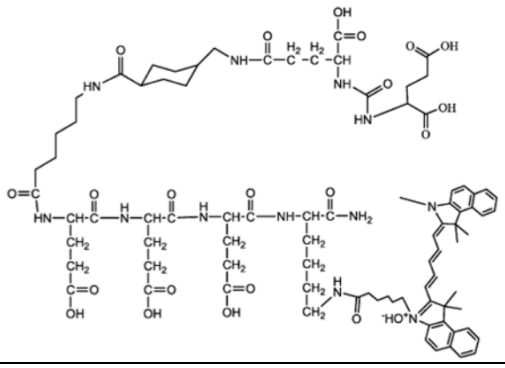	(15)
ICG	PSMA-MB	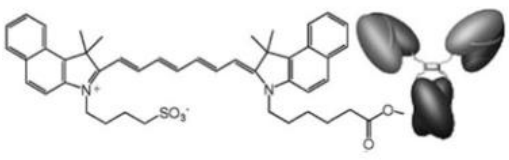	(65)

1.5. NIRF and Nuclear imaging dual probes for PSMA targeting

Intense efforts have been directed toward the development of dual PSMA-targeted probes for a variety of clinical applications ranging from diagnostic imaging using SPECT, PET, MRI, or optical methods toward innovative theranostic and therapeutic concepts[21].

Dual modality agents are expected to fulfill the unmet needs for specific imaging of PCa, which to some extent is inadequately assessed by conventional methods[9]. Several dual modality imaging agents are being developed to take advantage of the sensitivity of nuclear imaging, such as SPECT or PET, and the high sensitivity and resolution of NIRF for possible use in pre- and intraoperative applications, respectively[3],[66].

Nuclear imaging is an attractive modality for the detection and characterization of disease because it is non-invasive, quantitative, provides dynamic real-time data, and allows the diagnosis and follow-up of patients undergoing therapy[9]. In fact, for staging and preoperative assessment of tumor burden the RN component could initially be used to map disseminated lesions or lesions within the prostate at sub-centimeter resolution[66].

Optical imaging modalities could aid in image-guided surgery to more accurate real-time delineation of tumor margins precisely during and following resection, using a minimally invasive laparoscopic instrument equipped with a NIRF detection system (see figure 1.9.)[66],[67].

The NIRF approach shares common features with nuclear imaging techniques, such as the potential use of tracer administration of the probe, which enables the development of combinational use of both techniques for cancer imaging[9]. NIRF alone has inherent shortcomings such as its sensitivity and resolution being severely influenced by position and depth of the imaging probes in the body[9]. The positron- or gamma-emitting properties of the dual probe can overcome the shortcomings of NIRF and provide high sensitivity and deep-tissue spatial resolution for initial detection of primary tumors and their metastatic lesions, allowing also a sensitive intra-operative localization of tumor lesions using a gamma probe[9],[67]. Consequently, both nuclear and NIRF imaging might complement each other, merging the strength of both techniques, and dual-modality image-guided surgery may overcome limitations of the currently used single-modality imaging techniques[67],[68]. Some dual modality agents, developed so far, are presented in table 1.6.

Table 1.6. PSMA dual probes with both nuclear and optical imaging valences.

NIR dyes	Cancer Ligand	Chelator	RN	Ref
IRDye800CW	Glu-urea-Lys	DOTA	^{111}In	(66)
RDye800CW	D2B	DTPA	^{111}In	(67)
IRDye800CW	Glu-urea-Lys	HBED-CC	^{68}Ga	(68)
FITC	Glu-urea-Lys	HBED-CC	^{68}Ga	(68)
AlexaFluor488	Glu-urea-Lys	HBED-CC	^{68}Ga	(68)
DyLight800	Glu-urea-Lys	HBED-CC	^{68}Ga	(68)
Cy5	Glu-urea-Lys	DOTAGA	^{68}Ga ^{177}Lu	(69)

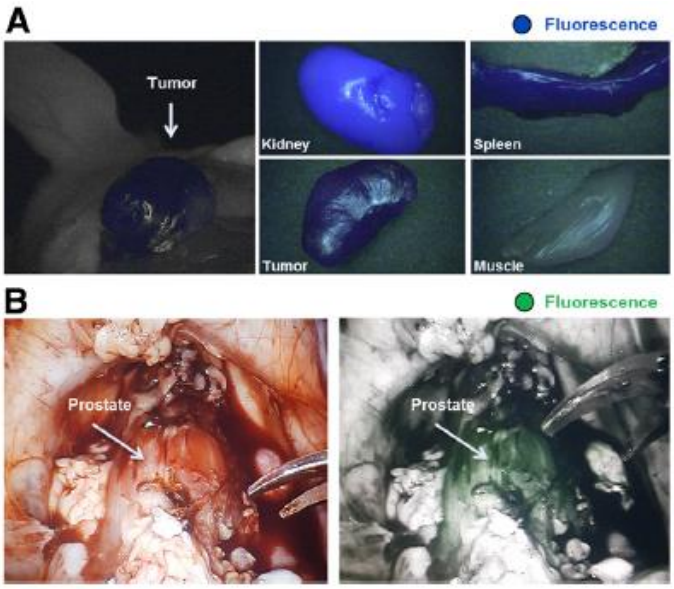

Figure 1.9. Proof-of-concept fluorescence-guided surgery studies in tumor-bearing mice and healthy pigs. (A) ^{68}Ga-Glu-urea-Lys-HBEDCC-IRDye800CW (0.5 nmol) was injected in mice (LNCaP tumor xenograft) for small-animal PET imaging, followed by *ex vivo* fluorescence detection after 120 min (IMAGE1 S system). (B) In healthy pigs, after pre-imaging acquisition of background fluorescence with da Vinci FireFly system, Glu-urea-Lys-HBED-CC-IRDye800CW (30 µg/kg) was intravenously injected. Fluorescence-guided prostatectomy accompanied by in vivo and ex vivo fluorescence detection was performed 1 h after injection. Adapted from(68).

1.6. Aim

As mentioned above, new PSMA radioactive probes have been developed recently and revealed high potential for detection and staging of PCa based on nuclear imaging techniques (SPECT or PET)[1-2],[25-26]. In particular, very promising results were obtained for complexes prepared with the ^{99m}Tc and ^{68}Ga radiometals and functionalized with a PSMA inhibitor containing the Glu and Lys amino acids[1-2],[10],[25-26]. ^{99m}Tc is the most widely used radioisotope in SPECT while ^{68}Ga is a radioisotope with increasing importance in PET, which justifies its interest in nuclear oncology, namely in the detection of PCa. It is noteworthy that one of the ^{68}Ga complexes directed to PSMA has already been clinically tested in numerous European NM Centers and has led to better results in the detection of PCa and its metastases when compared to other PET tracers or other imaging techniques[25],[42],[70-71].

Radioactive probes for PET or SPECT allow the detection of PCa and its metastases by acquisition of whole body images. However, the use of fluorescent congeners is more favorable in intraoperative procedures aiming at the most selective excision of tumor tissue. For this purpose, encouraging results have been described for PSMA inhibitors functionalized with ICG fluorophores[19],[65]. The design of specific dual probes for PSMA, containing a RN for PET or SPECT imaging or a fluorophore for optical imaging, profits from the inherent advantages of both nuclear and optical medical imaging modalities[9],[67].

Thus, the aim of the work was the design, synthesis and biological evaluation of bimodal probes (PET / SPECT and NIR) for the detection of PCa, starting from the base structure of complexes of ^{99m}Tc and ^{68}Ga functionalized with PSMA inhibitors that already showed clinical relevance, followed by further functionalization with indocyanine green (ICG) fluorophores. To tackle this goal, the following steps were thought:

1) Functionalization of bifunctional ligands (BFLs); with PSMA inhibitors and ICG derivatives;

2) Synthesis and characterization of ^{99m}Tc and ^{68}Ga complexes with the BFLs;

3) Biological evaluation of the ^{99m}Tc and ^{68}Ga complexes in cells of prostate carcinoma and in mice with induced tumor.

As one of the objectives of the work was to develop two bimodal probes for PSMA with SPECT and PET image capabilities, it was intended to synthesize a BFC for radiolabeling with ^{99m}Tc and another one for radiolabeling of ^{68}Ga, respectively. As referred above, in the design of the PSMA probe, the bifunctional ligands must present three components: the binding motif, a chelating unit and a linker spacer that connects the binding motif to the chelator. In this work,

the same binding motif (Glu-urea-Lys) and linker was used for the development of both dual probes, while two different chelators were tested. HBED-CC was the chelator chosen for labeling with ^{68}Ga, as it was already described in literature as an efficient chelator of ^{68}Ga[24],[40],[55]. Also, a pyrazolyl - diamine BFC was selected for radiolabeling with ^{99m}Tc, one of the most preferred RNs for SPECT imaging purposes. The pyrazolyl-diamine chelators have been introduced several years ago by the team of the Radiopharmaceutical Sciences group from C^{2}TN/IST and, since then, were successfully applied for the ^{99m}Tc-labeling of a variety of targeting biomolecules, spanning from bioactive peptides to small organic molecules and bis(phosphonates)[72-74]. For both dual probes, the optical image's capability would be added through the conjugation to a NIRF heptamethine dye. As known, ICG is the only FDA-approved NIRF cyanine agent for clinical use[9],[60],[75]. However, ICG can make normal tissues emit fluorescence signals with high intensity during some surgical procedures and, consequently, largely compromises its potential use for tumor visualization[60]. IR820 is structurally similar to ICG but the presence of sulfonic acid groups in both side chains allows better water solubility and lower toxicity through a quick clearance *in vivo*[60]. IR820 is also a better alternative than ICG when stability of the dye solution over time is a concern or when a consistent peak emission wavelength is desired[76]. The increased *in vitro* stability of IR820 translates into an increased stability *in vivo* as well, thus allowing for longer image collection times[76]. For these reasons, IR820 was selected as the NIRF chromophore to be evaluated in this work in the design of the dual probes.

Figure 1.10. represents the generic chemical structure of the proposed PSMA - bimodal probes studied in this work for both nuclear and optical imaging, as well as the BFCs selected for the labeling with two radioisotopes with clinical relevance for PET (^{68}Ga) and SPECT (^{99m}Tc).

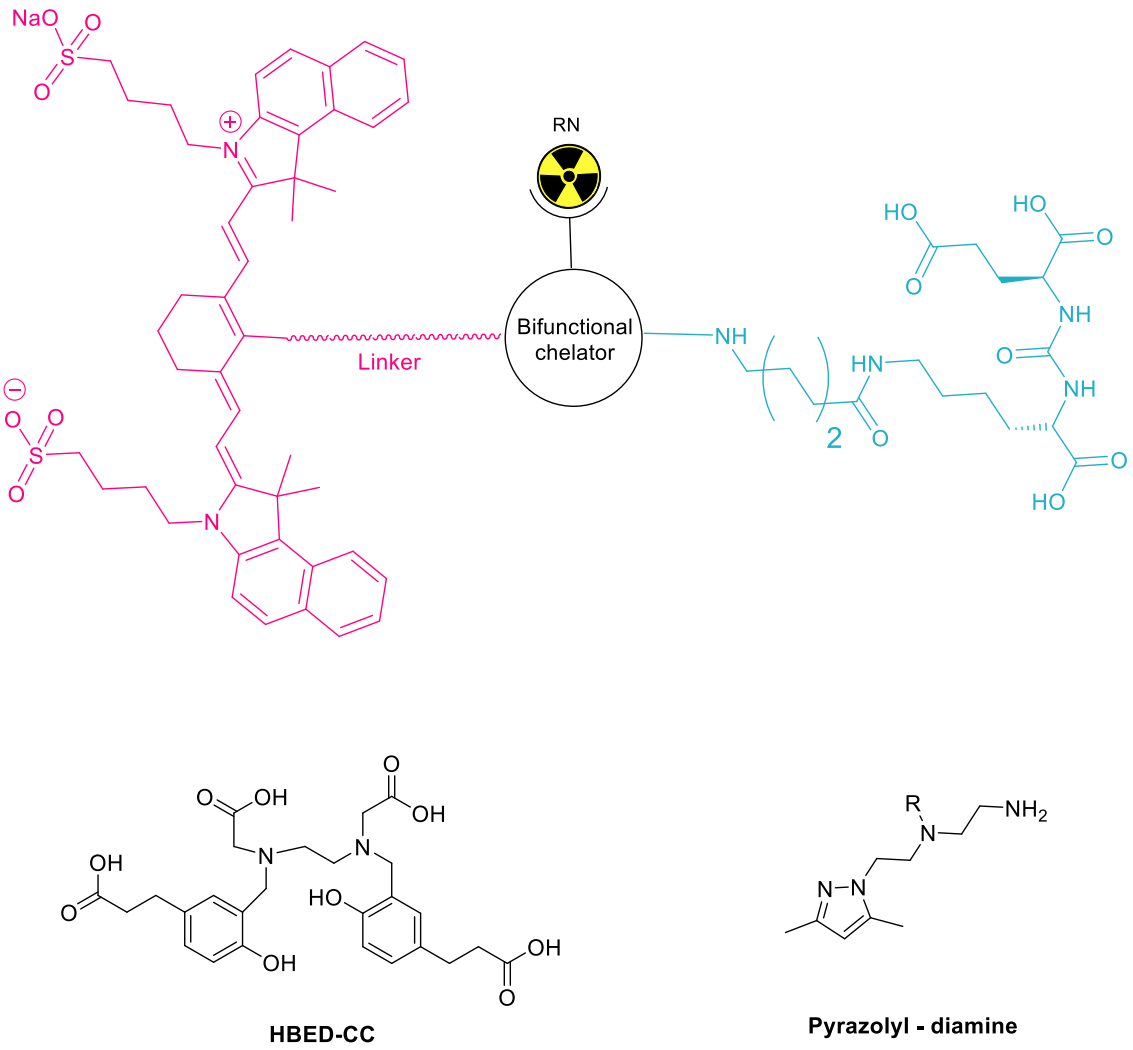

Figure 1.10. (A) Generic chemical structure of the dual probes. (B) BFCs for ^{68}Ga complexation (HBED-CC) and ^{99m}Tc coordination (pyrazolyl - diamine).

2. Synthesis and Characterization of Organic precursors: PSMA inhibitors and fluorescence dyes

2. Synthesis and Characterization of Organic precursors: PSMA inhibitors and fluorescence dyes

In this chapter the synthesis of the organic precursors (urea-based inhibitor and NIRF derivatives) for conjugation with the BFLs will be described, either for labeling with ^{99m}Tc or ^{68}Ga. In Scheme 2.1., the different steps needed for the synthesis of the proposed compounds are presented.

The synthesis of urea-based inhibitor involved the formation of an urea bond between two amino acids, Glu and Lys (see scheme 2.1.A). It was necessary to block or protect some functional groups of the reacting amino acids to prevent possible undesired side reactions during the urea bond formation, as detailed below. The desired urea-based inhibitor contains a flexible aminohexanoyl moiety as a spacer / linker that is accommodated at the spacious entrance funnel in the active site of PSMA, which is important for the binding affinity.

As for the synthesis of fluorophore derivatives, the functionalization of the NIRF dye – IR820- was attempted using two amino-containing linkers (see scheme 2.1.B), suitable for further coupling to the BFCs. This comprised the conjugation of the fluorophore with 4-aminothiophenol or with an hexamethylenediamine moiety. In both cases it was intended to obtain precursors with a terminal amine for conjugation with a carboxylic acid of the BFLs, through the formation of an amide bond.

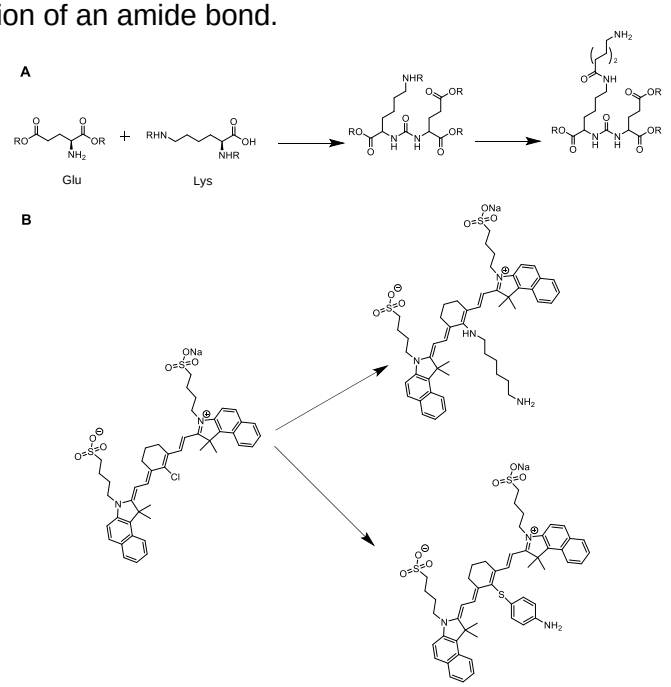

Scheme 2.1. Different steps needed for the synthesis of the organic precursors: urea-based inhibitor (A) and NIRF derivatives (B).

The various studied reactions and the synthesized compounds were followed-up and/or characterized by different methodologies, like TLC, ESI-MS, $^{1}H/^{13}C$ NMR and HPLC analysis.

2.1. Urea based PSMA Inhibitor

Two synthetic approaches were tested in this work to obtain the PSMA inhibitor moiety: liquid and solid phase synthesis. The synthesis of the PSMA inhibitor required the formation of a urea bond between protected Glu and Lys amino acids. Similarly to the work developed by other groups[23,24], we have studied the formation of the urea bond using triphosgene as reagent in a reaction involving two terminal amines (see table 2.1. and figure 2.1.), both for liquid and solid-phase synthesis.

Table 2.1. Triphosgene's reaction conditions for a urea bond formation.

Reagent	Conditions	Reaction Scheme
Triphosgene	Triphosgene is a solid reagent that is a less hazardous substitute for phosgene (gas) for a variety of chemical transformations including to bond one carbonyl group to two alcohols and to convert an amine group into isocyanate. The reagent order of addition can be important for avoiding the formation of symmetrical urea by-products.	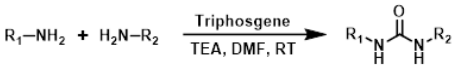

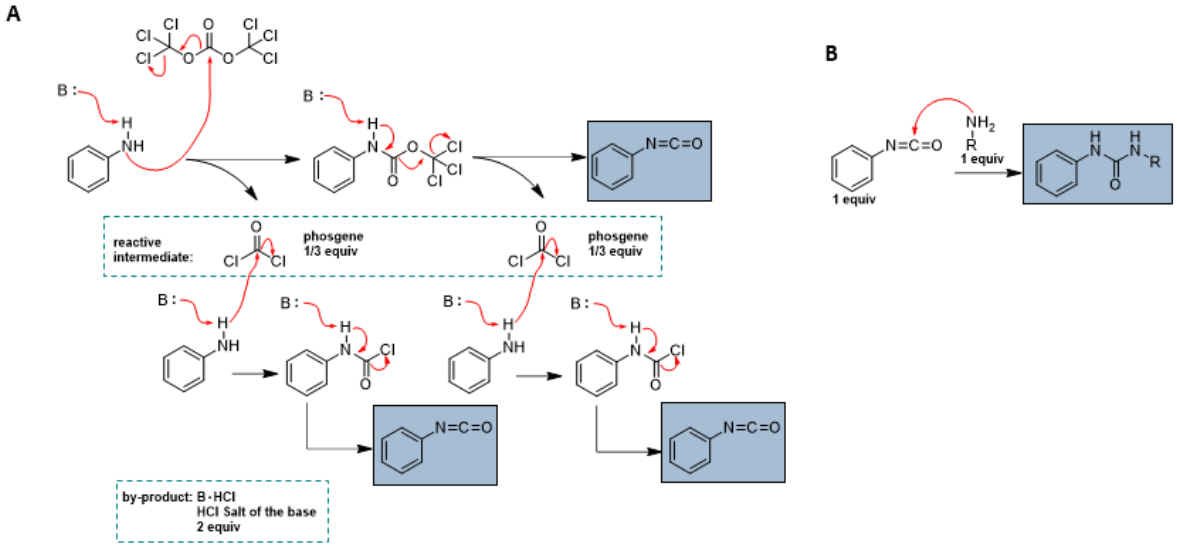

Figure 2.1. Mechanism for the formation of the isocyanate intermediate using triphosgene (A) and mechanism for the urea bond formation between the corresponding isocyanate and an amine (B).

2.1.1. Liquid-phase synthesis

Liquid-phase synthesis is a classical method used to synthesize peptides and it is still commonly used for large-scale synthesis. This method is slow and labor-intensive because the product must be manually removed from the reaction solution after each step. Additionally, this approach requires an appropriate chemical group to protect the C-terminus of the first amino acid. A benefit of liquid-phase synthesis, though, is that side reactions are easily detected because the product is purified after each step. Additionally, convergent synthesis can be performed, in which separate peptides are synthesized and then coupled together to create larger peptides.

Based on the methodology described by Banerjee *et al*[23], the reactions devised for the synthesis of the Glu-urea-Lys scaffold in solution are presented in scheme 2.2. It was also thought to introduce an aminohexanoyl spacer at the lateral amino group from the Lys amino acid (see scheme 2.2.) according to the work reported by Eder *et al*[24].

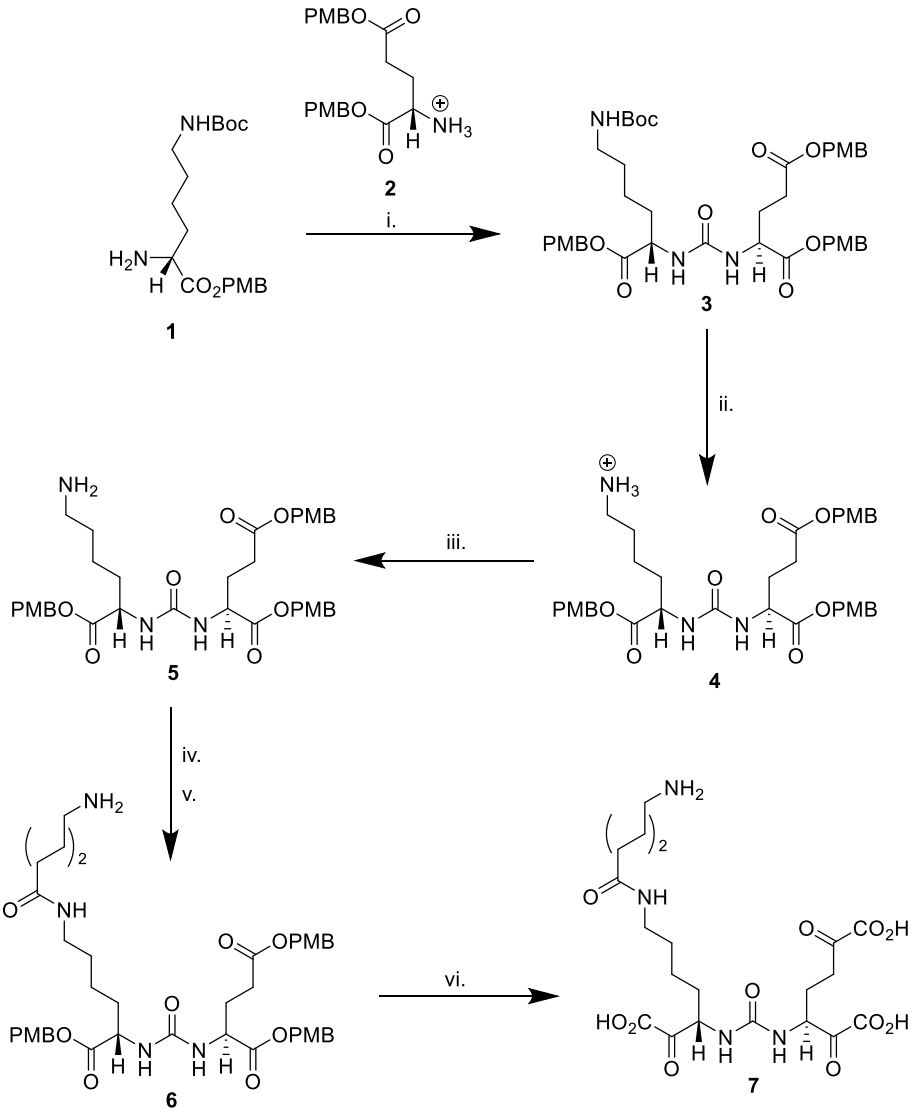

Scheme 2.2. Reactions devised for the synthesis of the Glu-urea-Lys scaffold starting from the protected amino acids **1** and **2**. i. Triphosgene, Et_3N; ii. TsOH; iii. 0.5 (N) $NaHCO_3$; iv. Fmoc-6-Ahx-OH, HBTU, DIPEA; v. 20% piperidine; vi. TFA, anisole.

The synthesis of the Glu-urea-Lys core required the previous protection with *p*-methoxybenzyl (PMB) of the carboxylic groups of both amino acids (Glu and Lys) before formation of the desired urea bond to afford the key intermediate 5 (see scheme 2.2.).

The synthetic strategy that was devised to obtain the protected lysine analogue **1** involved two steps, as shown in scheme 2.3. Nε-Boc-Nα-Fmoc-L-lysine (**8**) was reacted with 4-methoxybenzyl chloride and cesium carbonate in DMF. After removal of the solvent, an extraction with ethyl acetate followed by recrystallization in hexane/EtOAc afforded compound

9 in 70% yield. Compound **9** was characterized by ^{1}H NMR and ESI-MS analysis as shown in figures 2.2. and 2.3.

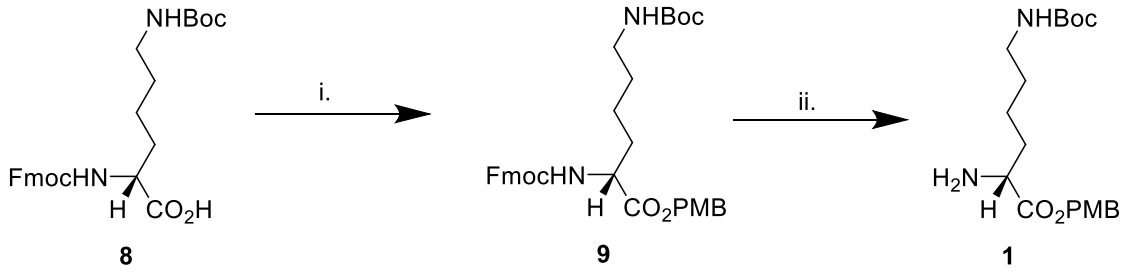

Scheme 2.3. Synthesis of protected Lys. i. 4-methoxybenzyl chloride, Cs_2CO3, DMF, RT, 4h; ii. 20% piperidine, DMF, RT, 20 min.

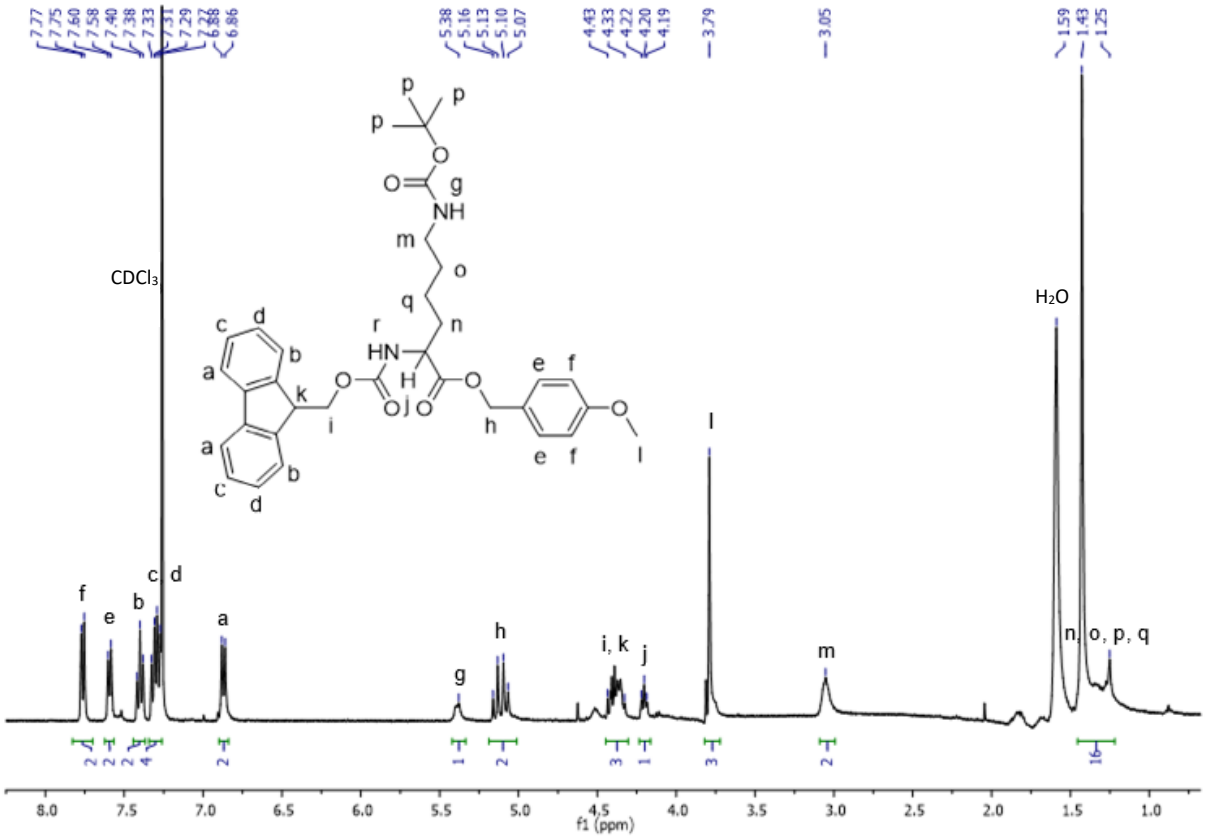

Figure 2.2. ^{1}H NMR spectrum of compound **9** in $CDCl_3$.

The ^{1}H NMR spectrum of compound **9** (see figure 2.2.) shows signals with chemical shifts and multiplicity similar to those described in the literature[23], namely:

- signals from δ = 6.86 to 7.77 ppm (H_{a-f}) with a total integration for 12 protons, corresponding to the CH aromatic protons from Fmoc and PMB system;

- broad signal (bs) at δ = 5.38 ppm (H_g), with integration for one proton corresponding to the BOC-NH proton;

- quadruplet at δ = 5.07-5.16 ppm (H_h) with integration for two protons, corresponding to the protons of the methylene protons (CH_2) of the PMB group;

- multiplet at δ = 4.33-4.43 ppm ($H_{i,k}$) with integration for three protons, corresponding to the CH and CH_2 protons of the Fmoc group;

- triplet (t) at δ = 4.20 ppm (H_j) with integration for one proton, corresponding to the CH proton of the Lys.

- singlet (s) at δ = 3.79 ppm (H_l) with integration for three protons, corresponding to the methyl groups (CH_3) present in the PMB structure;

- broad signal (bs) at δ = 3.05 ppm (H_m) with integration for two protons, corresponding to the protons of the methylene protons (CH_2) of the alkyl chain of Lys that are closer to the amide function;

- multiplet (m) at δ = 1.25-1.43 ppm (H_{n-q}) with integration for 16 protons, corresponding to the 9 protons of the three methyl groups (CH_3) present in the BOC group and also to the remaining methylene protons (CH_2) of the alkyl chain of Lys.

The ESI-MS spectrum in positive ion mode of compound **9** showed two peaks corresponding to the molecular ions $[M+H]^+$ and $[M+Na]^+$ and presenting patterns in agreement with the respective theoretical isotopic distributions, as shown in figure 2.3.

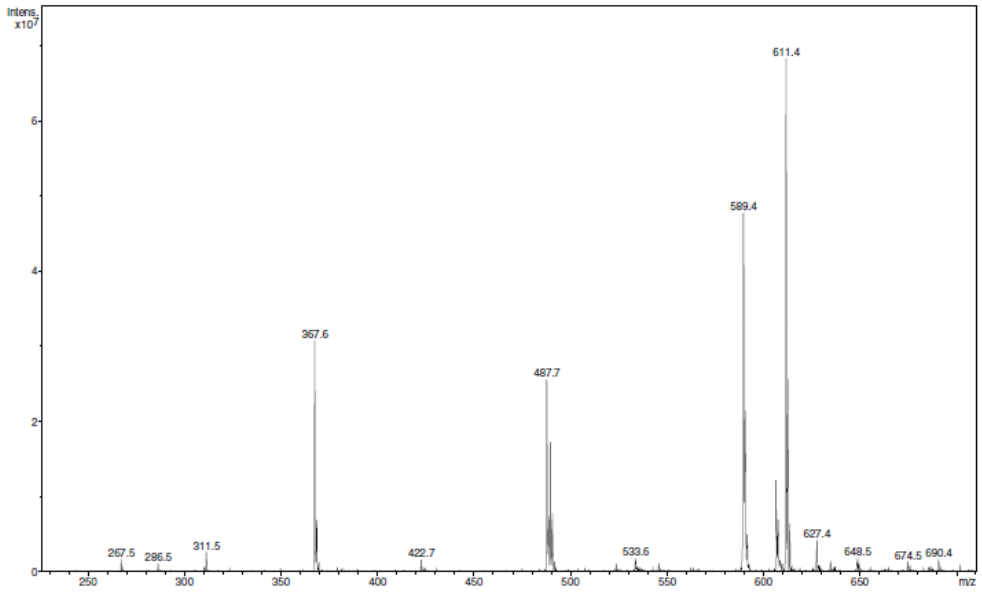

Figure 2.3. ESI-MS spectrum (positive mode) of compound **9**: The peaks observed at *m/z* = 589.4 and *m/z* = 611.4 correspond to the molecular ions $[M+H]^+$ and $[M+Na]^+$, respectively (theoretical values: $[M+H]^+$, *m/z*= 589.29; $[M+Na]^+$, m/z= 611.27).

The removal of the Fmoc group from compound **9** was performed using 20% piperidine in DMF, aiming to obtain compound **1** having a free amine group for the subsequent urea bond formation. After the FMOC deprotection reaction, the recovery of compound **1** was attempted by column chromatography purification, as described in the experimental section. ^{1}H NMR and ESI-MS analysis of the collected fractions showed that we could not obtain the desired compound.

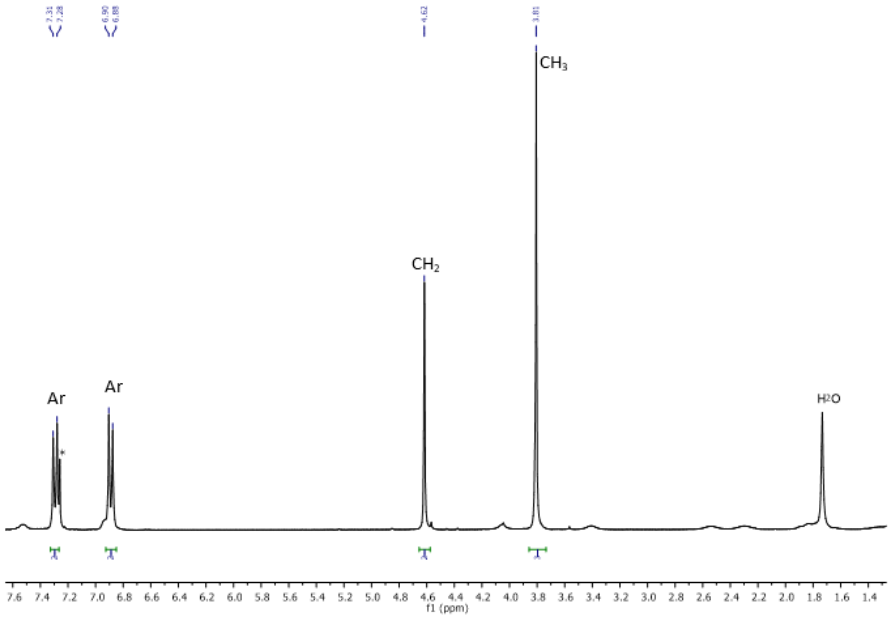

Figure 2.4. ^{1}H NMR spectrum of the collected fractions from the purification devised to obtain compound **1** in $CDCl_3$(*).

The ^{1}H NMR spectrum of the collected fractions showed that we were in the presence of PMB alcohol (see figure 2.4.), which indicated that the deprotection reaction was not selective, as the PMB protecting group was also removed together with Fmoc.

For the synthesis of the protected Glu analogue **2** (see scheme 4), bis-4-metoxybenzyl-L-glutamate.HCl (**2**), L(+) glutamic acid (**10**) was first treated with N,N,N',N' – tetramethylguanidine and then with ethyl acetoacetate to afford compound **11** (see scheme 2.4.). The intermediate **11** was not isolated and was further reacted with 4-methoxybenzyl chloride in order to guarantee the protection of the free carboxylic moieties through an esterification reaction. After the esterification reaction, the reaction mixture was treated with methanolic hydrogen chloride (HCl) to convert the imine function to a terminal NH_2 and afford compound **2**. The purification of compound **2** was performed by flash chromatography; compound **2** was isolated in 20% yield and was characterized by ^{1}H and ^{13}C NMR and ESI-MS analysis, as shown in figures 2.5., 2.6. and 2.7.

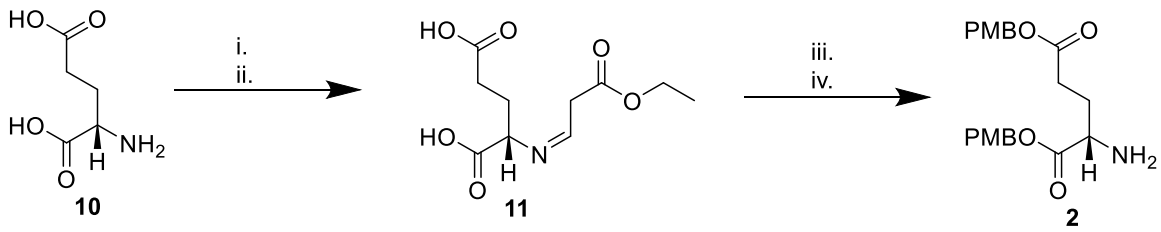

Scheme 2.4. Synthesis of protected Glu. i. N,N,N',N' – tetramethylguanidine, 0ºC, 30 min, RT; ii. Ethyl acetoacetate, RT, 24h; iii. 4-methoxybenzyl chloride, 16h, RT; iv. methanolic HCl, 30 min, RT.

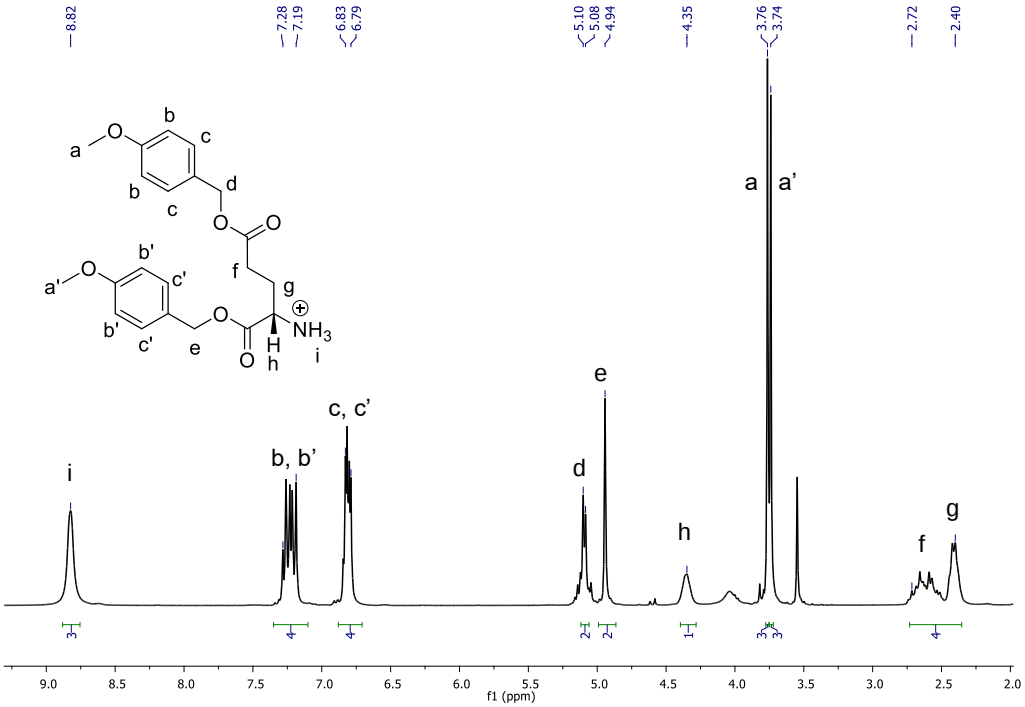

Figure 2.5. ^{1}H NMR spectrum of compound **2** in $CDCl_3$

The ^{1}H NMR spectrum of compound **2** (see figure 2.5.) shows signals with chemical shifts, relative integration areas and multiplicities compatible with the molecular structure of the compound and in accordance with the data described in the literature despite minor deviations in the chemical shifts[23]:

- singlet (s) at δ = 8.82 ppm (H_i) with integration for three protons corresponding to the NH_3^+ acidic protons of the protonated amine.

- multiplets (m) at δ = 7.19-7.28 ppm and δ = 6.79-7.83 ppm ($H_{b,b'-c,c'}$) with integration for four protons each, corresponding to the aromatic CH protons of the PMB group;

- doublet (d) at δ = 5.09 ppm (H_d), with integration for two protons corresponding to the methylene protons (CH_2) of PMB group;

- singlet (s) at δ = 4.94 ppm (H_e) with integration for two protons corresponding to the methylene protons (CH_2) of PMB group;

- broad signal (bs) at δ = 4.45 ppm (H_h) with integration for one proton corresponding to the CH proton.

- Two singlets (s) at δ =3.74 and 3.76 ppm ($H_{a,a'}$) with integration for three protons corresponding to CH_3 protons of PMB group;

- multiplet (m) at δ = 2.40 - 2.72 ppm (H_{f-g}) with integration for four protons, corresponding to CH_2 protons.

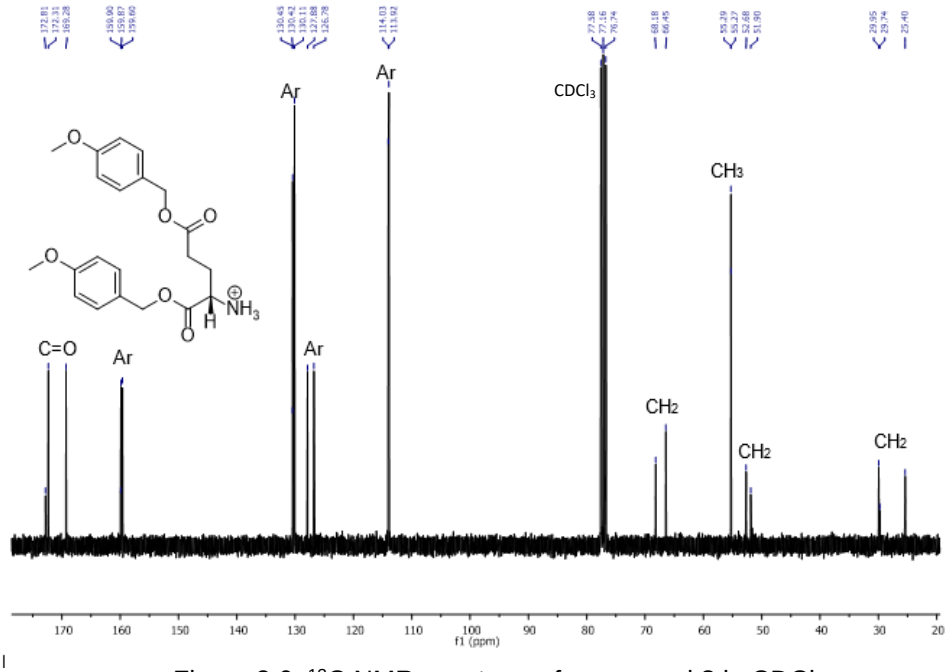

Figure 2.6. ^{13}C NMR spectrum of compound **2** in $CDCl_3$

In the ^{13}C NMR spectrum of compound **2** (see figure 2.6.), the two expected resonances for the C=O group of the –COOR function appeared at 172.31 and 169.28 ppm. The aromatic unit originated peaks between 113.92 and 159.90 ppm. The group -CH_2 attached to the aromatic ring originated a resonance at 66.45 ppm, while resonances appearing between 25.40 and 52.68 ppm correspond to carbons in the aliphatic chain of the amino acid. Finally, resonances for the -CH_3 carbons of the PMB protecting group appeared at 55.27 and 55.29 ppm.

Regarding the positive mode of the ESI-MS spectrum for compound **2**, it was observed a peak that matched to the molecular ion $[M+H]^+$, presenting a pattern corresponding to the theoretically expected, according to the isotopic distribution of the compound as shown in figure 2.7.

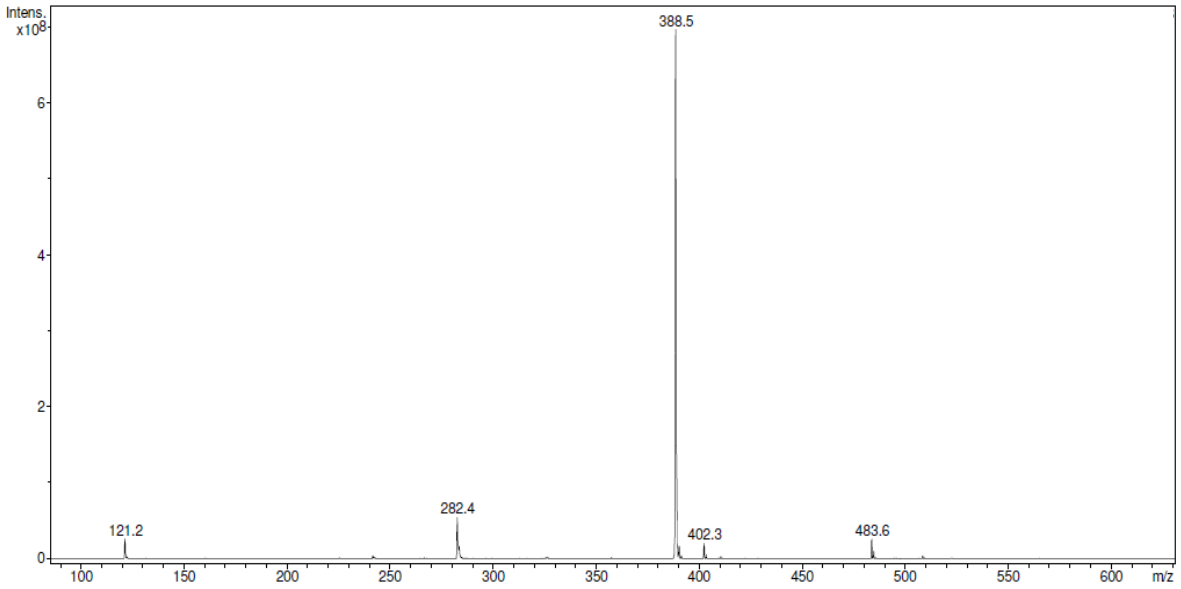

Figure 2.7. ESI-MS spectrum (positive mode) of compound **2**: The peak observed at *m/z* = 388.5 correspond to the molecular ion $[M+H]^+$ (theoretical value: $[M+H]^+$, *m/z*= 388.18).

2.1.2. Solid-phase synthesis

The liquid phase synthesis of the Glu-urea-Lys scaffold proved to be unsuccessful due to the inability to selectively deprotect compound **9**. Therefore, a solid-phase synthesis methodology was followed to perform the synthesis of this scaffold.

Solid-phase synthesis is a method in which molecules are covalently bound on a solid support material and synthesized step-by-step in a single reaction vessel using selective protecting group chemistry. Benefits compared with normal synthesis in a liquid state include: high efficiency and throughput and increased simplicity and speed. The reaction can be driven to

completion and high yields through the use of excess reagent. In this method, building blocks are protected at all reactive functional groups. The order of functional group reactions can be controlled by the order of deprotection. This method is usually used for the synthesis of peptides.

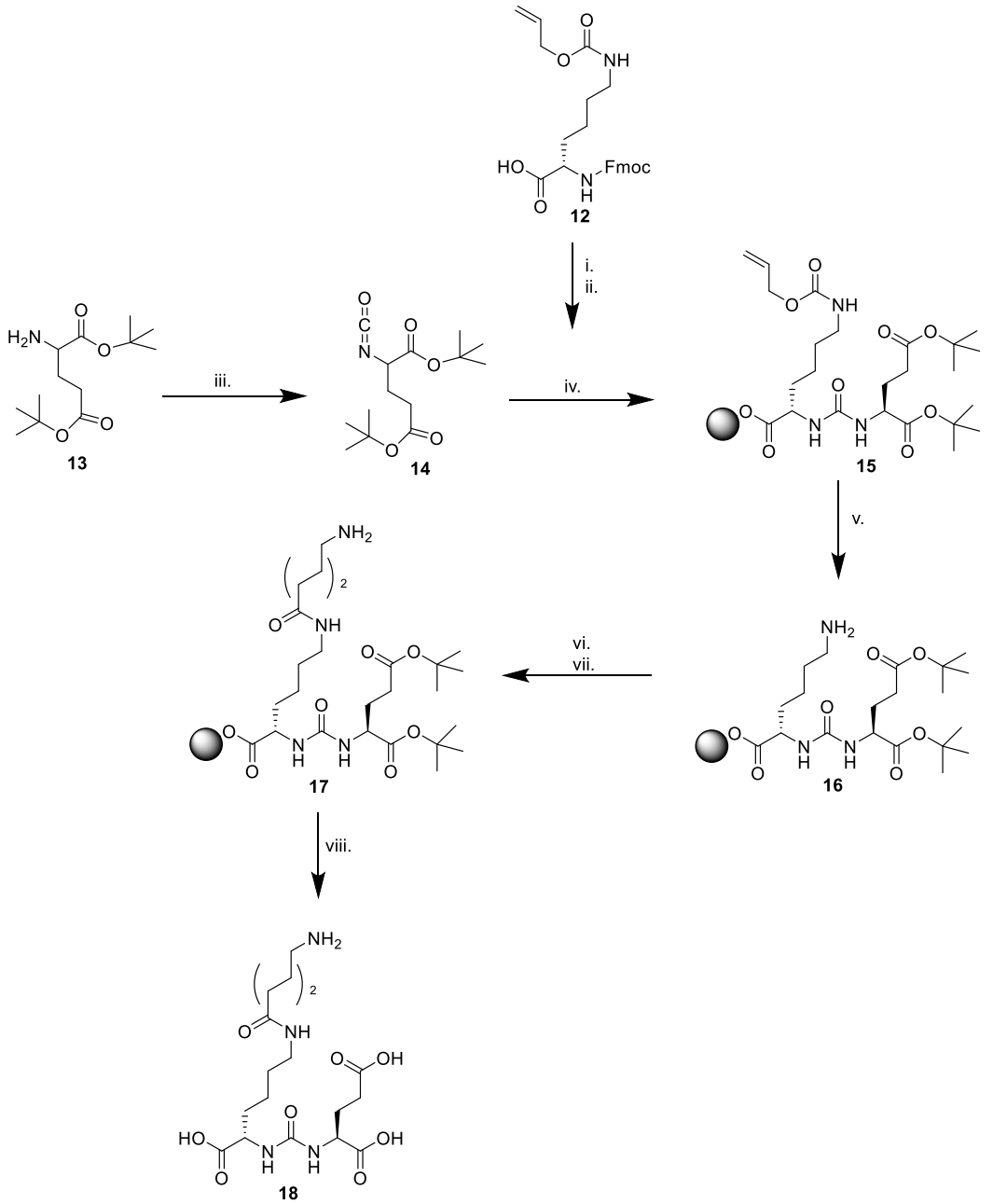

Scheme 2.5. Solid-phase synthesis of the Glu-urea-Lys scaffold. i. pyridine, 2,6- dichlorobenzoic acid, DMF, overnight, RT; ii. 20% of piperidine, DMF, 1h, RT; iii. Triphosgene, DIPEA, dry CH_2Cl_2, 1.5 h, -50°C; iv. H-Lys(Alloc)-Wang Resin; 72h, RT; v. $Pd[P(C_6H_5)_3]_4$, morpholine, dry CH_2Cl_2, 1 h, RT; vi. Fmoc-6-Ahx-OH, HBTU, DIPEA, DMF; vii. 20% piperidine, DMF, 1 h, RT; viii. TFA / TMS / H_2O (95: 2.5: 2.5), 30 min, RT.

The solid phase synthesis of the Glu-urea-Lys scaffold was performed according to the method developed by the Polatom team (see scheme 2.5.), which has an active collaboration with the C^{2}TN team under the framework of a FCT-funded bilateral project. The first step involved the loading of Fmoc-L-Lys (Alloc) (**12**) to a polystyrene Wang resin, under treatment of pyridine and 2,6- dichlorobenzoic acid in DMF over agitation overnight at RT. Subsequently, the deprotection of the Fmoc group was performed using 20% of piperidine in DMF to obtain the resin immobilized E-allyloxycarbonyl protected lysine. In a second step, the isocyanate of the glutamyl moiety (**14**) was generated in situ by slowly adding a mixture of bis(tert-butyl) L-glutamate hydrochloride (**13**) and DIPEA in dry CH_2Cl_2 to a solution of triphosgene, under agitation, in dry ice, over 1.5 h. Then, at RT, the L-Lys (Alloc) Wang resin was added to the previous solution and gently agitated over 72 h to form the urea bond leading to compound **15**. Subsequently, the allyloxyl-protecting group was removed using $Pd(PPh_3)_4$ and morpholine in dry CH_2Cl_2, leading to compound **16**. Next, it was performed the coupling of compound **16** to the aminohexanoic linker by reaction of the Fmoc-protected 6-aminohexanoic acid, in the presence of HBTU and DIPEA in DMF. Compound **17** was obtained by selective Fmoc deprotection under treatment with 20% piperidine in DMF. Finally, the cleavage from the resin allowed to obtain compound **18** upon treatment with trifluoroacetic acid (TFA) / trimethylsilane (TMS) / H_2O at RT under agitation. Regarding the positive mode of the ESI-MS spectrum for compound **18**, it was observed a peak that matched to the molecular ion $[M+H]^+$, presenting a pattern corresponding to the theoretically expected, according to the isotopic distribution of the compound as shown in figure 2.8.

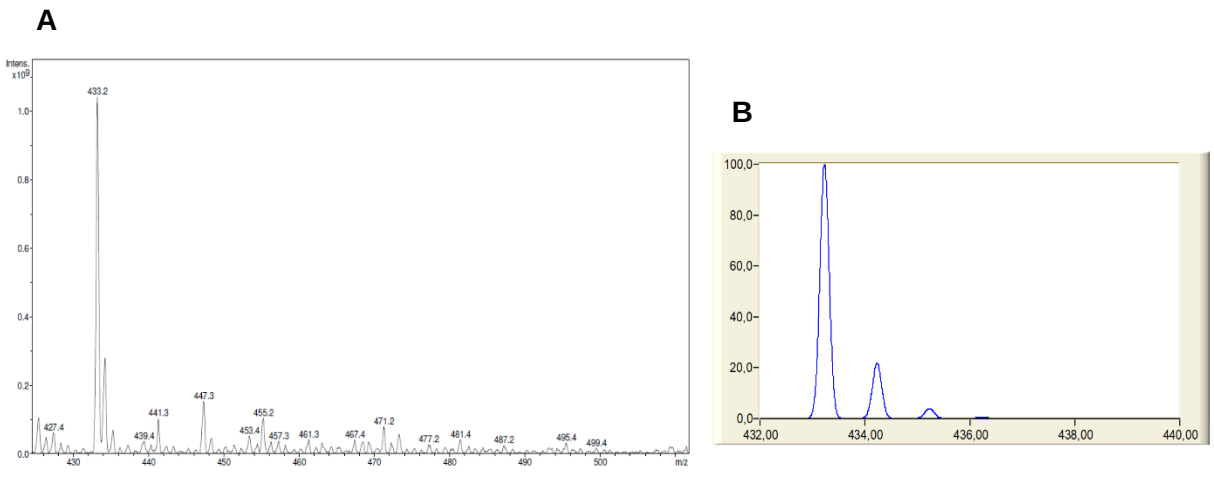

Figure 2.8. (A) ESI-MS spectrum (positive mode) of compound **18**: The peak observed at *m/z* = 433.2 correspond to the molecular ion $[M+H]^+$ (theoretical value: $[M+H]^+$, *m/z*= 433.23). (B) Isotopic abundances simulation for compound **18.**

2.2. Synthesis and characterization of IR820 derivatives

As mentioned above, the functionalization of the NIRF dye – IR820- for further coupling to the BFCs was attempted using two amino-containing linkers: 4-aminothiophenol and a hexamethylenediamine. As detailed below, the synthesis of the IR820 derivative containing an aminothiophenol linker was done in a similar way as reported by Iacono *et al* [77]. This synthesis started from a commercially available IR820 derivative containing a central cyclohexenyl with a meso-chlorine reactive site suitable for modification with the aminothiophenol moiety. A similar strategy was used to synthesize the IR820 derivative functionalized with the aliphatic hexamethylenediamine linker, and as reported by Masotti *et al* [78] to obtain related compounds.

2.2.1. Aromatic derivative of IR820

Several attempts were done to optimize the synthesis of the aromatic derivative of IR820 containing an aminothiophenol linker, which was previously described by Iacono *et al*[77]. The optimization of the synthesis of this compound required longest reaction times comparatively to the method described in the literature[77] and involved a distinct method to isolate the final product, as described below.

The aromatic derivative was synthesized by reacting the commercially available IR820 (**19**) with 4-aminothiophenol in DMF, during 72 h at RT and under light protection (see scheme 2.6.). Product purification was performed by flash chromatography affording IR820-S-Ph-NH_2 (**20**), which was obtained as a green solid in 51.7% yield. Compound **20** was characterized by ^{1}H NMR, ESI-MS and analytical HPLC (see figures 2.9-2.11). In the negative ESI-MS spectrum, it was observed a peak corresponding to the molecular ion $[M-Na]^-$ with a pattern in agreement with the one theoretically expected, as shown in figure 2.9.

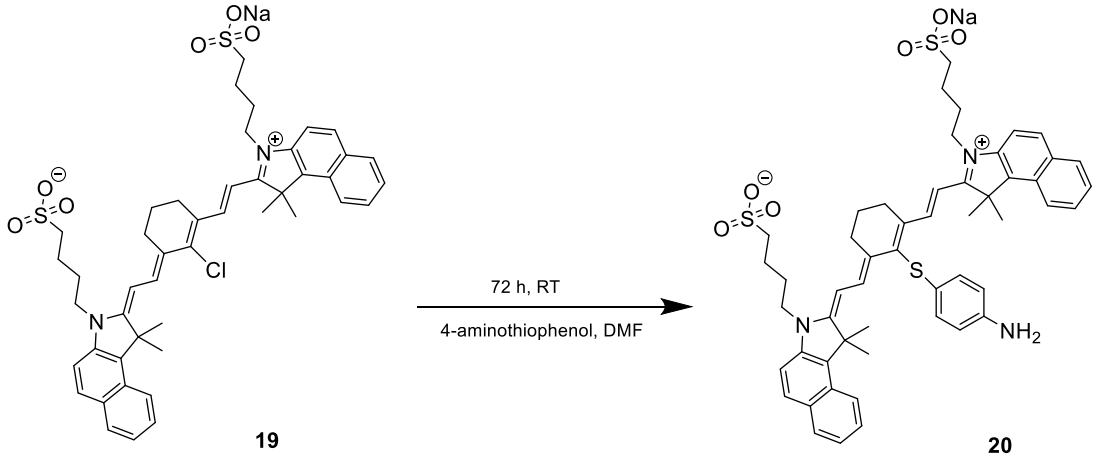

Scheme 2.6. Synthesis of the aromatic derivative of IR820 (**20**).

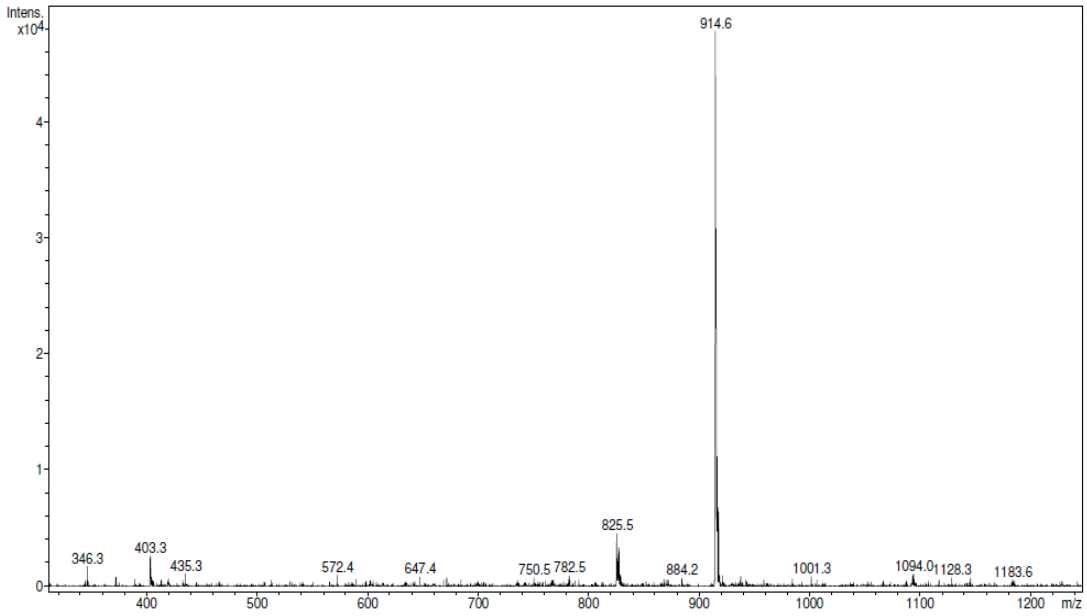

Figure 2.9. ESI-MS spectrum (negative mode) of compound **20**: The peak observed at *m/z* = 914.6 corresponds to the molecular ion $[M\text{-}Na]^-$ (theoretical value: $[M\text{-}Na]^-$, *m/z* = 914.33).

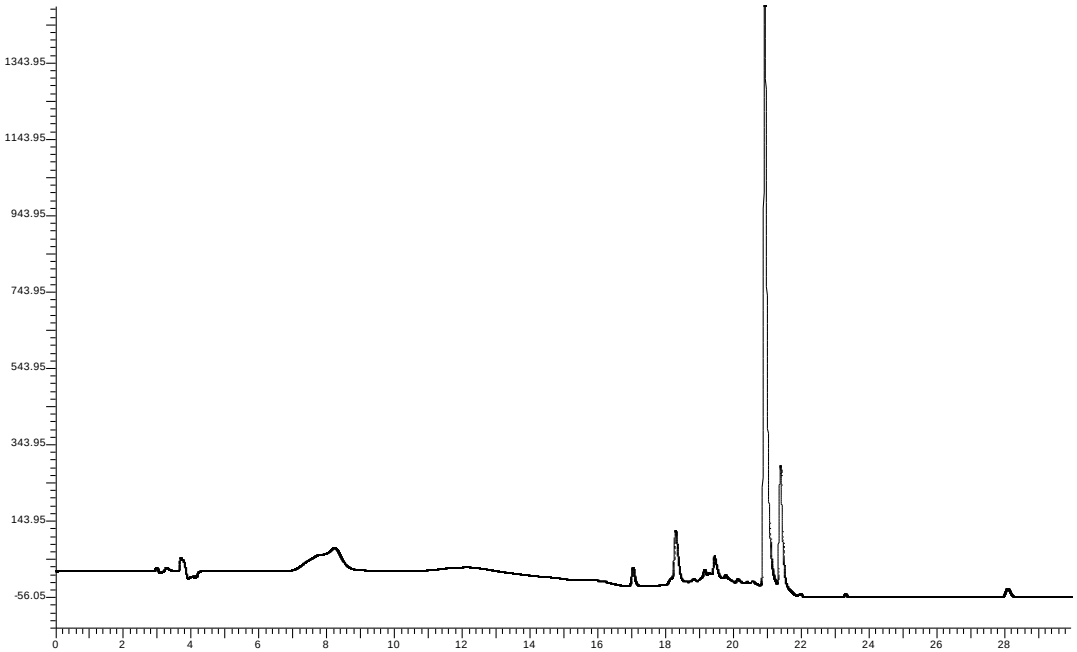

Figure 2.10. HPLC chromatogram of IR820-S-PH-NH_2 (**20**) (rt = 20.92 min).

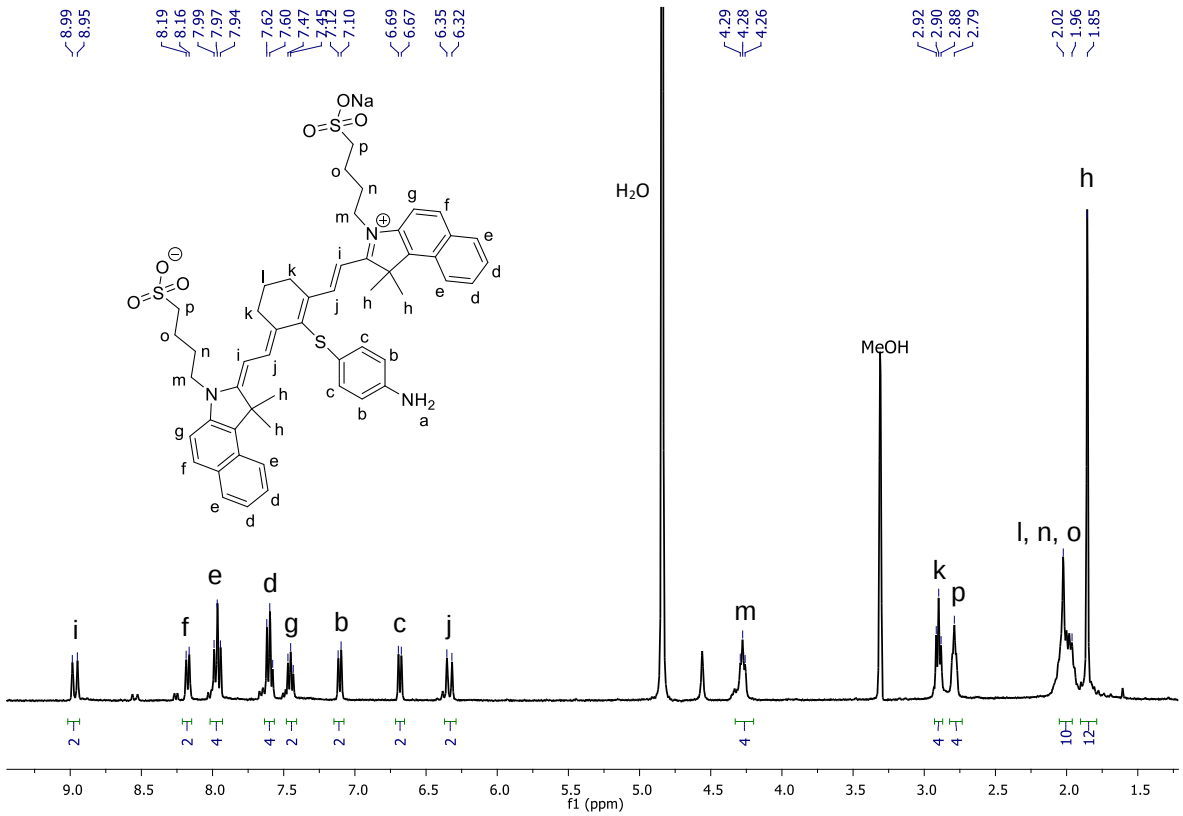

Figure 2.11. ^{1}H NMR spectrum in MeOH of compound **20**.

The ^{1}H NMR spectrum of compound **20** (see figure 2.11.) shows signals with chemical shifts and multiplicity compatible with the identity of the compound and similar to those as described in the literature[77], namely:

- doublet (d) at δ = 8.97 ppm (H_i) with integration for two protons, corresponding to the vinylic CH protons of the heptamethine chain;

- doublet (d) at δ = 8.18 ppm (H_f) with integration for two protons, corresponding to the protons of the aromatic CH of indoline;

- triplet at δ = 7.97 (H_e) ppm with integration for four protons, corresponding to the aromatic CH protons of the benzene moiety of the benzo-fused indoline;

- multiplet at δ = 7.60 ppm (H_d) with integration for four protons, corresponding to the aromatic CH protons of the benzene moiety of the benzo-fused indoline;

- triplet at δ = 7.45 ppm (H_g) with integration for two protons, corresponding to the aromatic CH protons of indoline;

- doublet (d) at δ = 7.11 ppm (H_b) with integration for two protons, corresponding to the aromatic CH protons of the aminothiophenol moiety;

- doublet (d) at δ = 6.68 ppm (H_c) with integration for two protons, corresponding to the aromatic CH protons of the aminothiophenol moiety;

- doublet (d) at δ = 6.34 ppm (H_j) with integration for two protons, corresponding to the vinylic CH protons of the heptamethine chain;

- triplet at δ = 4.28 ppm with integration for four protons (H_m), corresponding to the protons of methylene protons (CH_2) that are the more unshielded, due to electroatractive effect of the adjacent heteroaromatic ring;

- triplet at δ = 2.90 ppm (H_k) with integration for four protons, corresponding to the methylene protons (CH_2) protons of central cyclohexene;

- singlet at δ = 2.79 ppm (H_p) with integration for four protons, corresponding to the methylene protons (CH_2) of the alkyl chain that are adjacent to the sulfo-groups;

- multiplet at δ = 1.96-2.02 ppm ($H_{l,n,o}$) with integration for ten protons, corresponding to eight aliphatic CH_2 protons of the alkyl chain and the remaining CH_2 protons of central cyclohexene;

- singlet at δ = 1.85 ppm (H_h) with integration for twelve protons, corresponding to the protons of the four methyl groups (CH_3) adjacent to the benzoindoline core of the compound.

2.2.2. Aliphatic derivative of IR820

As discussed above, two strategies were followed to synthesize the aliphatic derivative of IR-820. The first synthesis was made based on the work developed by Masotii *et al*[78]. Firstly, unprotected hexamethylenediamine was used to functionalize the fluorophore under study. The protocol was the subject of some optimizations, such as the increase of reaction time and the method of purification through flash chromatography. After purification of the product, ESI-MS analysis of the collected fractions showed that a dimeric compound was also formed, besides the desired product. The dimeric compound resulted from the N-alkylation of each NH_2 group from the diamine.

As the synthesis using the unprotected diamine did not yield the desired product in good yield, an alternative method was adopted, using hexamethylenediamine protected with BOC only at one of the NH_2 groups, being available the second one for the N-alkylation reaction (see scheme 2.7). This synthetic methodology involved two steps. The first step involved the protection of one of the terminal amines from hexamethylenediamine with the BOC protecting

group, while the second step involved the conjugation of the protected amine to the fluorophore and the subsequent deprotection.

The BOC-protection of the diamine was achieved by reaction of hexamethylenediamine (**21**) with di-*tert*-butyl dicarbonate [$(Boc)_2O$)] in dioxane, as detailed in the experimental section. The resulting mono-protected diamine, compound **22,** was isolated in 39.6% yield. Compound **22** was characterized by ^1H NMR and ESI-MS analysis, as shown in figures 2.12. and 2.13.

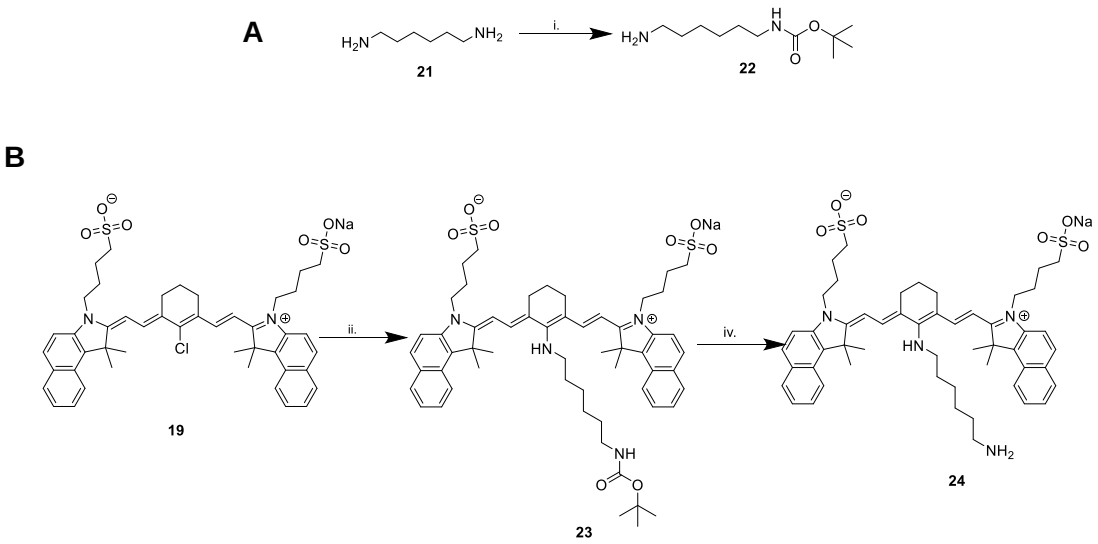

Scheme 2.7. Synthesis the aliphatic derivative of IR820 (**24**). A. i. dioxane, $[(Boc)_2O)]$, 24 h, RT; B. ii. Dry DMF, Hxmda-Boc, Et_3N, overnight, RT; iii. TFA/DCM (50:50), 3h, RT.

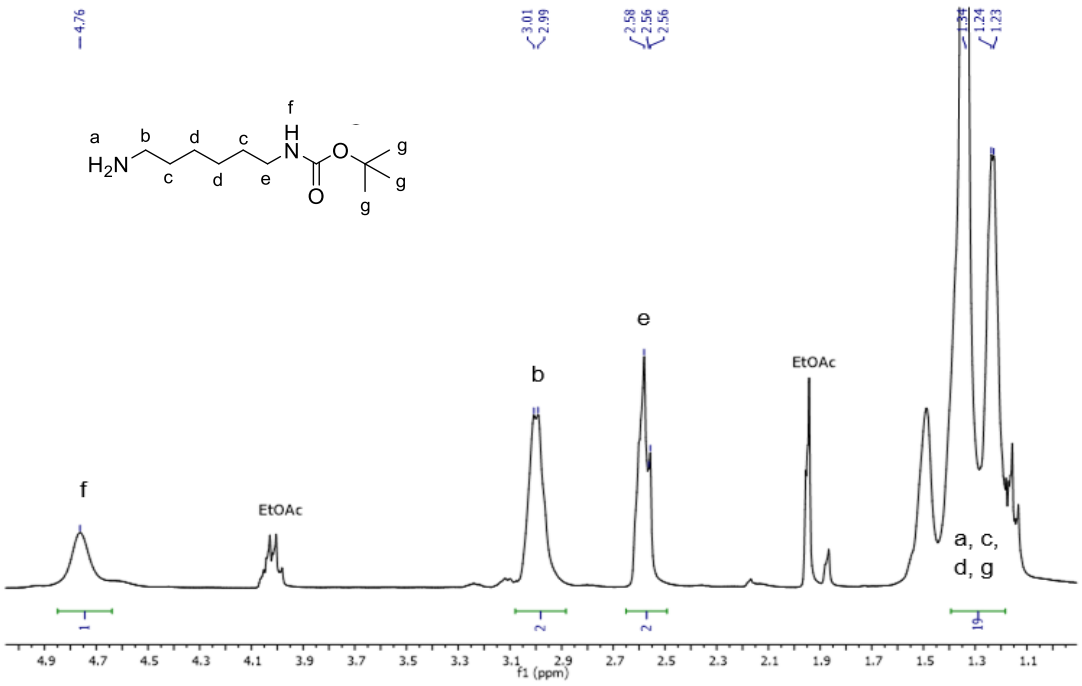

Figure 2.12. ^1H NMR spectrum of compound **22** in $CDCl_3$.

The ^{1}H NMR spectrum of compound **22** (see figure 2.12) shows signals with chemical shifts and multiplicity compatible with the identity of the compound:

- singlet (s) at d = 4.76 ppm (H_f) with integration for one proton corresponding to the BOC-NH proton;

- doublet (d) at d = 2.99 ppm (H_b) with integration for two protons corresponding to the aliphatic CH_2 protons adjacent to the amine function;

- triplet (t) at d = 2.58 ppm (H_e) with integration for two protons corresponding to the aliphatic CH_2 protons adjacent to the amide function;

- multiplet (m) d = 1.23-1.34 ppm ($H_{a,c,d,g}$) with integration for nineteen protons corresponding to the 9 CH_3 protons from the BOC group, the 2 protons of the NH_2 terminal amine and the 8 protons corresponding to the methylene protons (CH_2) of the alkyl chain.

In the positive mode of the ESI-MS spectrum, it was observed a peak corresponding to the molecular ion $[M+Na]^+$, presenting a pattern in agreement with the theoretical one, as shown in figure 2.13.

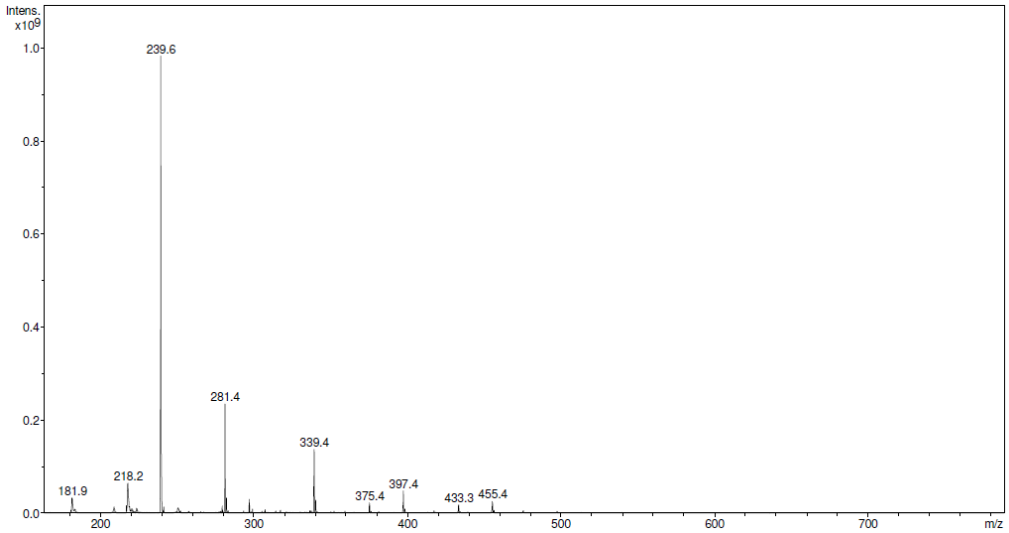

Figure 2.13. ESI-MS spectrum (positive mode) of compound **22**: the peak observed at *m/z* = 239.6 corresponds to the molecular ion $[M+Na]^+$ (theoretical value: $[M+Na]^+$, *m/z* = 239.17).

Then, it was studied the conjugation of the protected diamine, Hxmda-BOC (**22**), to the fluorophore IR820 (**19**). For that, **22** was reacted with **19** in dry DMF in the presence of dry Et_3N, under a nitrogen atmosphere and with magnetic stirring overnight at RT. Product purification was performed by flash chromatography, which afforded compound **23** as a blue solid (28% yield). Compound **23** was characterized by ^{1}H and ^{13}C NMR and ESI-MS.

The ESI-MS spectrum of **23** (negative mode) showed a prominent peak corresponding to the molecular ion $[M-Na]^-$, with a pattern in agreement with the theoretical one, as shown in figure 2.14.

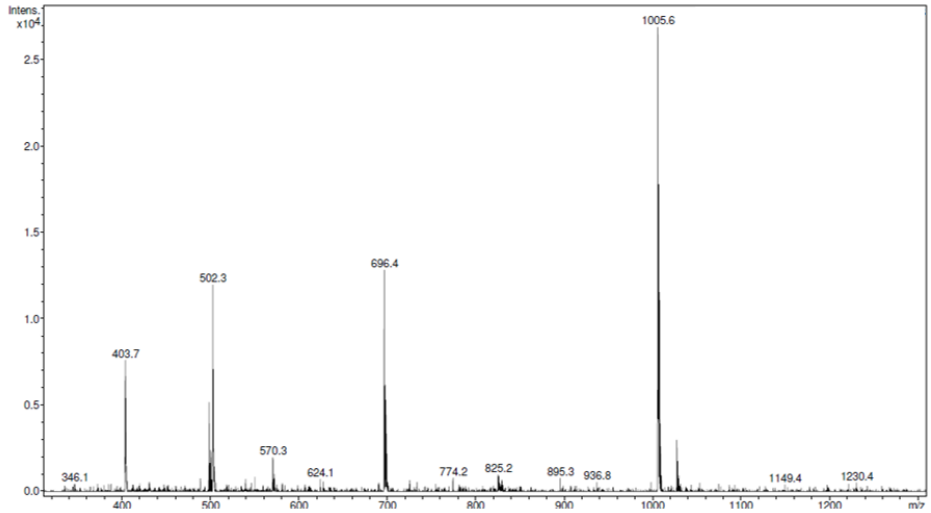

Figure 2.14. ESI-MS spectrum (negative mode) of compound **23**: The peak observed at *m/z* =1005.6 corresponds to the molecular ion $[M-Na]^-$ (theoretical value: $[M-Na]^-$; *m/z* = 1005.49).

The ^1H NMR spectrum of **23** (see figure 2.15.) showed signals due to its different protons, in the aromatic and aliphatic regions (see figure 2.15). However, it was not possible to make a full interpretation of the spectrum, due to its complexity and broadness of the signals. Moreover, the intensity of the signals due to the aliphatic protons were higher than expected.

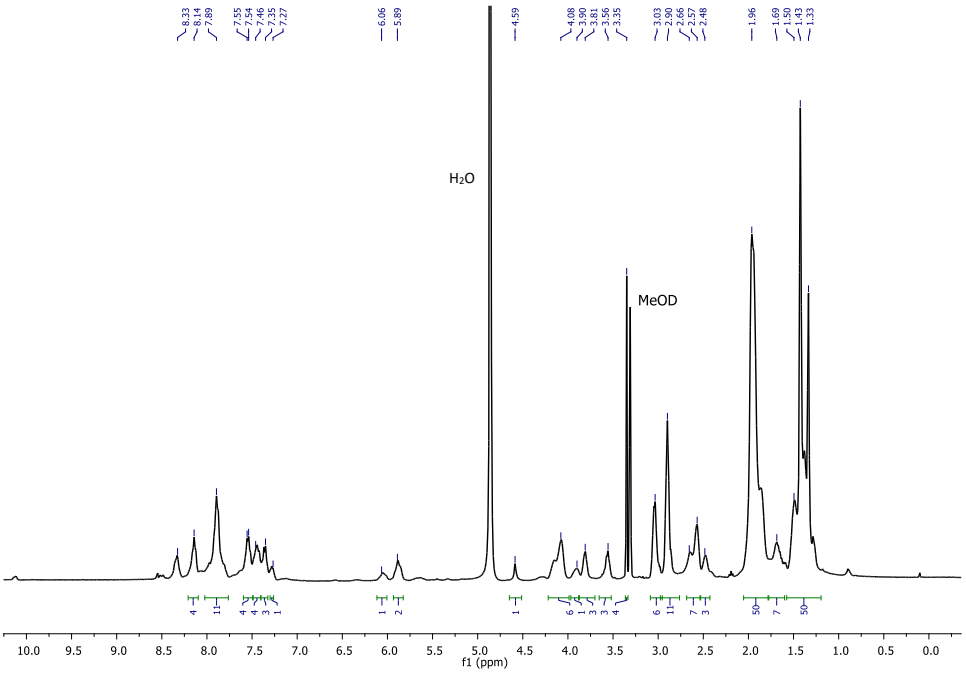

Figure 2.15. ^1H NMR spectrum in MeOH of compound **23**.

As compound **23** was positively identified by ESI-MS analysis we have pursued with the removal of BOC protecting group to obtain the final compound **24** (see Scheme 2.7). The removal of the BOC-protecting group was done by reacting **23** with TFA at RT for 3 h. Preparative HPLC was performed to purify **24**, leading to the isolation of 2 fractions that were analyzed by ^{1}H NMR, ESI-MS analysis and analytical HPLC. However, the obtained analytical and spectroscopic data did not confirm the formation of the compound **24**.

3. Synthesis and characterization of bifunctional chelators and its functionalization

3. Synthesis and characterization of bifunctional chelators and its functionalization

The synthesis of two bifunctional ligands was attempted in this work. Regarding PET imaging with the positron emitter ^{68}Ga, we have thought on HBED-CC. HBED-CC is a two-fold carboxylic acid substituted HBED that was synthesized as the chelating agent for ^{68}Ga according to the methods described in the literature[79]. Additionally, HBED-CC provides functional groups for coupling to the PSMA inhibitor and the cyanine dye[79]. For labeling with ^{99m}Tc and for SPECT imaging a pyrazolyl-diamine ligand was envisaged as the chelating agent, according to strategies previously developed by the RSG from C^{2}TN/IST[73].

3.1. HBED-CC derivatives

The synthesis of HBED-CC was performed using the methods described in the literature[79], based on a Mannich reaction between N,N' ethylenediamine diacetic acid (EDDA) and formaldehyde, followed by an electrophilic addition of the resulting imine to the phenolic compound as showed in the mechanism presented in figure 3.1.

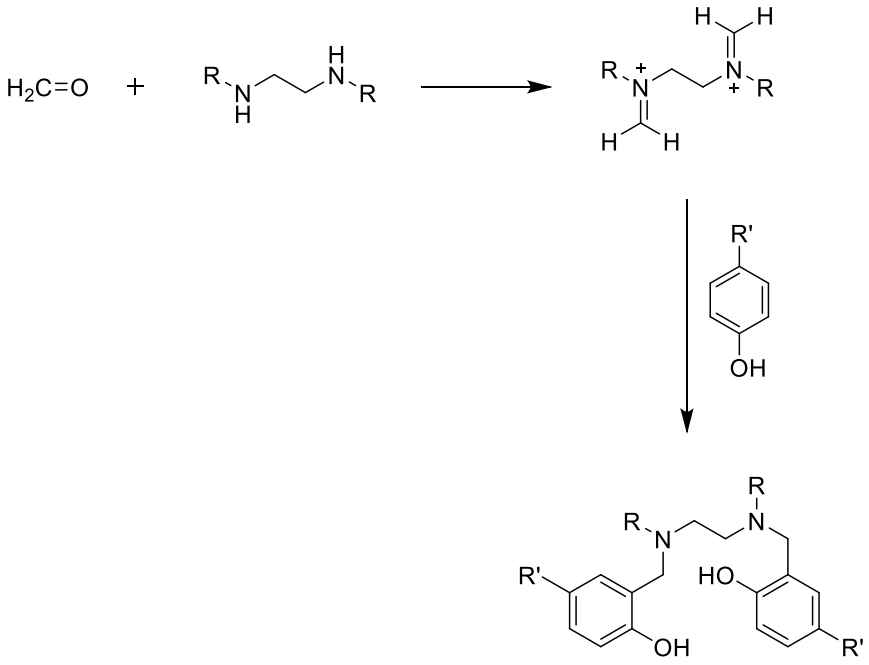

Figure 3.1. Mechanism of the electrophilic addition between an imine and a phenolic compound.

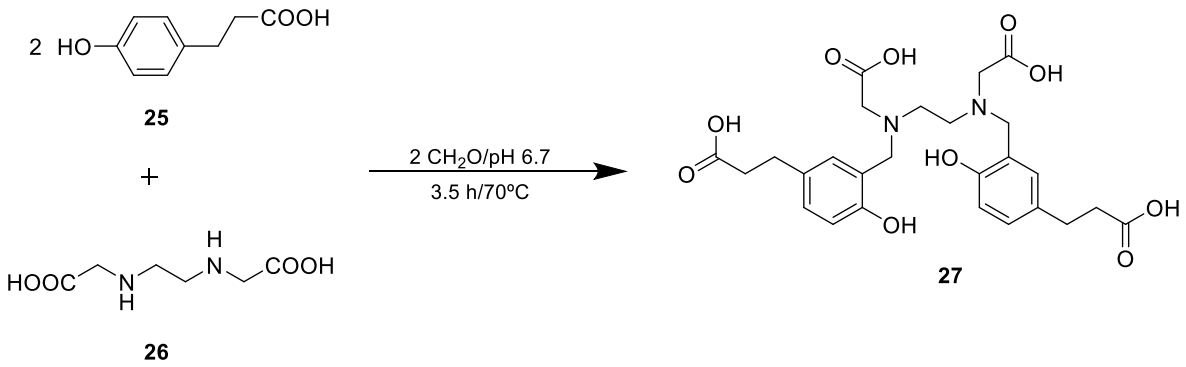

Scheme 3.1. Synthesis of HBED-CC (**27**).

The HBED-CC synthesis was done based on the above mentioned Mannich reaction, as presented in scheme 3.1. 3-(o-hydroxyphenyl)propionic acid (**25**) was treated with EDDA (**26**) while the pH of this mixture was adjusted to 6.7 and the solution was cooled in an ice bath. Subsequently, formaldehyde (aqueous solution 37%) was added while maintaining the pH at the previous referred value. After refluxing the mixture for 3.5 h, the solvent was removed and the remaining aqueous solution was acidified with HCl to pH 5.5 and lyophilized. The residue was washed/extracted with methanol and dried under vacuum to afford compound **27**.

Despite the presence of impurities in the isolated product **27**, it was confirmed the presence of compound **27** by ESI-MS analysis. In the positive mode of ESI-MS spectrum, it was observed a peak at m/z = 555.4 corresponding to the molecular ion $[M+Na]^+$ and presenting a pattern in accordance with the theoretical isotopic distribution of the compound, as shown in figure 3.2.

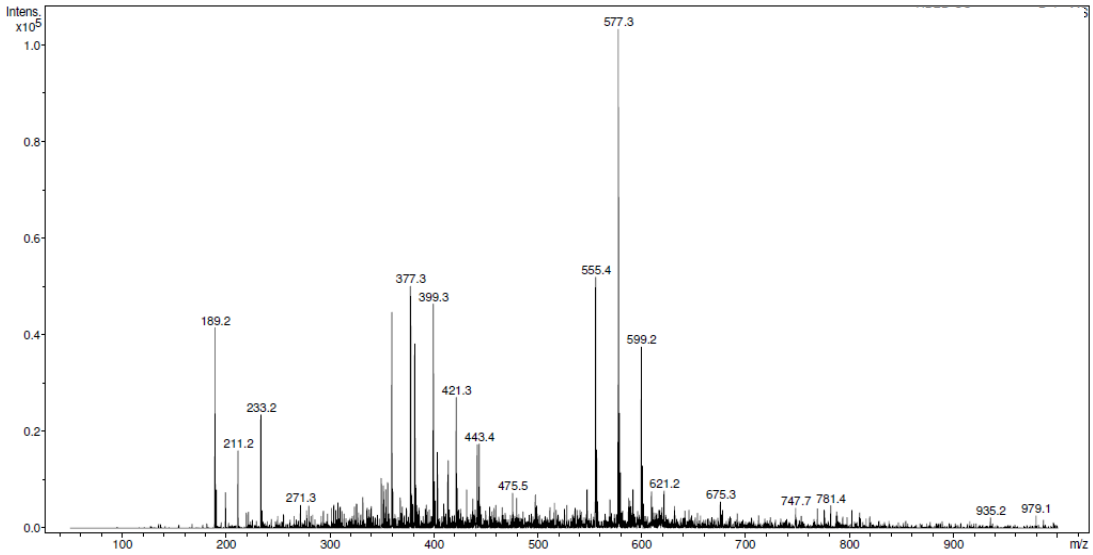

Figure 3.2. ESI-MS Spectrum (positive mode) of compound **27**: The peak observed at *m/z* = 555.4 corresponds to the molecular ion $[M+Na]^+$ (theoretical value: $[M+Na]^+$; *m/z* = 555.20).

^{1}H NMR analysis of the recovered solid was also consistent with the presence of desired compound, **27**, but contaminated with the starting reagents, including an excess of EDDA (**26**). It was decided to use the obtained compound **27** for subsequent generation of the iron complex (see 3.1.1.) expecting a more efficient purification for the Fe(III) complex of HBED-CC.

3.1.1. [Fe(HBED-CC)]$^-$

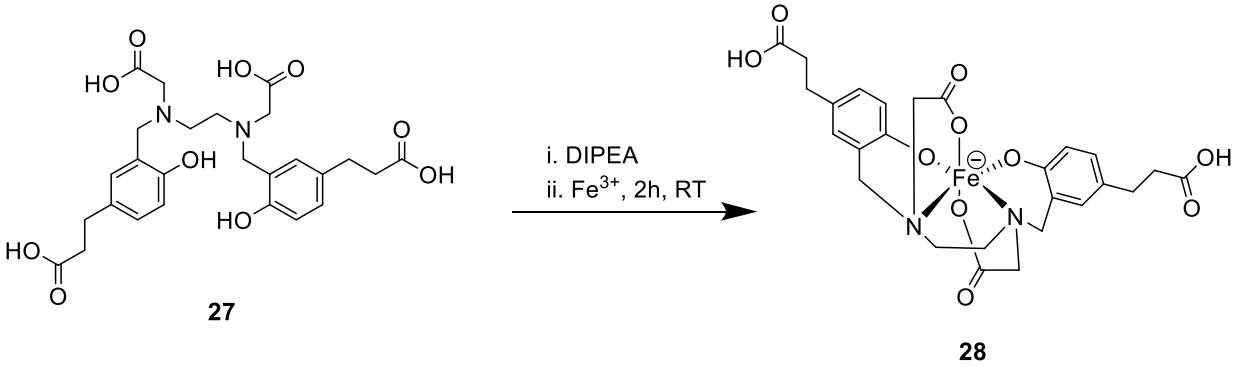

27 **28**

Scheme 3.2. Synthesis of [Fe(HBED-CC)]$^-$ (**28**).

The synthesis of the Fe(III) complex with HBED-CC is presented in scheme 3.2 and was performed based on the methodologies described in literature[6, 54]. HBED-CC (**27**) was treated with DIPEA in H_2O/MeOH (50:50 V/V) to obtain complete dissolution and to this solution was added 0.1 M $FeCl_3$ in water, while kept stirring for 2 hours at RT. The reaction mixture was evaporated to dryness, and the crude HBED-CC-Fe complex was purified by flash chromatography. The [Fe(HBED-CC)]$^-$ complex (**28**) was recovered in 21% yield as a purple solid, after evaporation of the solvents from the collected fractions. The recovered product was analyzed by TLC that confirmed the presence of a single spot. The identity of the [Fe(HBED-CC)]$^-$ complex (**28**) was confirmed only by ESI-MS (see figure 3.3.), because it was not able to perform NMR analysis due to paramagnetic character of the Fe (III) complex. In the negative ESI-MS spectrum, it was observed a peak that corresponded to the molecular ion [M]$^-$, presenting a pattern consistent with the theoretically expected, according to the isotopic distribution of the compound as shown in figure 3.3.

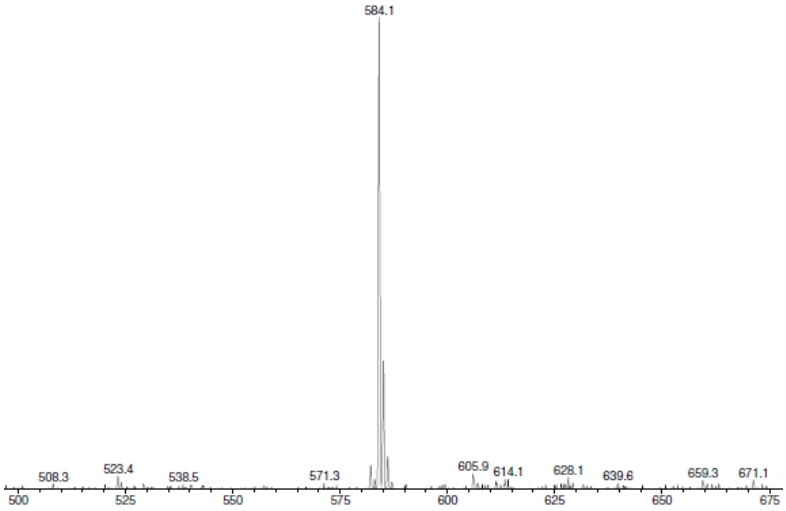

Figure 3.3. ESI-MS spectrum (negative mode) of compound **28**: The peak observed at *m/z* = 584.1 corresponds to $[M]^-$ (theoretical value: $[M]^{-}$; *m/z* = 584.11).

3.1.2. (HBED-CC)TFP_2

The formation of the activated diester of the HBED-CC chelator was attempted similarly to the methods described previously for the synthesis of the corresponding monoactived ester[6, 54], as shown in scheme 3.3.

The strategy followed for the synthesis of the desired product **30** initially involved the esterification of complex **28**, followed by selective hydrolysis for Fe (III) decomplexation. The complexation of Fe (III) allows the protection of the other carboxylic groups that could react with tetrafluorophenol (TFP).

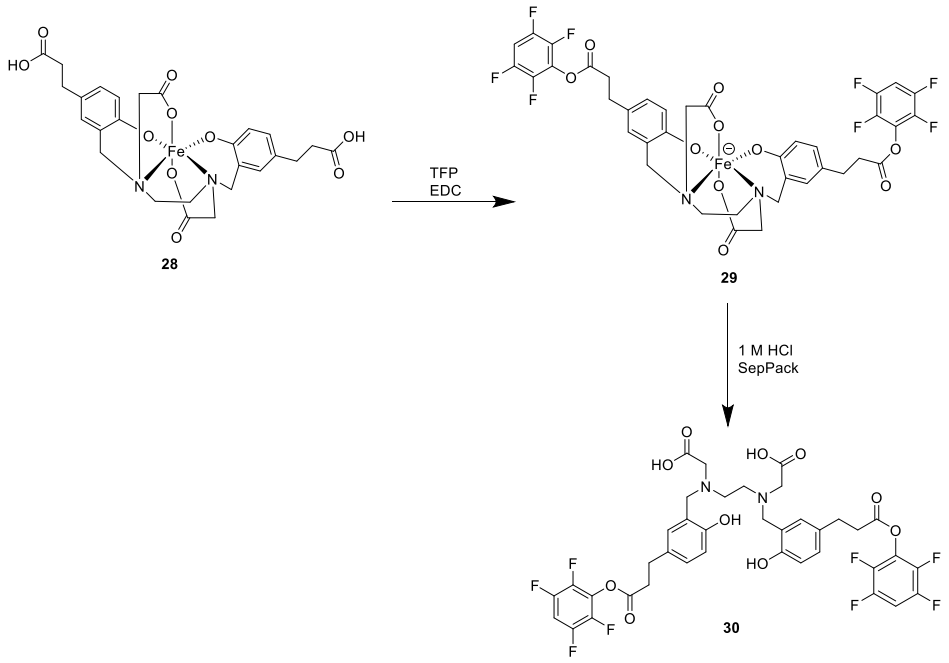

Scheme 3.3. Synthesis of [Fe(HBED-CC)TFP_2] (**29**) and (HBED-CC)TFP_2 (**30**)

To a solution of $[Fe(HBED\text{-}CC)]^-$ (**28**) in dry DMF were added TFP and ethyl(dimethylaminopropyl) carbodiimide (EDC), and the reaction mixture was stirred for 3 days at RT. The completion of the reaction was checked by TLC and then the solvent was evaporated to dryness. The purification of **29** was done uniquely by extraction processes instead of preparative HPLC [as described in the literature[6]]. The crude bis-activated ester $[Fe(HBED\text{-}CC)TFP_2]$ was dissolved in $CHCl_3$, washed with H_2O and the organic phase was evaporated to dryness affording a purple solid. TLC analysis of the collected solid revealed the presence of a single spot. ESI-MS analysis confirmed the formation of the desired complex **29**. The negative ESI-MS spectrum showed an intense peak corresponding to the molecular ion $[M]^-$, presenting a pattern in agreement with the theoretical one, according to the isotopic distribution of the compound, as shown in figure 3.4.

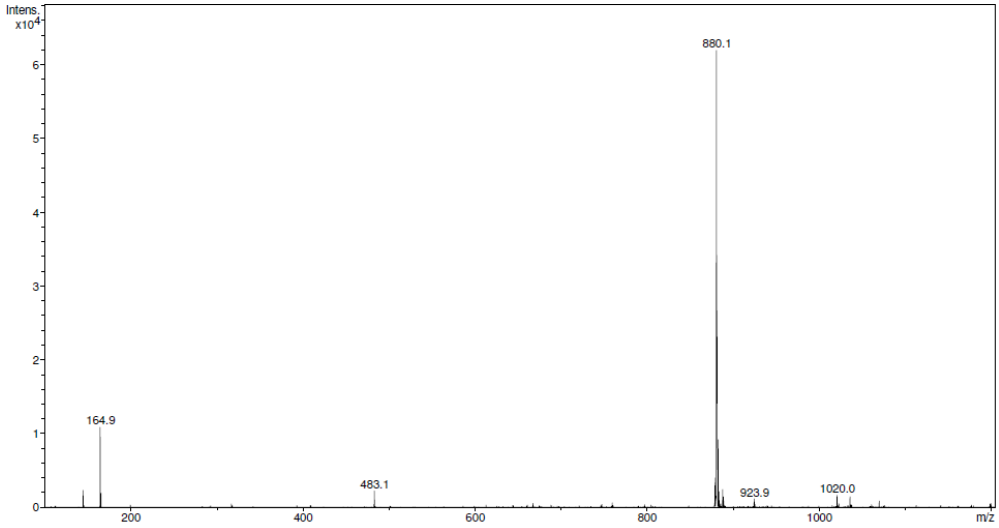

Figure 3.4. ESI-MS spectrum (negative mode) of compound **29**: The peak observed at *m/z* = 880.1 corresponds to the molecular ion $[M]^-$ (theoretical value: $[M]^-$; *m/z* = 880.10).

The removal of Fe^{3+} from $[Fe(HBED\text{-}CC)TFP_2]$ (**29**) was performed as described in the literature[6]. Complex **29** was dissolved in MeOH and trapped on a preconditioned RP18 cartridge, in order to remove the complexed Fe^{3+} through treatment with 1 M HCl. The expected $(HBED\text{-}CC)TFP_2$ ester was eluted with CH_3CN. The solvent from the collected fraction was evaporated to dryness affording a white solid. Despite its low solubility in most common solvents, the recovered product was analyzed by analytical HPLC, ESI-MS analysis and ^1H NMR.

HPLC analysis showed the presence of two major peaks at rt=15.25 min and rt=17.97 min, as shown in figure 3.5. Concerning the ESI-MS spectrum (see figure 3.6.), it was not possible to detect any peak corresponding to compound **30**. The ^{1}H NMR spectrum (see figure 3.7.) also did not show the expected resonances, namely those corresponding to the aromatic protons from the TFP and phenolic rings.

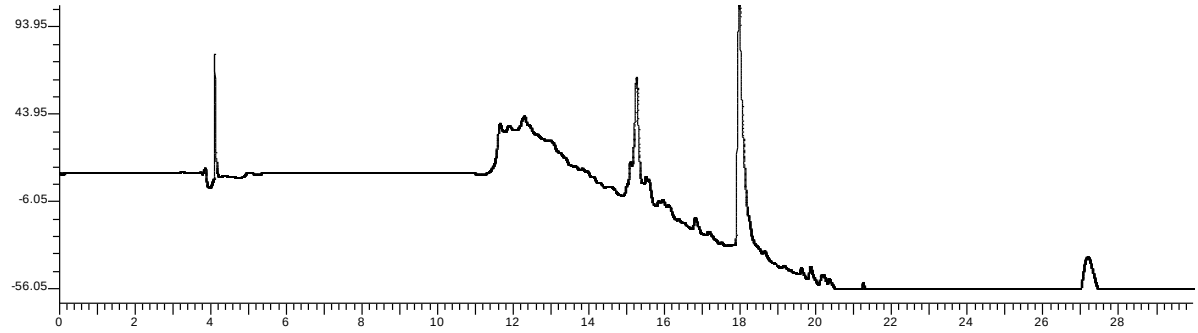

Figure 3.5. Analytical HPLC chromatogram of the collected fraction in the reaction attempted to obtain compound **30**.

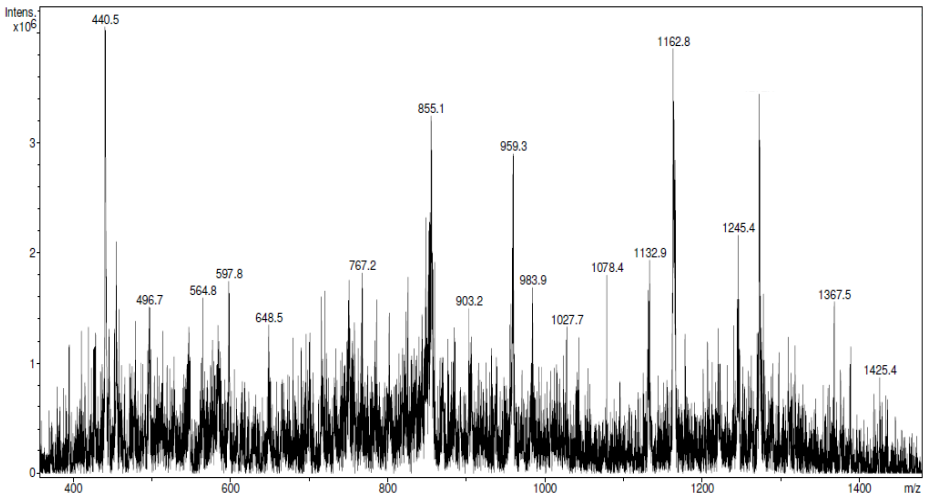

Figure 3.6. ESI-MS spectrum (positive mode) of the collected fraction in the reaction attempted to obtain compound **30**. The expected molar mass of (HBED-CC)TFP_2 (**30**) is 828.67.

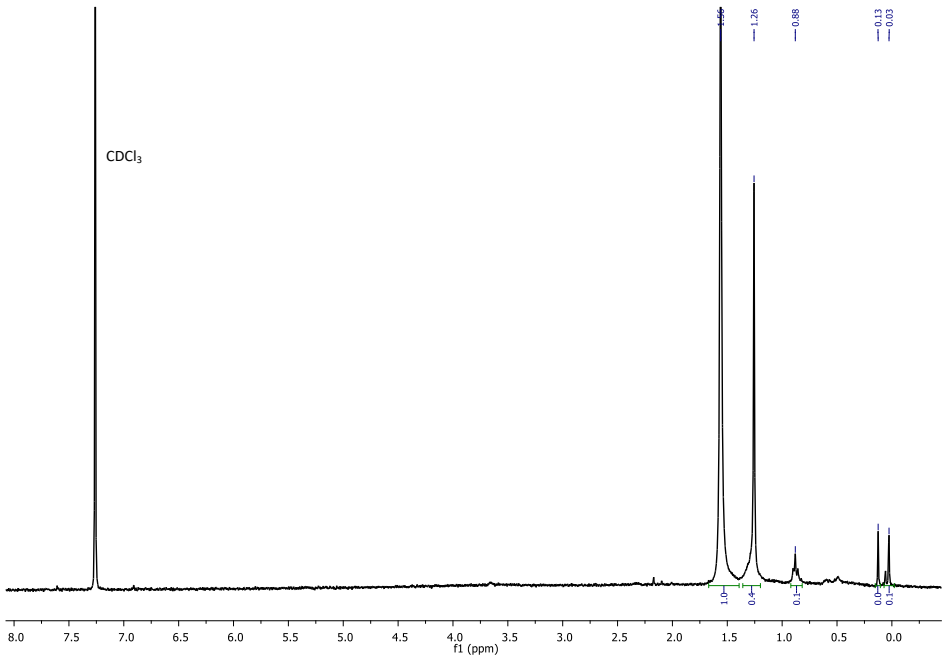

Figure 3.7. ^{1}H NMR spectrum of the collected fraction in the reaction attempted to obtain compound **30**.

It is worthwhile to mention that the solutions of the recovered white solid acquired with time a faint violet color which is indicative of the presence of Fe^{3+}. Hence, the obtained results may be due to the inefficient decomplexation of Fe^{3+}, in addition to the low amount of complex **29** used in this step.

Alternatively, it was thought to use complex **29** for coupling to the PSMA and cyanine dye derivatives synthesized in the previous chapter. A similar strategy was already described in the literature[80], where complex **29** was directly used for coupling with other organic molecules, followed by a successful iron decomplexation leading to the desired products. This strategy could lead to the successful synthesis of the desired ligands for future ^{68}Ga radiolabeling. However, the study of this approach was not attempted due to time limitations.

3.2. Pyrazolyl diamine derivatives

The synthesis of the precursor of the bifunctional ligand with a pyrazolyl unit (**36**) was previously performed by researchers from the RSG of C^{2}TN (see scheme 3.4.) and was kindly provided for conjugation to the molecules designed in this work and to the radioisotope selected for SPECT, ^{99m}Tc. Thus, a pyrazolyl diamine ligand was synthesized for functionalization with the organic precursors studied in this work, through the 4 position of the

pyrazolyl ring or a butyric arm attached to the secondary amine of the coordinating pyrazolyl diamine unit.

The full synthesis of the pyrazolyl diamine ligand **37** involves several steps, as shown in scheme 3.4. In the present work, only the last step was performed. This last step corresponds to the formation of an activated ester at the 4- position of the pyrazolyl ring, starting from compound **36**. This result in the formation of compound **37** that has an activated ester function which was intended to react with the amine groups of the fluorophores studied in this work.

N-Hydroxysuccinimide (NHS) is commonly used as an activating reagent for carboxylic acids, leading to esters with a good leaving group that can react with amines to form amides. A common way to synthesize a NHS-activated acid is to mix NHS with the desired carboxylic acid and a small amount of an organic base in an anhydrous solvent. A coupling reagent such as dicyclohexylcarbodiimide (DCC) or EDC is then added to form a highly reactive activated acid intermediate. The general mechanism of the reaction in presented in figure 3.8.

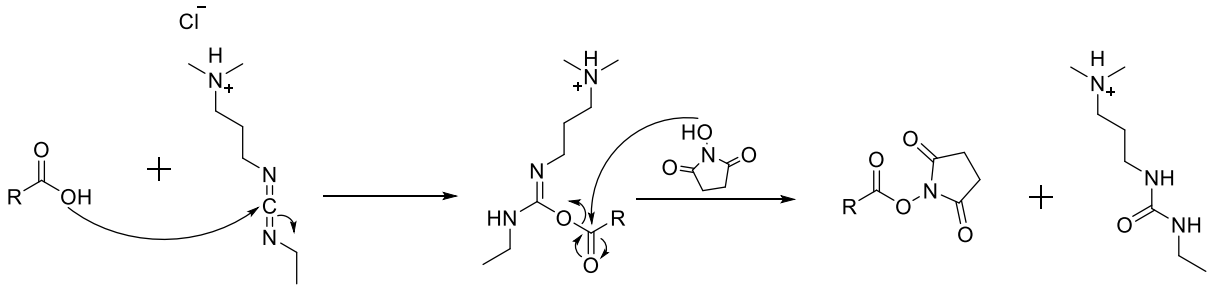

Figure 3.8. Mechanism of formation of NHS-activated esters in the presence of carbodiimides.

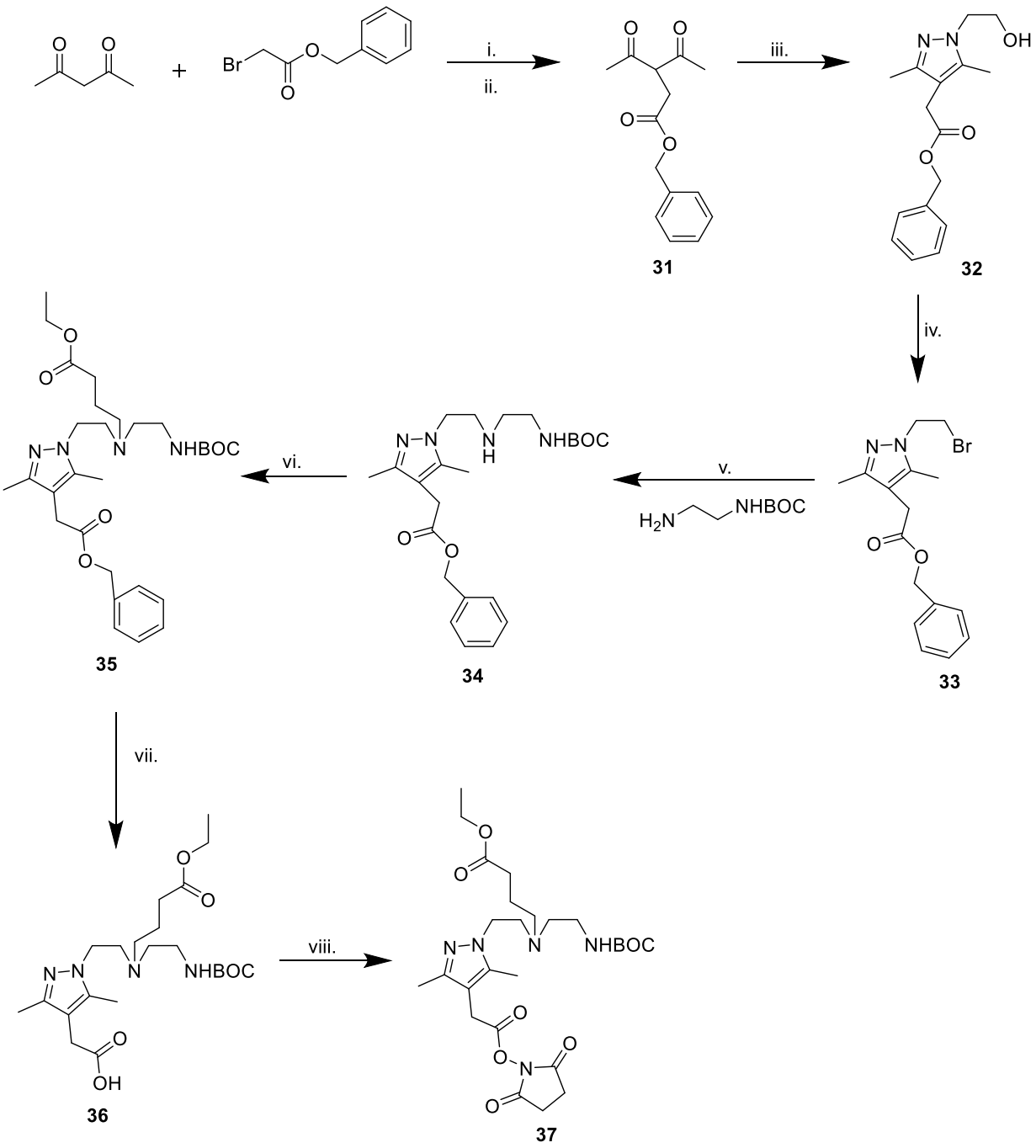

Scheme 3.4. Synthesis of pyrazolyl diamine ligand **37**. i. NaH, dry THF, 0 ° C; ii. HCl 2N; iii. EtOH, 0°C, 2-hydroxyethylhydrazine; iv. CBr_4, THF, PPh_3; v. CH_3CN, K_2CO_3, KI, reflux; vi. 4-bromobutyrate, Et_3N, NaI, reflux, 48 hours; vii. H_2/Pd, dry EtOH; viii. NHS, EDC, dry CH_2Cl_2, rt.

As shown in scheme 3.4, the compound 2-(1-(2 -((2-(tert-butoxycarbonylamino) ethyl) (4-ethoxy-4-oxobutyl) amino) ethyl)-3,5-dimethylpyrazole) acetic acid (**36**) was reacted with NHS in dry CH_2Cl_2 in the presence of EDC yielding ethyl-4 - ((2- (tert-butoxycarbonylamino) ethyl) (2- (4- (2- (2,5-dioxopyrrolidinyloxy) 2-oxoethyl) -3,5-dimethylpyrazole) ethyl) amino) butanoate (**37**) in 77.8 % yield. In this reaction step, to remove the excess NHS and the urea formed during the reaction, the dry residue was diluted with water and extracted with CH_2Cl_2. Characterization of compound **37** by ^1H NMR and ESI-MS analysis confirmed the identity of the desired compound.

Concerning the positive mode of ESI-MS spectrum, it was observed a peak that corresponded to the molecular ion $[M+H]^+$, presenting a pattern corresponding to the theoretically expected, according to the isotopic distribution of the compound as shown in figure 3.9.

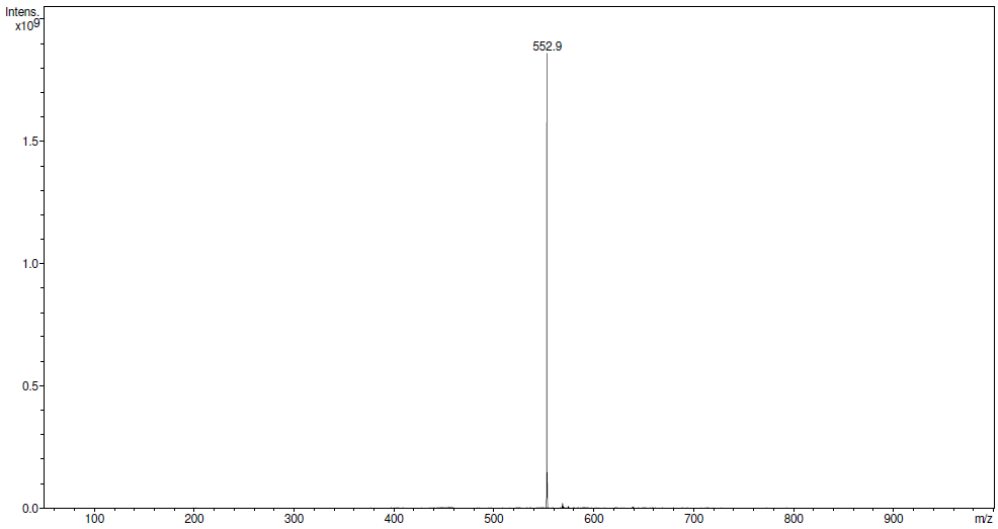

Figure 3.9. ESI-MS Spectrum (positive mode) of compound **37**: The peak observed at *m/z* = 552.9 corresponds to molecular ion $[M+H]^+$ (theoretical value: $[M+H]^+$; *m/z* = 552.30).

3.2.1. IR-820-S-Ph-Nh-Pz

The NHS ester-activated, compound **37**, was used for the coupling of the aromatic derivative of the IR820 fluorophore (compound **20**) being expected the formation of a stable amide bond and the release of NHS, as depicted in figure 3.10.

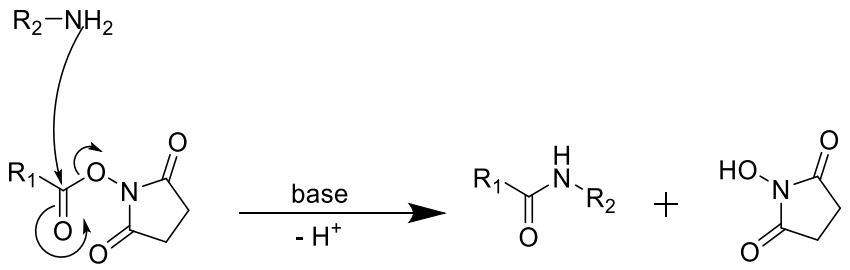

Figure 3.10. Mechanism of formation of an amide group with release of NHS.

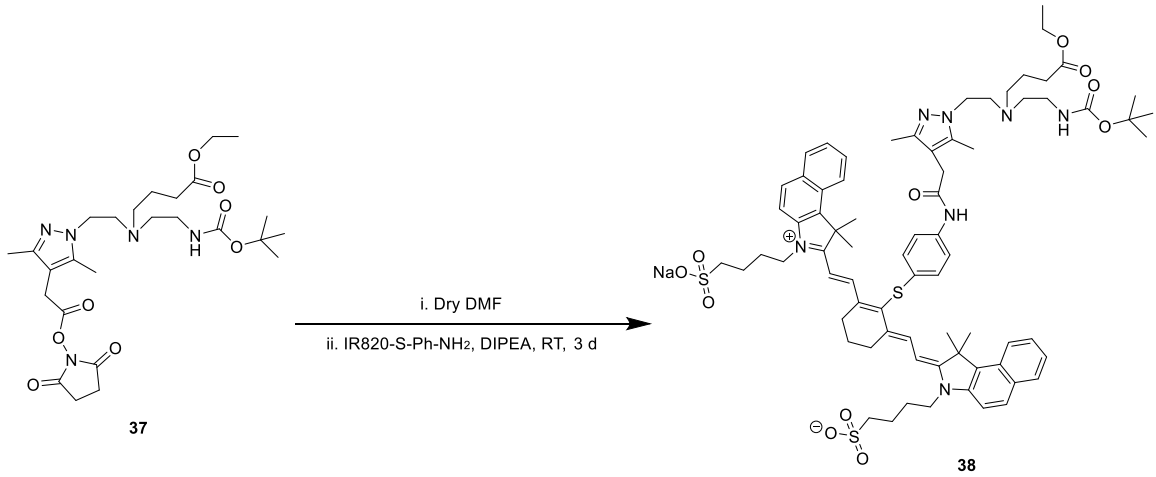

Scheme 3.5. Synthesis of IR-820-S-Ph-NH-Pz (**38**).

The reaction studied to synthesize the IR-820-S-Ph-NH-Pz ligand (**38**) is presented in scheme 3.5. The NHS activated-ester, compound **37**, was dissolved in dry DMF and the aromatic derivative of IR820 (**20**) and DIPEA were added to this solution under stirring at RT for 3 days. The solvent was evaporated to afford a purple solid. Before stopping the reaction, control TLC and preparative HPLC were performed and confirmed the formation of a new product. ESI-MS analysis was performed on the crude product and the spectrum revealed a weak peak that corresponded to the molecular ion $[M-Na+2H]^+$, presenting a pattern corresponding to the theoretically expected, according to the isotopic distribution of the compound (see figure 3.11). The product purification was tried out by preparative HPLC being isolated the two major peaks found in the chromatogram (see figure 3.12.). Then, these samples were characterized by ESI-MS analysis, but none of the peaks observed in the spectra corresponded to the desired product.

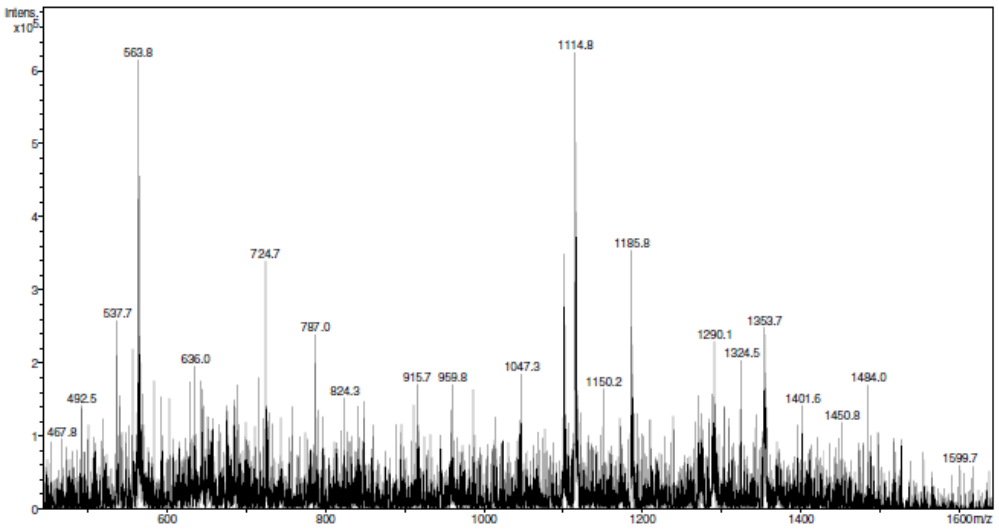

Figure 3.11. ESI-MS spectrum (positive mode) of the crude from the reaction studied to obtain compound **38**: The peak observed at *m/z* = 1353.7 might corresponds to molecular ion $[M\text{-}Na+2H]^+$ (theoretical value: $[M\text{-}Na+2H]^+$; *m/z* = 1352.62).

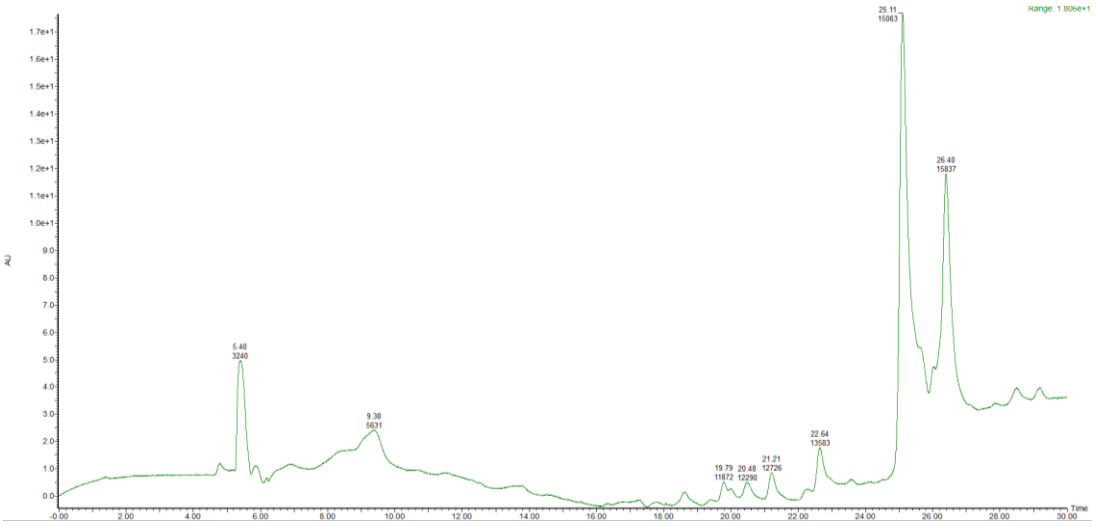

Figure 3.12. Preparative HPLC chromatogram of the crude from the reaction studied to obtain compound **38**.

At this point and due to time limitations, it was not possible to go further in optimizing an appropriate purification method that should avoid the tendency of the compound to degrade in solution.

4. Final considerations and future perspectives

4. Final considerations and future perspectives

During the development of this work it should be noted that several difficulties were encountered in obtaining the products in their pure state, namely in their purification.

The optimization of the proposed synthesis, especially in terms of the choice and testing of purification methods, led to the delay in obtaining the compounds studied in this work. For these reasons, it was not possible to obtain the proposed final compounds. Nevertheless, it was possible to obtain several precursors necessary for the synthesis of the proposed dual probes.

In the synthesis of the organic precursors, it was possible to obtain the PSMA inhibitor through solid phase synthesis (compounds **17** and **18**), as well as the aromatic fluorophore derivative IR820-S-Ph-NH_2 (**20**). In the future and taking advantage of the synthesis strategy already developed for the aliphatic derivative of IR820 (**24**), consideration should be given to optimize the proposed synthesis and purification methods of compound **24**. It should be emphasized that it is expected an easier formation of the amide bonds during the functionalization of the BFCs with the fluorophores in the case of **24,** when compared to **20**. This is due to the higher reactivity of aliphatic amines in this type of reactions, comparatively to aromatic amines.

Regarding the synthesis of BFCs, it was possible to obtain the two desired molecules - HBED-CC and pyrazolyl diamine derivatives - for subsequent conjugation to the organic precursors (PSMA inhibitor and fluorescent dye).

During the synthesis of HBED-CC derivatives, different optimizations in the synthesis and purification methods of compounds **27** to **30** were tested, and the greatest difficulties were encountered in obtaining pure compound **30**. Efforts should be done to optimize the method of decomplexation tested for Fe^{3+} removal, as the resulting ligand could not be correctly characterized by the tested identification techniques. Alternatively and as a priority, as it was not possible to obtain pure compound **30**, the conjugation of compound [Fe(HBED-CC)TFP_2] (**29**) to the organic precursors should be considered, as already described in the literature for the coupling of this Fe(III) complex to other bioactive molecules[80].

Concerning the coupling between the pyrazolyl diamine ligand (**37**) and the fluorophore aromatic derivative of IR820 (**20**), the proposed synthesis did not prove to be effective. It is suggested in the future, to optimize the synthesis strategy as well as the purification methods to obtain the final ligand **38**. The failure of this coupling may be explained by the lower reactivity

of the aromatic derivative of IR820 (**20**) compared to an aliphatic one. It is also important to note that the NHS-activated ester **37** tends to hydrolyze in the presence of residual water and even during storage, according to the experience of the RSG researchers who have developed this compound.

The fact that it was not possible to synthesize any of the bimodal probes, either for PET or SPECT imaging, precluded the biological studies that were initially thought, namely the evaluation of the dual ^{99m}Tc and ^{68}Ga complexes in cells of PCa and in mice with induced tumor. In the future, once the final ligands and radiolabeled complexes will be available, it will be crucial to conduct such biological evaluation to have an insight on the performance of the designed complexes as dual probes for the imaging and detection of prostate cancer.

5. Experimental

5. Experimental

5.1. Solvents, reagents and purification and characterization techniques

5.1.1. Solvents and Reagents

All used solvents were of pro-analytical quality and were used without additional purification. The dry solvents were treated and maintained according to described methods[81]. Commercially purchased reagents were not subjected to any previous purification.

5.1.2. Thin Layer chromatography (TLC)

TLC was used to check the chemical synthesis reactions and to identify the reaction products. Strips of silica gel 60-F254 (Merck) on aluminum support or strips of aluminum oxide on aluminum support (Merck) were used and then the chromatograms were revealed by ultraviolet light irradiation with wavelength of 254 nm. Exposure of the plates to a iodine chamber (I_2) and/or a solution of ninhydrin (3% w/v in a solution of 5% acetic acid in MeOH) followed by heating were also used, in some cases, for revelation of the chromatograms.

5.1.3. Flash chromatography

This technique was performed to purify some of the synthesized compounds. Depending on the compound to be purified, silica gel 60 (0.060 mesh granulometry, Merck) or aluminum oxide (Macherey-Nagel) were used as the stationary phase. Columns of glass of appropriate size to the amount of sample to be purified, were filled with a stationary phase/eluent mixture. The eluent system was chosen according to the characteristics (polarity) of the compounds to be purified. After application of the sample to the top of the column, elution was performed by the action of gravity and fractions of appropriate volume were collected. The collected fractions were analyzed by TLC to select those that corresponded to the desired product. The fractions containing the purified product were combined and dried under vacuum on the rotary evaporator (Büchi) and in the vacuum line.

5.1.4. High Pressure Liquid Chromatography (HPLC)

Analysis and purification of some synthesized compounds were performed on an HPLC system equipped with a Perkin-Elmer LC 200 pump and a Perkin-Elmer LC 290 visible / UV detector, and/ or a HPLC system of Waters 2535 Quaternary Gradient. The water was bi-distilled in a quartz apparatus and filtered using 0.22 µm millipore filters. All solvents used were of HPLC grade and were previously deaerated with helium. Chromatograms were obtained by detection of absorbance at 220 nm or 254 nm. Analytical control and/or purification of the fluorophore derivatives, the fluorophore-pyrazolyl diamine conjugate and esterification product of the complex $[Fe(HBEC\text{-}CC)]^{-}$ (samples prepared in MeOH) were carried out according to the following methods.

Method 1

Pre-column and column: Supelco C18; 25 cm x 4,6 mm, 5 µm

Flow: 1 mL/minute

Eluents/Solvents: (A) 0.1% TFA aqueous; (B) MeOH

Gradients:

TIME (min)	A (%)	B (%)	Curve
0	100	0	0
20	0	100	1
25	0	100	0
26	100	0	1
30	100	0	0

Method 2

Pre-column and column: Supelco C18; 25 cm x 10 mm, 10 µm

Flow: 3 mL/minute

Eluents/Solvents: (A) 0.1% TFA aqueous; (B) MeOH

Gradients:

TIME (min)	A (%)	B (%)	Curve
0	100	0	0
20	0	100	1
25	0	100	0
26	100	0	1
30	100	0	0

Method 3

Pre-column and column: Supelco C18; 25 cm x 10 mm, 10 µm

Flow: 3 mL/minute

Eluents/Solvents: (A) 0.1% TFA aqueous; (B) MeOH

Gradients:

TIME (min)	A (%)	B (%)	Curve
0	80	20	0
20	0	100	1
25	0	100	0
26	80	20	1
30	80	20	0

Method 4

Pre-column and column: Supelco C18; 25 cm x 4,6 mm, 5 µm

Flow: 1 mL/minute

Eluents/Solvents: (A) 0.1% TFA aqueous; (B) ACN

Gradients:

TIME (min)	A (%)	B (%)	Curve
0	100	0	0
20	0	100	1
25	0	100	0
26	100	0	1
30	100	0	0

5.2. Chemical Synthesis

5.2.1. Synthesis of 4-methoxybenzyl N2-(((9H-fluoren-9-yl)methoxy)carbonyl)-N6-(tert-butoxycarbonyl)lysinate (9)

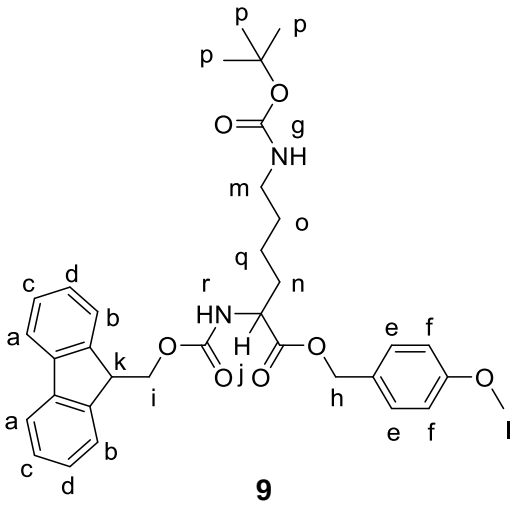

9

Under nitrogen, Nε-Boc-Nα-Fmoc-L-lysine (1 g, 0.002 mol) was dissolved in dry DMF and to this solution was added cesium carbonate (0.98 g, 0.003 mol) and 4-methoxybenzyl chloride (289 µl, 0.0021 mol). The suspension was stirred at RT under nitrogen for 4 h, then filtered. After removal of the solvent under vacuum, the residue was extracted with ethyl acetate and the resulting solution washed with 5% Na_2CO_3 and water [EtOAc (40 ml), 5% Na_2CO_3 (2 x 20 ml), H_2O (2 x 20 ml)]. The ethyl acetate solution was dried over $MgSO_4$ and the solvent

removed in the rotary evaporator. The resulting residue was recrystallized in 60/40 (v/v) hexane/EtOAc to give 3 crops of a colorless solid (**9**) (0.795 g, 0.0014 mol, η = 70%).

TLC Rf (70/30 hexane/EtOAc): 0.33

ESI-MS ($C_{34}H_{40}N_2O_7$): *m/z (calculated)* = 589.29 $[M+H]^+$; 611.27 $[M+Na]^+$; *m/z (found)* = 589.4 $[M+H]^+$; 611.4 $[M+Na]^+$

^{1}H NMR [$CDCl_3$, δ (ppm)]: 7.76 [d, 2H, 2ArCH (f)]; 7.59 [d, 2H, 2ArCH (e)]; 7.40 [(t, 2H, 2ArCH (b)]; 7.27-7.33 [m, 4H, 4ArCH (c,d)]; 6.87 [d, 2H, 2ArCH (a)]; 5,38 [bs, 1H, CH (g)]; 5,07-5,16 [q, 2H, CH_2 (h)]; 4,33-4,43 [m, 3H, CH_2, CH (i,k)]; 4,20 [t, 1H, CH (j)]; 3.79 [s, 3H, CH_3 (l)]; 3,05 [bs, 2H, CH_2 (m)]; 1.25-1,43 [m, 16H, $3CH_3$, $3CH_2$ (p, n, o, q)].

5.2.2. Attempted synthesis of 2-Amino-6-tert-butoxycarbonylamino-hexanoic acid 4-methoxybenzyl ester (1)

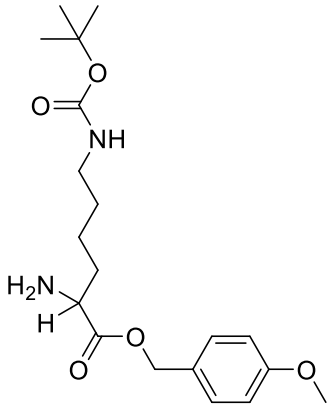

1

Under nitrogen, compound **9** (105.5 mg, 0. 179 mmol) was treated with a 20% solution of piperidine in 10 ml DMF in order to remove the Fmoc group. The reaction was stirred at RT temperature for 2 h. After removal of the solvent, the residue was dissolved in CH_2Cl_2 and the resulting solution washed with water. The CH_2Cl_2 fraction was dried over Mg_2SO_4 and the solvent removed under vacuum. The residue was applied in an alumina column that was eluted with MeOH/$CHCl_3$ (5/95). An oil was recovered from the collected fractions, which was analyzed by ^{1}H NMR in $CDCl_3$. The ^{1}H NMR analysis showed that we were in the presence of *p*-methoxybenzyl alcohol and not the desired compound **1**.

5.2.3. Synthesis of bis-4-methoxybenzyl-L-glutamate.HCl (2)

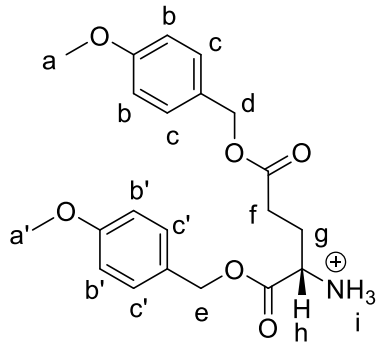

2

L(+) glutamic acid (161.8 mg, 1.1 mmol) was dissolved in dry DMF (20 ml). The mixture was stirred at 0ºC and slowly N,N,N',N' – tetramethylguanidine (147 µl, 1.17 mmol) was added. After 30 minutes, ethyl acetoacetate (148 µl, 1.17 mmol) was added to the mixture. Stirring was continued at RT for 24 h. Then, 4-methoxybenzyl chloride (317 µl, 2.345 mmol) was added and stirring was continued for another 16 h under nitrogen gas. The reaction mixture was then diluted with 1 M $NaHCO_3$ (30 ml) and EtOAc (55 ml); the organic phase was washed with 1 M $NaHCO_3$ (20 ml) and H_2O (2 x 30 ml) and then dried with $MgSO_4$. After evaporation under vacuum, the product was acidified with methanolic HCl (1M, 15 ml); the mixture was shaken gently until the solid had dissolved. After 30 minutes at RT, the solution was evaporated to dryness to yield an oil which solidified when triturated with diethyl ether. Compound **2** was purified by flash chromatography [MeOH/CH_2Cl_2 (5/95)] affording a yellow solid (86 mg, 0.22 mmol, η = 20%).

TLC Rf (MeOH/CH_2Cl_2 (5/95)): 0.40

ESI-MS ($C_{21}H_{25}NO_6$): *m/z (calculated)*= 388.18 $[M+H]^+$; *m/z (found)* = 388.5 $[M+H]^+$

^{1}H NMR [$CDCl_3$, δ (ppm)]: 8.82 [s, 3H, NH_3 (i)]; 7.19-7.28 [m, 4H, 4ArCH (b,b')]; 6.79-7.83 [m, 4H, 4ArCH (c,c')]; 5.10 [d, 2H, CH_2 (d)]; 4.94 [s, 2H, CH_2 (e)]; 4.45 [bs, H, CH (h)]; 3.76 [s, 3H, CH_3 (a)]; 3.74 [s, 3H, CH_3 (a')]; 2.40 - 2.72 [m, 4H, $2CH_2$ (f,g)].

^{13}C NMR [$CDCl_3$), δ (ppm)] 172.31 (C=O); 169.28 (C=O); 159.90 (Ar); 159.87 (Ar); 159,60 (Ar); 130.45 (Ar); 130.42 (Ar); 130.11 (Ar), 127.88 (Ar); 126.78 (Ar); 114.03 (Ar); 113.92 (Ar); 68.18 (CH_2); 66.45 (CH_2); 55.29 (CH_3); 55.27 (CH_3); 52.68 (CH_2); 51.90 (CH_2); 29.95 (CH_2); 25.40 (CH_2).

5.2.4. Solid-phase synthesis of the Glu-urea-Lys scaffold

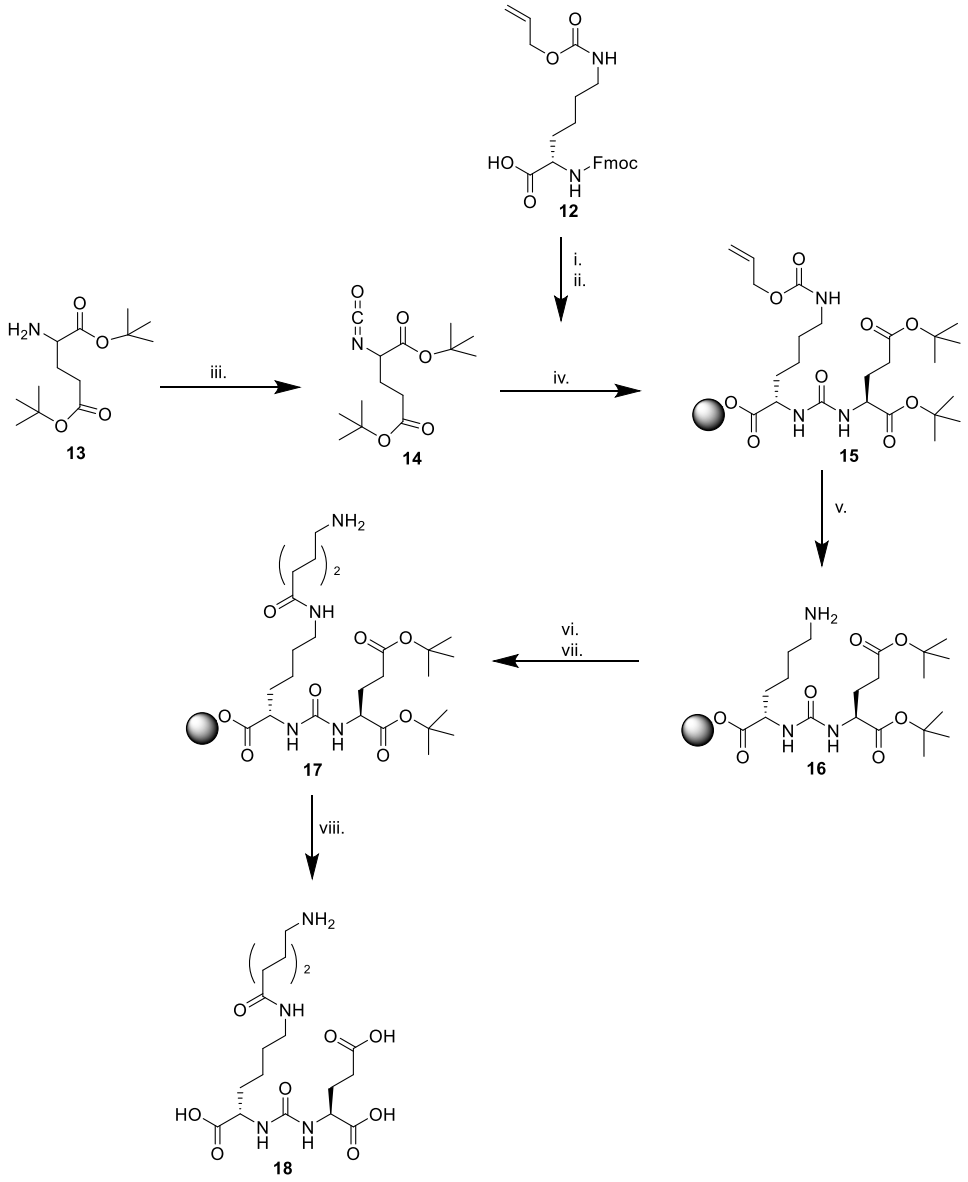

In a 20 ml syringe with a filter, the polystyrene Wang resin (1 g, 0.45 mmol/g, 0.45 mmol) in 20 ml of dry DMF was agitated over 40 minutes. Then, the protected amino acid Fmoc-L-Lys (Alloc) (**12**) (1.02 g, 2.254 mmol) was dissolved in a minimum volume of DMF and to this solution was added pyridine (300 µL, 3.71 mmol) and 2,6- dichlorobenzoic acid (322 µL, 2.247mmol) and it was agitated and then loaded to the syringe that contained the resin. The reaction mixture was agitated overnight and then the resin was washed (5x15 ml of DMF). In order to remove the Fmoc group, the mixture was treated with 15 ml of 20% of piperidine in DMF and agitated over 1 hour. The solvent was dried and the mixture was washed (3x15 ml of DMF, followed by 3x50% DMF and 50% of DCM and 3x15 ml of DCM). Finally the solvents were dried out under vacuum to obtain the resin immobilized E-allyloxycarbonyl protected lysine.

In a round flask, triphosgene (147 mg, 0.495 mmol) was dissolved in 15 ml of dry DCM over magnetic stirring and cooled with dry ice until -50ºC. Meanwhile in a closed dropping funnel, to the bis(tert-butyl) L-glutamate hydrochloride (13) (400 mg, 1.352 mmol) were added 40 ml of dry DCM and 2 ml of DIPEA and the mixture was agitated until obtain a complete dissolution. The solution of triphosgene was kept stirring while the solution of glutamic acid was slowly added over 1.5 hour. Finally the dry ice was removed and the solution was kept under stirring while reaching RT. Then, the L-Lys (Alloc) Wang resin was added to the previous solution and gently shaken over 72 hours to form the urea bond. The mixture was washed (3x15 ml DCM) and leaded to compound **15**.

Subsequently, compound **15** was shaken in 20 ml of dry DCM over 20 min at RT and a solution of $Pd(PPh_3)_4$ (200 mg, 0.173 mmol) and 2 ml morpholine in 20 ml of dry DCM was prepared under light protection. In order to remove the allyloxyl-protecting group, 10 ml of the last solution were added to the solution of compound **15** over agitation for 1 hour. The solvents were removed and the procedure was repeated with the remaining 10 ml of the $Pd(PPh_3)_4$ and morpholine solution. The mixture was washed (5x15ml DMF; 10x15 ml 2% DIPEA in DMF; 5x15 ml 20 mg/ml of sodium diethylthiocarbamate in DMF; 5x15 ml DMF; 5x15 ml DCM) and dried over vacuum leading to compound **16**. Next, it was performed the coupling of compound **16** to the aminohexanoic linker by reaction of the Fmoc-protected 6-aminohexanoic acid, in the presence of HBTU and DIPEA in DMF, followed by selective Fmoc deprotection under treatment with 20% piperidine in DMF to afford compound **17**. Compound **17** was then treated with TFA/ TMS / H_2O (95: 2.5: 2.5) under stirring at RT for 30 min to afford compound **18**.

ESI-MS of compound **18** ($C_{18}H_{32}N_4O_8$): *m/z (calculated)*= 433.23 $[M+H]^+$; *m/z (found)* = 433.2 $[M+H]^+$

5.2.5. Synthesis of IR820-S-Ph-NH_2 (20)

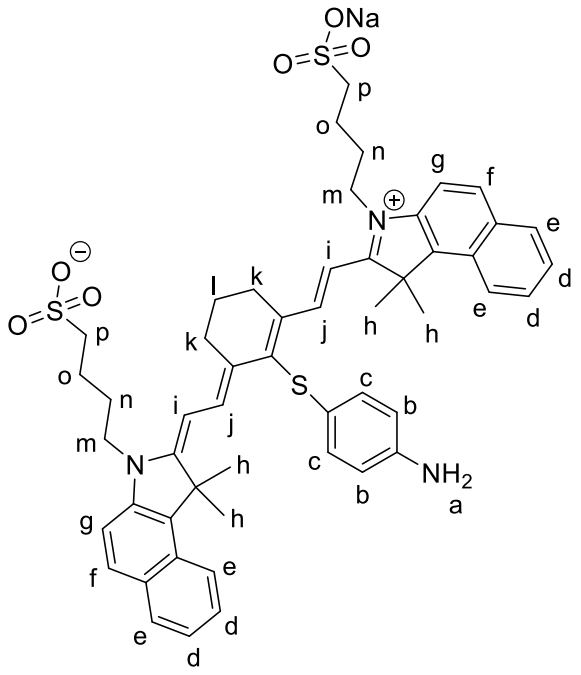

20

IR820 (100 mg, 0.118 mmol) was treated with 2 Eq of 4-aminothiophenol (29.5 mg, 0.236 mmol) in 3 ml of DMF and stirred 72 h at RT under light protection. The solution was concentrated, precipitated out of diethyl ether, centrifuged and washed two times with diethyl ether. Product purification was then performed by flash chromatography (CH_2Cl_2/MeOH 90/10 to 0/100) to afford compound **20** as a green solid (57 mg, 0.061 mmol, η = 51.7%).

TLC Rf (90/10 CH_2Cl_2/MeOH): 0.6

ESI-MS ($C_{52}H_{56}N_3NaO_6S_3$): *m/z (calculated)*= 914.33 $[M-Na]^-$; *m/z (found)* = 914.6 $[M-Na]^-$

^{1}H NMR [CD_3OD, δ (ppm)]: 8,97 [d, 2H, 2CH (i)]; 8,18 [d, 2H, 2ArCH (f)]; 7,97 [t, 4H, 4ArCH (e)]; 7,60 [m, 4H, 4ArCH (d)]; 7,45 [t, 2H, 2ArCH (g)]; 7,11 [d, 2H, 2ArCH (b)]; 6,68 [d, 2H, 2ArCH (c)]; 6,34 [d, 2H, 2CH (j)]; 4,28 [t, 4H, $2CH_2$ (m)]; 2,90 [t, 4H, $2CH_2$ (k)]; 2,79 [s, 4H, $2CH_2$ (p)]; 1,96-2,02 [m, 10H, $5CH_2$, (l ,n, o)}; 1,85 [s, 12H, $4CH_3$ (h)].

HPLC: Method 1; rt = 20.92 min.

5.2.6. Synthesis of Hxmda-BOC (22)

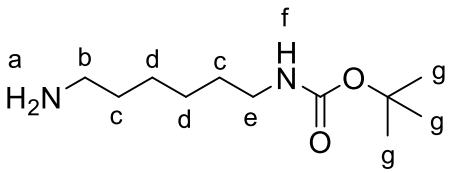

22

To a solution of hexamethylenediamine (957.3 mg, 8.238 mmol) in 30 ml dioxane, was added a solution of $(BOC)_2O$ (221.5 mg, 1.015 mmol) in 30 ml of dioxane over 3 hours and the reaction mixture was then stirred for 24 hours at RT. After evaporation of the solvent, the solution was redissolved in EtOAc (30 ml) and washed with a saturated NaCl solution (3 x 15 ml). The organic phase was dried over $MgSO_4$, filtered and evaporated affording compound **22** (87 mg, 0.402 mmol, η = 39.6%).

ESI-MS ($C_{11}H_{24}N_2O_2$): *m/z (calculated)*= 239.17 $[M+Na]^+$.; *m/z (found)* = 239.6 $[M+Na]^+$.

^{1}H NMR [CD_3OD, δ (ppm)]: 4.76 [s, 1H, NH (f)]; 2.99 [d, 2H, CH_2 (b)]; 2.58 [t, 2H, CH_2 (e)]; 1.23-1.34 [m, 19H, $3CH_3$, NH_2, $4CH_2$ (a,c,d,g)].

5.2.7. Synthesis of IR820-HXMDA-BOC (23)

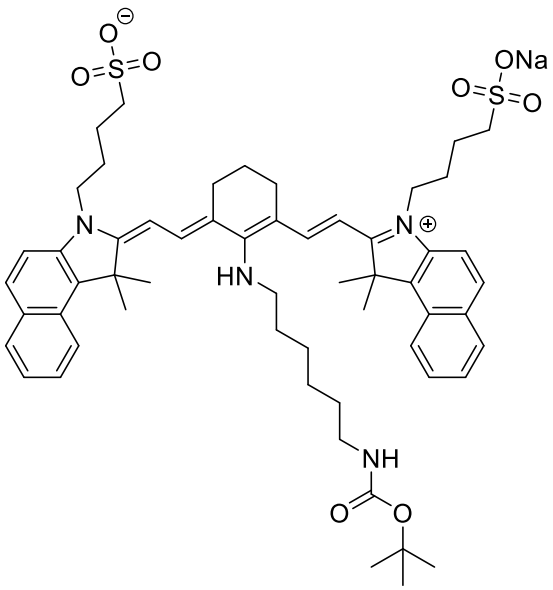

23

IR820 (100 mg, 0.118 mmol) was reacted with 3 Eq of Hxmda-BOC (87 mg, 0.4022 mmol) and 3 Eq of dry triethylamine (56.1 µL, 0.4022 mmol) in 2 ml of dry DMF in a corked flask, under nitrogen atmosphere and magnetic stirring overnight at RT. The solution was dried out to afford a green solid. The compound was purified by flash chromatography using EtOAc/MeOH (80/20) as eluent, affording compound **23** as a blue solid (34 mg, 0.033 mmol, η = 28%).

TLC Rf (80/20 EtOAc/MeOH): 0.42

ESI-MS ($C_{57}H_{73}N_4NaO_8S_2$): *m/z (calculated)* = 1005.49 $[M-Na]^-$; *m/z (found)* = 1005.6 $[M-Na]^-$

5.2.8. Attempted synthesis of IR820-Hxmda (24)

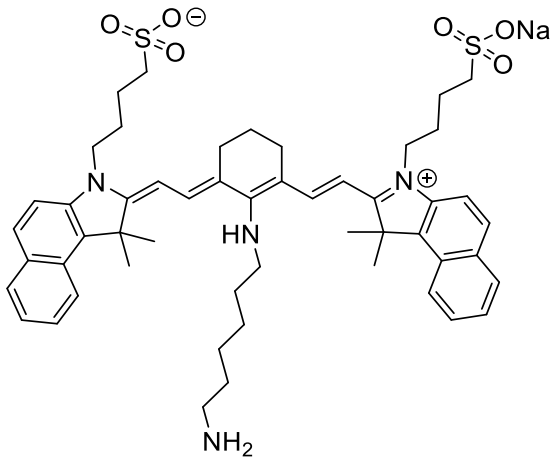

24

IR820-Hxmda-BOC (**23**) (34 mg, 0.033 mmol) was dissolved in 500 µL of DCM and treated with TFA/DCM (50:50) at RT over stirring for 3 h and the solvents were removed in vacuum.

Preparative HPLC (method 2) was performed to purify the compound, leading to the isolation of 2 fractions that were analyzed by ^{1}H NMR, ESI-MS analysis and analytical HPLC (method 1). The performed analysis did not confirm the formation of the desired compound.

5.2.9. Synthesis of HBED-CC (27)

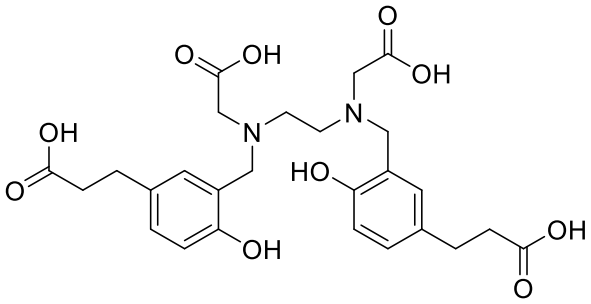

27

3-(o-hydroxyphenyl)propionic acid (1 g, 5.98 mmol) was dissolved in 6 ml of methanol, 1.6 ml of H_2O and 0.8 ml of 4.0 M NaOH. To this solution, EDDA (526.74 mg, 2.99 mmol) in 2 ml of 2.0 M NaOH was added with continual stirring. The pH of this mixture was adjusted to 6.7 and the solution was cooled in an ice bath. Subsequently, formaldehyde (aqueous solution 37%) (5.98 mmol, 485.35 µl) was added in several portions while maintaining the pH at 6.7 by intermittent addition of 4.0 M NaOH. After refluxing the mixture for 3.5 h, MeOH was removed on a rotary evaporator. The remaining aqueous solution was acidified with HCl to pH 5.5 and lyophilized. Finally, the solid was washed/extracted with MeOH and dried under vacuum to afford a white solid. It was obtained 1.0402 g of the product but the ^{1}H NMR analysis showed that **27** was contaminated with some of the starting reagents.

ESI-MS ($C_{26}H_{32}N_2O_{10}$): *m/z (calculated)*= 555.20 $[M+Na]^+$; *m/z (foundl)* = 555.4 $[M+Na]^+$

5.2.10. Synthesis of [Fe(HBED-CC)]$^-$ (28)

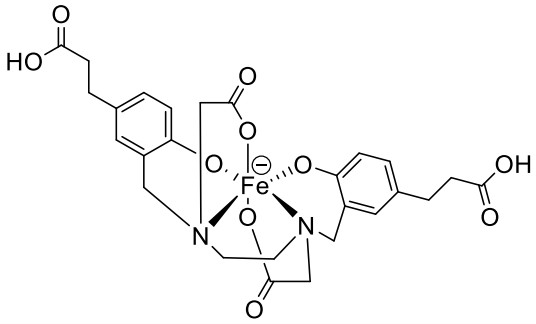

28

HBED-CC (**27**) (835.6 mg, 1.57 mmol) was dissolved in 80 ml of H_2O/MeOH (50:50 V/V) and 1.2 ml of DIPEA was added to obtain complete dissolution, while stirring for 30 minutes.

To this solution, 16 ml of 0.1 M $FeCl_3$ in water was added while the solution's color turned burgundy and it was kept stirring for 2 hours at RT. The reaction mixture was evaporated to dryness, and the resulting solid was dissolved in CH_3CN and, once again, the solution was evaporated to dryness to remove remaining water. Purification of the crude by silica-gel chromatography using MeOH/EtOH/$CHCl_3$ (70/15/15) as eluent afforded the $[Fe(HBED\text{-}CC)]^-$ (**28**) complex as a purple solid (190 mg, 0.325 mmol, η = 21%).

TLC Rf (70/15/15 MeOH/EtOH/$CHCl_3$): 0.56

ESI-MS ($C_{26}H_{28}FeN_2O_{10}$): *m/z (calculated)*= 584.11 $[M]^-$; *m/z (found)* = 584.1 $[M]^-$

5.2.11. Synthesis of [Fe(HBED-CC)]TFP_2 (29)

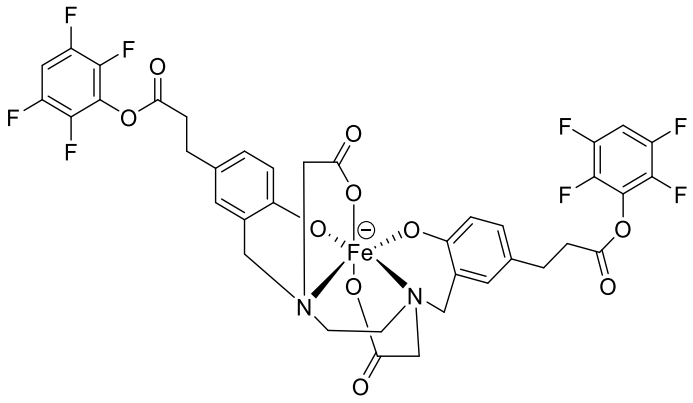

29

To a 0.01 M $[Fe(HBED\text{-}CC)]^-$ (**28**) solution in dry DMF (26.4 ml) were added TFP (438.4 mg, 2.64 mmol) and EDC (202.4352, 1.056 mmol). The solution was maintained under magnetic stirring for 3 days at RT and then evaporated to dryness. The crude bis-activated ester $[Fe(HBED\text{-}CC)TFP_2]$ (**29**) was dissolved in $CHCl_3$, washed with H_2O and the organic phase was evaporated to dryness affording a purple solid. The purity of the product was checked by TLC and the identity of $[HBED\text{-}CC\text{-}Fe]TFP_2$ (**29**) was confirmed by ESI-MS.

TLC Rf (90/10 $CHCl_3$/MeOH): 0.4

ESI-MS ($C_{38}H_{28}F_8FeN_2O_{10}$): *m/z (calculated)*= 880.10 $[M]^-$; *m/z (found)* = 880.1 $[M]^-$

5.2.12. Attempted synthesis of (HBED-CC)]TFP_2 (30)

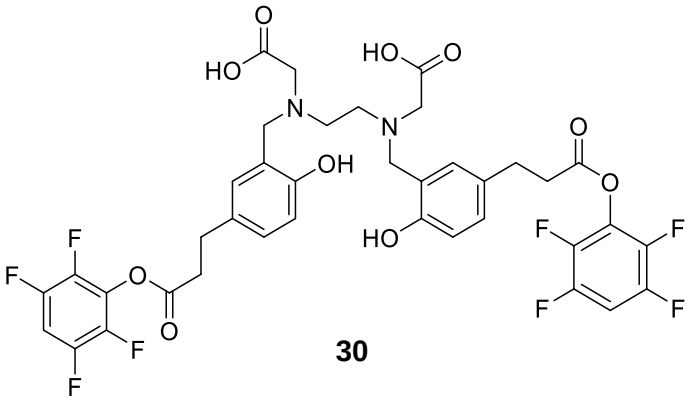

30

Complex **29** was dissolved in MeOH and loaded on a preconditioned RP18 cartridge (Waters SepPack-Classic C18). Preconditioning was performed by purging with 5 ml of CH_3CN and 5 ml of HCl. To remove complexed Fe^{3+}, the cartridge was flushed with 1 M HCl and washed with 4 ml H_2O. The disappearance of the violet color seemed to indicate completion of the deprotection reaction. The remaining (HBED-CC)TFP_2 ester was eluted with 4 ml CH_3CN and evaporated to dryness affording a white solid. HPLC analysis (method 4) of this solid showed the presence of two major species (rt=15.25 min and rt=17.97 min). The analysis of the recovered solid by ESI-MS and ^1H NMR did not corroborate the formation of the desired compound.

5.2.13. Synthesis of ethyl-4 - ((2- (tert-butoxycarbonylamino) ethyl) (2- (4- (2- (2,5-dioxopyrrolidinyloxy) 2-oxoethyl) -3,5-dimethylpyrazole) ethyl) amino) butanoate (37)

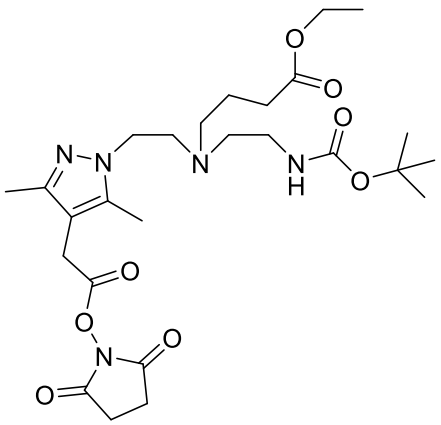

37

To a solution of **36** (16.4 mg, 0.036 mmol) in 10 ml of dry CH_2Cl_2, was added NHS (4.6 mg, 0.0396 mmol) in an ice bath and the mixture was stirred for 30 minutes. Then, EDC (7.6 mg, 0.0396 mmol) was added and the reactional mixture was stirred for 24 hours at RT. The solvent was evaporated under vacuum and the remaining residue was dissolved in H_2O (10 ml) and extracted with CH_2Cl_2 (15 ml). The organic phase was dried over MgSO4, filtered and evaporated to obtain a yellow oil (15.5 mg, 0.028 mmol, η = 77.8 %).

ESI-MS ($C_{26}H_{41}N_5O_8$): *m/z (calculated)*= 552.30 $[M+H]^+$; *m/z (found)* = 552.9 $[M+H]^+$

^{1}H NMR (CDCl3): δ (ppm): 1.21 (t, 3H, CH_3); 1.41 (s, 9H, $3CH_3$, BOC); 1.57 (m, 2H, CH_2); 2.09 (m, 2H, CH_2); 2.15 (m, 6H, $2CH_3$); 2.39 (t, 2H, CH_2); 2.41 (t, 1H, CH); 2.78 (m, 6H, $3CH_2$); 3.03 (m, 1H, CH); 3.61 (m, 4H, $2CH_2$); 3.97 (t, 2H, CH_2); 4.13 (q, 2H, CH_2); 5.42 (s br, 1H, NH)

5.2.14. Attempted synthesis of IR-820-S-Ph-NH-Pz ligand (38)

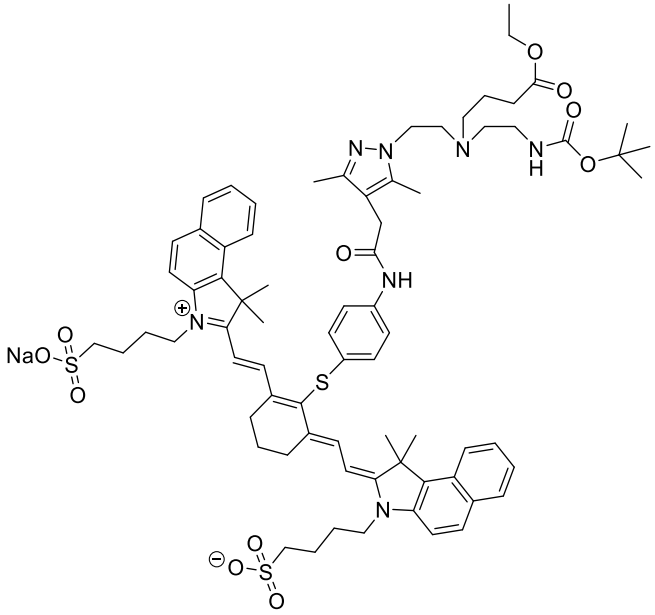

38

The NHS activated-ester **37** (15.5 mg, 0.028 mmol) was dissolved in 5 ml of dry DMF. To the resulting solution, a solution of the aromatic derivative of IR820 (**20**) (27.58 mg, 0.0294 mmol) and DIPEA (5.12 µL, 0.0294 mmol) in DMF was added, and the reaction mixture was then stirred at RT for 3 days. The solvent was evaporated to afford a purple solid. Before stopping the reaction, control TLC and analytical HPLC were performed and confirmed the formation of a new product. Purification of **38** was attempted by preparative HPLC (method 3). However, the ESI-MS analysis of the collected peaks did not confirm the presence of **38**.

ESI-MS of crude compound **38** ($C_{74}H_{92}N_7O_{11}S_3Na$): *m/z (calculated)*= 1352.62 $[M–Na+2H]^+$; *m/z (found)* = 1353.7 $[M–Na+2H]^+$

6. References

6. References

1. Gourni E, Henriksen G, Gamez P, Caballero AB. Metal-based PSMA radioligands. *Molecules*, **2017**, 22(4), 1–34.
2. Eiber M, Fendler WP, Rowe SP, Calais J, Hofman MS, Maurer T, et al. Prostate-Specific Membrane Antigen Ligands for Imaging and Therapy. *J Nucl Med*, **2017**, 58 (Supplement 2), 67S–76S.
3. Kovar JL, Cheung LL, Simpson MA, Olive DM. Pharmacokinetic and Biodistribution Assessment of a Near Infrared-Labeled PSMA-Specific Small Molecule in Tumor-Bearing Mice. *Prostate Cancer*, **2014**, 104248.
4. Chen Y, Pullambhatla M, Banerjee. SR, Byun Y, Stathis M, Rojas C, et al. SYnthesis and biological evaluation of low molecular weight fluorescent imaging agents for the prostate-specific membrane antigen. *Bioconjug Chem*, **2012**, 23(12), 2377–85.
5. Ferlay J, Steliarova-Foucher E, Lortet-Tieulent J, Rosso S, Coebergh JWW, Comber H, et al. Cancer incidence and mortality patterns in Europe: Estimates for 40 countries in 2012. *Eur J Cancer*, **2013**, 49(6), 1374–403.
6. Schäfer M, Bauder-Wüst U, Leotta K, Zoller F, Mier W, Haberkorn U, et al. A dimerized urea-based inhibitor of the prostatespecific membrane antigen for 68Ga-PET imaging of prostate cancer. *EJNMMI Res*, **2012,** 2(1), 1–11.
7. Eder M, Neels O, Müller M, Bauder-Wüst U, Remde Y, Schäfer M, et al. Novel preclinical and radiopharmaceutical aspects of [68Ga]Ga-PSMA-HBED-CC: A new PET tracer for imaging of prostate cancer. *Pharmaceuticals,* **2014**, 7(7), 779–96.
8. Pillai MRA, Nanabala R, Joy A, Sasikumar A, Russ Knapp FF. Radiolabeled enzyme inhibitors and binding agents targeting PSMA: Effective theranostic tools for imaging and therapy of prostate cancer. *Nucl Med Biol,* **2016**, 43(11), 692–720.
9. Wu J, Pan D, Chung LWK. Near-infrared fluorescence and nuclear imaging and targeting of prostate cancer. *Transl Androl Urol*, **2013**, 2(6), 254–64.
10. Haberkorn U, Eder M, Kopka K, Babich JW, Eisenhut M. New strategies in prostate cancer: Prostate-specific membrane antigen (PSMA) ligands for diagnosis and therapy. *Clin Cancer Res*. **2016**, 22(1), 9–15.
11. Beyer T, Freudenberg LS, Townsend DW, Czernin J. The future of hybrid imaging—part 1: hybrid imaging technologies and SPECT/CT. *Insights Imaging*, **2011**, 2(2), 161–9.
12. Beyer T, Townsend DW, Czernin J, Freudenberg LS. The future of hybrid imaging—part 2: PET/CT. *Insights Imaging*. **2011**, 2(3), 225–34.

13. Kratochwil C, Bruchertseifer F, Giesel FL, Weis M, Verburg FA, Mottaghy F, et al. 225Ac-PSMA-617 for PSMA-Targeted-Radiation Therapy of Metastatic Castration-Resistant Prostate Cancer. *J Nucl Med*, **2016**, 57(12), 1941–4.
14. Chakravarty R, Siamof CM, Dash A, Cai W. Targeted α-therapy of prostate cancer using radiolabeled PSMA inhibitors: a game changer in nuclear medicine. *Am J Nucl Med Mol Imaging*, **2018**, 8(4), 247–67.
15. Wang X, Huang SS, Heston WDW, Guo H, Wang B-C, Basilion JP. Development of Targeted Near-Infrared Imaging Agents for Prostate Cancer. *Mol Cancer Ther*, **2014**, 13(11), 2595–606.
16. Luo S, Zhang E, Su Y, Cheng T, Shi C. A review of NIR dyes in cancer targeting and imaging. *Biomaterials*, **2011**, 32(29), 7127–38.
17. Yuan J, Yi X, Yan F, Wang F, Qin W, Wu G, et al. Nearinfrared fluorescence imaging of prostate cancer using heptamethine carbocyanine dyes. *Mol Med Rep*, **2015**, 11(2), 821–8.
18. Zhang Z, Zhu Z, Yang D, Fan W, Wang J, Li X, et al. Preparation and affinity identification of glutamic acid-urea small molecule analogs in prostate cancer. *Oncol Lett*, **2016**, 12(2), 1001–6.
19. Nakajima T, Mitsunaga M, Bander NH, Heston WD, Choyke PL, Kobayashi H. Targeted, activatable, in vivo fluorescence imaging of prostate-specific membrane antigen (PSMA) positive tumors using the quenched humanized J591 antibody-ICG conjugate. *Bioconjugate Chem*, **2011**, 22, 8, 1700-1705.
20. Wang L, Switalska M, Wang N, Du ZJ, Fukumoto Y, Diep NK, et al. Design, synthesis, and biological evaluation of artemisinin-indoloquinoline hybrids as potent antiproliferative agents. *Molecules*, **2014**, 19(11), 19021–35.
21. Robu S, Schottelius M, Eiber M, Maurer T, Gschwend J, Schwaiger M, et al. Preclinical Evaluation and First Patient Application of 99mTc-PSMA-I&S for SPECT Imaging and Radioguided Surgery in Prostate Cancer. *J Nucl Med*, **2016**, 58(2), 235–42.
22. Vallabhajosula S, Nikolopoulou A, Babich JW, Osborne JR, Tagawa ST, Lipai I, et al. 99mTc-Labeled Small-Molecule Inhibitors of Prostate-Specific Membrane Antigen: Pharmacokinetics and Biodistribution Studies in Healthy Subjects and Patients with Metastatic Prostate Cancer. *J Nucl Med*, **2014**, 55(11), 1791–8.
23. Banerjee SR, Foss CA, Castanares M, Mease RC, Byun Y, Fox JJ, et al. Synthesis and evaluation of technetium-99m- and rhenium-labeled inhibitors of the prostate-specific membrane antigen (PSMA). *J Med Chem*, **2008**, 51(15), 4504–17.
24. Eder M, Schäfer M, Bauder-Wüst U, Hull WE, Wängler C, Mier W, et al. 68Ga-complex lipophilicity and the targeting property of a urea-based PSMA inhibitor for PET imaging. *Bioconjug Chem*, **2012**, 23(4), 688–97.

25. Lütje S, Heskamp S, Cornelissen AS, Poeppel TD, van den Broek SAMW, Rosenbaum-Krumme S, et al. PSMA ligands for radionuclide imaging and therapy of prostate cancer: Clinical status. *Theranostics*, **2015**, 5(12), 1388–401.
26. Kopka K, Benešová M, Bařinka C, Haberkorn U, Babich J. Glu-Ureido–Based Inhibitors of Prostate-Specific Membrane Antigen: Lessons Learned During the Development of a Novel Class of Low-Molecular-Weight Theranostic Radiotracers. *J Nucl Med*, **2017**, 58(Supplement 2), 17S–26S.
27. Yang X, Mease RC, Pullambhatla M, Lisok A, Chen Y, Foss CA, et al. Fluorobenzoyllysinepentanedioic Acid Carbamates: New Scaffolds for Positron Emission Tomography (PET) Imaging of Prostate-Specific Membrane Antigen (PSMA). *J Med Chem*, **2016**, 59(1), 206–18.
28. Jeelani S, Jagat Reddy RC, Maheswaran T, Asokan GS, Dany A, Anand B. Theranostics: A treasured tailor for tomorrow. *J Pharm Bioall Sci*, **2014**, 6, S6-8.
29. Ballinger JR, Decristoforo C, Farstad B, Mccoubrey B, O'reilly G, Ryder H, et al. The Radiopharmacy A Technologist's Guide. *European Association of Nuclear Medicine*, **2008**.
30. Yeong C-H, Cheng M, Ng K-H. Therapeutic radionuclides in nuclear medicine: current and future prospects. J *Zhejiang Univ Sci B*, **2014**,15(10), 845–63.
31. Bhattacharyya S, Manish D. Metallic radionuclides in the development of diagnostic and therapeutic radiopharmaceuticals. *Dalton Trans*, **2011**, 40(23), 6112–6128.
32. Perkins AC. In vivo molecular targeted radiotherapy. *Biomed Imaging Interv J*, **2005**, 1(2), e9.
33. Ünak P. Imaging and therapy with radionuclide labeled magnetic nanoparticles. *Brazilian Arch Biol Technol*, **2008**, 51(spe), 31–7.
34. Dash A, Knapp FFR, Pillai MRA. Targeted radionuclide therapy - an overview. *Curr Radiopharm*, **2013**, 6(3), 152–80.
35. Welch MJ, Redvanly CS. Handbook of radiopharmaceuticals: radiochemistry and applications. *John Wiley and Sons*, ***2003***.
36. Grupen C. Introduction to Radiation Protection. *Springer Berlin Heidelberg*, **2010**.
37. Pimlott SL, Sutherland A. Molecular tracers for the PET and SPECT imaging of disease. *Chem Soc Rev*, **2011**, 40(1), 149–62.
38. Bazañez-Borgert M. Basics of SPECT , PET and PET/CT Imaging. *JASS*, **2006**.
39. Parvez S, Hasan MR, Islam MR, Hossain MB, Khan HR, Paul AK. Determination of Elution Profile of a Radionuclide Generator System 99Mo/99mTc. *Bangladesh Res Pub J*, **2016**, 12(2), 155-158.
40. Banerjee SR, Pullambhatla M, Byun Y, Nimmagadda S, Green G, Fox JJ, et al. 68Ga-labeled inhibitors of prostate-specific membrane antigen (PSMA) for imaging prostate

cancer. *J Med Chem*, **2010**, 53(14), 5333–41.

41. Velikyan I. 68Ga-based radiopharmaceuticals: Production and application relationship. *Molecules*, **2015**, 20(7), 12913-12943.
42. Kratochwil C, Afshar-Oromieh A, Kopka K, Haberkorn U, Giesel FL. Current Status of Prostate-Specific Membrane Antigen Targeting in Nuclear Medicine: Clinical Translation of Chelator Containing Prostate-Specific Membrane Antigen Ligands Into Diagnostics and Therapy for Prostate Cancer. *Semin Nucl Med*, **2016**, 46(5), 405–18.
43. Barrett JA, Coleman RE, Goldsmith SJ, Vallabhajosula S, Petry NA, Cho S, et al. First-in-Man Evaluation of 2 High-Affinity PSMA-Avid Small Molecules for Imaging Prostate Cancer. *J Nucl Med*, **2013**, 54(3), 380–7.
44. Zechmann CM, Afshar-Oromieh A, Armor T, Stubbs JB, Mier W, Hadaschik B, et al. Radiation dosimetry and first therapy results with a 124I/ 131I-labeled small molecule (MIP-1095) targeting PSMA for prostate cancer therapy. *Eur J Nucl Med Mol Imaging*, **2014**, 41(7), 1280–92.
45. Mease RC, Dusich CL, Foss CA, Ravert HT, Dannals RF, Seidel J, et al. N-[N-[(S)-1,3-dicarboxypropyl]carbamoyl]-4-[18F]fluorobenzyl-L-cysteine, [18F]DCFBC: A new Imaging probe for prostate cancer. *Clin Cancer Res*, **2008**, 14(10), 3036–43.
46. Rowe SP, Macura KJ, Mena E, Blackford AL, Nadal R, Antonarakis ES, et al. PSMA-Based [18F]DCFPyL PET/CT Is Superior to Conventional Imaging for Lesion Detection in Patients with Metastatic Prostate Cancer. *Mol Imaging Biol*, **2016**, 18(3), 411–9.
47. Chen Y, Pullambhatla M, Foss CA, Byun Y, Nimmagadda S, Senthamizhchelvan S, et al. 2-(3-{1-carboxy-5-[(6-[18F]fluoro-pyridine-3-carbonyl)-amino]- pentyl}-ureido)-pentanedioic acid, [18F]DCFPyL, a PSMA-based PET imaging agent for prostate cancer. *Clin Cancer Res*, **2011**, 17(24), 7645–53.
48. Weineisen M, Schottelius M, Simecek J, Baum RP, Yildiz A, Beykan S, et al. 68Ga- and 177Lu-Labeled PSMA I&T: Optimization of a PSMA-Targeted Theranostic Concept and First Proof-of-Concept Human Studies. *J Nucl Med*, **2015**, 56(8), 1169–76.
49. Schottelius M, Wirtz M, Eiber M, Maurer T, Wester HJ. [111In]PSMA-I&T: expanding the spectrum of PSMA-I&T applications towards SPECT and radioguided surgery. *EJNMMI Res*, **2015**, 5(1), 1–5.
50. Benešová M, Schafer M, Bauder-Wust U, Afshar-Oromieh A, Kratochwil C, Mier W, et al. Preclinical Evaluation of a Tailor-Made DOTA-Conjugated PSMA Inhibitor with Optimized Linker Moiety for Imaging and Endoradiotherapy of Prostate Cancer. *J Nucl Med*, **2015**, 56(6), 914–20.
51. Han X-D, Liu C, Liu F, Xie Q-H, Liu T-L, Guo X-Y, et al. 64Cu-PSMA-617: A novel PSMA-targeted radio-tracer for PET imaging in gastric adenocarcinoma xenografted mice model. *Oncotarget*, **2017**, 8(43), 74159–69.

52. Cardinale J, Schäfer M, Benešová M, Bauder-Wüst U, Leotta K, Eder M, et al. Preclinical Evaluation of 18F-PSMA-1007, a New Prostate-Specific Membrane Antigen Ligand for Prostate Cancer Imaging. *J Nucl Med*, **2016**, 58(3), 425–31.
53. Zöller M, Schuhmacher J, Reed J, Maier-Borst W, Matzku S. Establishment and characterization of monoclonal antibodies against an octahedral gallium chelate suitable for immunoscintigraphy with PET. *J Nucl Med*, **1992**, 33(7), 1366–72.
54. Eder M, Wängler B, Knackmuss S, LeGall F, Little M, Haberkorn U, et al. Tetrafluorophenolate of HBED-CC: A versatile conjugation agent for 68Ga-labeled small recombinant antibodies. *Eur J Nucl Med Mol Imaging*, **2008**, 35(10), 1878–86.
55. Jamous M, Haberkorn U, Mier W. Synthesis of peptide radiopharmaceuticals for the therapy and diagnosis of tumor diseases. *Molecules*, **2013**, 18(3), 3379–409.
56. Maresca KP, Marquis JC, Hillier SM, Lu G, Frank J, Zimmerman CN, et al. Novel polar single amino acid chelates for technetium-99m tricarbonyl-based radiopharmaceuticals with enhanced renal clearance: application to octreotide. *Bioconjug Chem*, **2010**, 21(6), 1032-42.
57. Rahbar K, Afshar-Oromieh A, Jadvar H, Ahmadzadehfar H. PSMA Theranostics: Current Status and Future Directions. *Mol Imaging*, **2018**, 17, 1–9.
58. Narayanan N, Patonay G. A New Method for the Synthesis of Heptamethine Cyanine Dyes: Synthesis of New Near-Infrared Fluorescent Labels. *J Org Chem*, **1995**, 60(8), 2391–5.
59. Yang X, Shi C, Tong R, Qian W, Zhau HE, Wang R, et al. Near IR heptamethine cyanine dye-mediated cancer imaging. *Clin Cancer Res*, **2010**, 16(10), 2833–44.
60. Shi C, Wu JB, Pan D. Review on near-infrared heptamethine cyanine dyes as theranostic agents for tumor imaging, targeting, and photodynamic therapy. *J Biomed Opt*, **2016**, 21(5), 50901.
61. Lee H, Mason JC, Achilefu S. Synthesis and Spectral Properties of and Phenyl-Substituted Heptamethine Cyanines. *J Org Chem*, **2008**, 73(9), 723–5.
62. Matsuoka D, Watanabe H, Shimizu Y, Kimura H, Ono M, Saji H. Synthesis and evaluation of a novel near-infrared fluorescent probe based on succinimidyl-Cys-C(O)-Glu that targets prostate-specific membrane antigen for optical imaging. *Bioorganic Med Chem Lett*, **2017**, 27(21), 4876–80.
63. Liu T, Wu LY, Hopkins MR, Choi JK, Berkman CE. A targeted low molecular weight near-infrared fluorescent probe for prostate cancer. *Bioorganic Med Chem Lett*, **2010**, 20(23), 7124–6.
64. Chen Y, Dhara S, Banerjee SR, Byun Y, Pullambhatla M, Mease RC, et al. A low molecular weight PSMA-based fluorescent imaging agent for cancer. *Biochem Biophys Res Commun*, **2009**, 390(3), 624–9.

65. Watanabe R, Sato K, Hanaoka H, Harada T, Nakajima T, Kim I, et al. Minibody-indocyanine green based activatable optical imaging probes: The role of short polyethylene glycol linkers. *ACS Med Chem Lett*, **2014**, 5(4), 411–5.
66. Banerjee SR, Pullambhatla M, Byun Y, Nimmagadda S, Foss CA, Green G, et al. Sequential SPECT and optical imaging of experimental models of prostate cancer with a dual modality inhibitor of the prostate-specific membrane antigen. *Angew Chemie Int Ed Engl*, **2011**, 50(39), 9167–70.
67. Lutje S, Rijpkema M, Franssen GM, Fracasso G, Helfrich W, Eek A, et al. Dual-Modality Image-Guided Surgery of Prostate Cancer with a Radiolabeled Fluorescent Anti-PSMA Monoclonal Antibody. *J Nucl Med*, **2014**, 55(6), 995–1001.
68. Baranski A-C, Schäfer M, Bauder-Wüst U, Roscher M, Schmidt J, Stenau E, et al. PSMA-11–Derived Dual-Labeled PSMA Inhibitors for Preoperative PET Imaging and Precise Fluorescence-Guided Surgery of Prostate Cancer. *J Nucl Med*, **2017**, 59(4), 639–45.
69. Schottelius M, Wurzer A, Wissmiller K, Beck R, Koch M, Gorpas D, et al. Synthesis and Preclinical Characterization of the PSMA-Targeted Hybrid Tracer PSMA-I&F for Nuclear and Fluorescence Imaging of Prostate Cancer. *J Nucl Med*, **2018**, 60(1), 71–8.
70. Rauscher I, Maurer T, Beer AJ, Graner F, Haller B, Weirich G, et al. Value of 68Ga-PSMA HBED-CC PET for the Assessment of Lymph Node Metastases in Prostate Cancer Patients with Biochemical Recurrence: Comparison with Histopathology After Salvage Lymphadenectomy. *J Nucl Med*, **2016**, 57(11), 1713-1719.
71. Afshar-Oromieh A, Holland-letz T, Giesel FL, Kratochwil C, Mier W, Haufe S, et al. Diagnostic performance of 68Ga-PSMA-11 (HBED-CC) PET/CT in patients with recurrent prostate cancer: evaluation in 1007 patients. *Eur J Nucl Med Mol Imaging*, **2017**, 44(8), 1258-1268.
72. Santos I, Vitor RF, Alves S, Correia JDG. Rhenium (I) - and technetium (I) tricarbonyl complexes anchored by bifunctional pyrazole-diamine and pyrazole-dithioether chelators. *Journal of Organometallic Chemistry*, **2004**, 689(25), 4764-4774.
73. Maria L, Garcia R, Gano L, Santos IC, Santos I. Tris(pyrazolyl)methane 99mTc tricarbonyl complexes for myocardial imaging. *Dalton Trans*., **2009**, 603–6.
74. Esteves T, Marques F, Jose P, Smith CJ, Santos I. Nuclear targeting with cell-specific multifunctional tricarbonyl M(I) (M is Re, 99mTc) complexes : synthesis, characterization, and cell studies. *Journal of Biological Inorganic Chemistry*, **2011**, 16(8), 1141-53.
75. Zhou L, Zhang M, Fu Q, Li J, Sun H. Targeted near infrared hyperthermia combined with immune stimulation for optimized therapeutic efficacy in thyroid cancer treatment. *Oncotarget*, **2016**, 7(6), 6878-90.

76. Fernandez-Fernandez A, Manchanda R, Lei T, Carvajal DA, Tang Y, Raza SZ, et al. Comparative Study of the Optical and Heat Generation Properties of IR820 and Indocyanine Green. *Mol Imaging*, **2012**, 11(2), 99–113.
77. Iacono P, Karabeber H, Kircher MF, Iacono P. A “schizophotonic” all-in-one nanoparticle coating for multiplexed SE(R)RS biomedical imaging. *Angew Chemie - Int Ed*, **2014**, 53(44), 11756–61.
78. Masotti A, Vicennati P, Boschi F, Calderan L, Sbabati A, Ortaggi G. A novel near-infrared indocyanine dye-polyethylenimine conjugate allows DNA delivery imaging in vivo. *Bioconjug Chem*, **2008**, 19(5), 983–7.
79. Zöller M, Schuhmacher J, Reed J, Maier-Borst W, Matzku S. Establishment and characterization of monoclonal antibodies against an octahedral gallium chelate suitable for immunoscintigraphy with PET. *J Nucl Med*, **1992**, 33(7), 1366–72.
80. Arndt C, Feldmann A, Koristka S, Schäfer M, Bergmann R, Mitwasi N, et al. A theranostic PSMA ligand for PET imaging and retargeting of T cells expressing the universal chimeric antigen receptor UniCAR. *Oncoimmunology*, **2019**, 8(11), 1659095.
81. Perrin D., Armarego W. Purification of Laboratory Chemicals. 3rd edition, **1988**, *Pergamon Press*, Oxford.